QATAR UNIVERSITY

COLLEGE OF PHARMACY

CURCUMIN-CONJUGATED CHITOSAN OLIGOMERS DERIVED FROM MICROWAVE IRRADIATION FOR NANOFORMULATION IN COLON CANCER TREATMENT

BY

DOAA ELSAYED ABDELRAHMAN MAHMOUD

A Thesis Submitted to

the College of Pharmacy

in Partial Fulfillment of the Requirements for the Degree of

Masters of Science in Pharmacy

June 2024

COMMITTEE PAGE

The members of the Committee approve the Thesis of

Doaa Elsayed Abdelrahman Mahmoud defended on 15/05/2024.

Nashiru Billa, PhD
Thesis/Dissertation Supervisor

Saghir Akhtar, PhD
Co-supervisor

Yousef Hijji, PhD
Committee Member

Amjad Shraim, PhD
Committee Member

Approved:

Mohammed Izham, Dean, College of Pharmacy

ABSTRACT

Mahmoud, Doaa E. Masters : June [2024], Pharmaceutical Sciences

Title: Curcumin-conjugated Chitosan Oligomers Derived from Microwave Irradiation for Nanoformulation in Colon Cancer Treatment

Supervisor of Thesis: Prof. Nashiru Billa

Colon cancer remains as one of the leading causes of deaths worldwide, whilst current treatment options are not optimal. Chemotherapy is the mainstay in cancer therapy but is associated with severe side effects. Some anticancer agents of plant origin such as curcumin (CURC), have gained recognition as formidable alternatives to chemotherapeutic drugs. However, the full therapeutic potential of CURC can best be harnessed following formulation or chemical intervention. In this proposal we developed a curcumin-conjugated-chitosan nanoparticles (CCC NPs) delivery system based on a novel approach comprising of fragmentation of chitosan (Ct) by microwave (MW) irradiation at 300W, conjugation with CURC through a Schiff base reaction, and then constructing into CURC-Ct NPs by ionic gelation. Fragmentation of Ct as well as conjugation to CURC was confirmed by UV-vis, FTIR, XRD, DSC, viscometry and CN elemental analyses. The MW treated CCC NPs were 71.19 ± 0.52 nm, significantly smaller than the control CCC NPs (95.31±0.17nm). Both control and 300W CCC NPs had a spherical morphology and CURC release was higher in 300W CCC NPs than control, which was sustained over 96 hrs. Preliminary in-vitro cell cytotoxicity studies indicate a promising dose-dependent cytotoxic effect of the CURC-Ct NPs against colon cancer. This approach will help in providing a more convenient, cost effective and accessible oral dosage form to patients. The next phase of the study will involve an in-depth understanding of the molecular basis of action and in-vivo anti-colon cancer evaluation.

Keywords: Chitosan, Curcumin, Conjugation, Nanoparticles, Ionic gelation, Colon cancer.

DEDICATION

I dedicate this work to cancer patients who suffer in silence.

ACKNOWLEDGMENTS

I would like to thank Allah, my strength, my support, my fortress, my strong corner, my refuge, and the one I rely on, for all the blessings he has given me throughout my entire life, and for granting me the strength and knowledge to be able to complete this work. I hope HE accepts this work and makes it sincerely for the sake of HIS noble face.

I would like to express my gratitude to my primary supervisor, Prof. Nashiru Billa for all the assistance, guidance, and support he has provided throughout my MSc program, and my co-supervisors, Dr. Yousef Hijji, Dr. Saghir Akhtar and Dr. Amjad Shraim for their support, assistance, and provision of needed guidance and materials. I acknowledge the support and the assistance of:

My family: my beloved mama, papa and siblings for their unconditional love and support.

Qatar University: for providing all the needs to achieve the requirements of this study.

CPH Professors: Dr. Ashraf Khalil and the faculty members Dr. Ala-aldin Alkilany, Dr. Abdelbary Elhissi, Dr. Hesham Korashy, Dr. Zaid Alma'ayah, Dr. Ousama Rachid, Dr. Anis Dou, Dr. Abdelali, Dr. Hassan Rathore, for their support, encouragement, and kindness.

I06 faculty: Dr. Wisam - Ms. Jensa, Ms. Aarti - Ms. Badrya, Dr. Noora Al- Zaidan.

CLU Team: Dr. Mohammad Ibrahim - Dr. Ahmed Easa. – Ms. Muneera Al-qahtani – Dr. Essam – Dr. Sherin Ahmed – Mr. Mohammed Akbik – Mr. Nandagopal – Mr. Anzar – Mr. Jassim.

BCR Team: Mr. Mohammed Jaber – Dr. Siham Alqaradawy - Dr. Yahia Hussein Shoeb – Dr. Kifah Saleh **H10 Research complex team**: Mr. Hamood Alsaadi – Ms Thuraya Alyafei – Mr. Ahmed. **I06 colleagues**: Sourour Idoudi - Mahmoud Alruwaidi - Arij Hassan - Tahseen Sayed - Areej Alhams - Nindya – Heba Iqbal - Azza Sulaiman – Hadeel – Shadya - Diya – Security: Manal, Nafeesa, Doaa, Rose, Razni, Dolvin and all – janitors for maintaining healthy and clean work environment.

TABLE OF CONTENTS

DEDICATION iv

ACKNOWLEDGMENTS v

LIST OF TABLES x

LIST OF FIGURES xi

LIST OF ABBREVIATIONS xiii

CHAPTER I: INTRODUCTION 1

1.1 Colon cancer (CoC) and Colorectal cancer (CoRC): Overview: 1

1.1.1 Anatomy and histology of colon 2

1.1.2 Pathophysiology and Stages 5

1.1.3 Treatment modalities and constraints 8

1.2 Nanotechnology in cancer treatment: 11

1.2.1 Nanoparticles preparation and parameters optimization: 13

1.2.2 Factors affecting the stability of NPs: 14

1.3 Curcumin: 15

1.3.1 Physicochemical properties 16

1.3.2 Thermal and photo stability 18

1.3.3 Effect on colon cancer 20

1.3.4 Limitations of pure curcumin use 23

1.3.5 Methods to improve curcumin solubility/bioavailability: 24

1.4 Chitosan (Ct): 28

1.4.1 Physical and chemical properties of Ct 29

1.4.2 Degree of deacetylation (DD) 30

1.4.3 Molecular weight (Mw) and methods of chitosan depolymerization 31
1.4.4 Effect of Microwave depolymerization on chitosan 33
1.4.5 Proposed mechanisms by which microwave depolymerizes Ct 41
1.5 Research gaps and study rationale 42
1.6 Aims of research 43
CHAPTER II: MATERIALS AND METHODOLOGY 45
2.1 Materials 45
2.2 Microwave treatment of Ct: 45
2.3 Conjugation of CURC to Ct 46
2.3.1 Scheme 1: Microwave assisted conjugation of CURC to Ct (134): 47
2.3.2 Scheme 2: Conjugation of CURC to Ct using poly(ethylene-alt-maleic anhydride) PEAMA as a crosslinker: 47
2.3.3 Scheme 3: Conjugation by Schiff base formation between CURC and Ct 48
2.4 Preparation of Ct and CURC-Ct conjugate nanoparticles (CCC NPs) 49
2.5 Physical characterization of the microwave treated Ct and CCC 50
2.5.1 UV-Vis spectra of microwave treated and untreated Ct 50
2.5.2 Ascertaining the presence of relevant chemical moieties in Ct after microwave treatment 50
2.5.3 Assessment of the crystalline nature of Ct after microwave treatment 50
2.5.4 Carbon-nitrogen (CN) elemental analyses 51
2.5.5 Flow time (viscosity) of microwave treated and untreated Ct 51
2.5.6 Thermal profile of microwave treated and untreated Ct 52
2.5.7 Solubility studies of microwave treated Ct 51
2.5.8 Percent yield and drug loading capacity 52

2.5.9 CURC quantification by high-performance liquid chromatography (HPLC) 53
2.5.10 Solubility and stability studies on CCC in different pHs of CCC: 53
2.6 Physical properties of nanoparticles 53
2.6.1 Size and zeta potential analysis.....53
2.6.2 Morphological studies using Atomic Force Microscopy (AFM) and Transmission electron microscopy (TEM).....54
2.6.3 Stability studies of Ct NPs 54
2.7 In vitro studies.....55
2.7.1 In vitro drug release studies 55
2.7.2 Cell thawing and incubation 55
2.7.3 Cell subculturing.....56
2.7.4 Cell counting using a hemocytometer.....56
2.7.5 Cell cytotoxicity using CCK8 assay 57
2.8 Statistical analyses 57
CHAPTER III: Results 59
3.1 Physicochemical Characterization of Microwave Treated Ct: 59
3.1.1 Characterization Using Ultraviolet-visible (UV-Vis) Spectroscopy 60
3.1.2 Characterization Using Fourier Transform Infrared (FTIR) Spectroscopy 61
3.1.3 Assessment of the crystalline nature of Ct after microwave treatment 62
3.1.4 Carbon-nitrogen (CN) elemental Analyses.....63
3.1.5 Flow time (viscosity) of microwave treated and untreated Ct.....64
3.1.6 Thermal profile of microwave treated and untreated Ct (DSC) 66
3.1.7 Solubility studies of microwave treated Ct.....67
3.2 Physicochemical Characterization of Chitosan-Curcumin Conjugates (CCC): 68

3.1.2 Characterization Using Fourier Transform Infrared (FTIR) Spectroscopy 68
3.2.2 X-Ray diffraction analysis (XRD) and assessment of the crystalline nature.....69
3.2.3 Thermal profiles and differential scanning calorimetry (DSC) 71
3.2.4 Carbon-nitrogen (CN) elemental Analyses.....72
3.2.5 Percent yield and drug loading efficiency 73
3.2.6 Solubility and stability studies of CCC in different solvents and pHs: 74
3.3 Physicochemical Characterization of Chitosan-Curcumin Conjugates Nanoparticles (CCC NPs): 76
3.3.1 Size, polydispersity (PDI) and zeta potential (ZP) analysis 76
3.3.2 Morphological studies using Atomic Force Microscopy (AFM) and Transmission electron microscopy (TEM) 78
3.3.3 Stability studies on Ct and CCC NPs.....80
3.4 In vitro Studies 82
3.4.1 In vitro drug release studies: 82
3.4.2 In vitro cytotoxicity assay: 83
CHAPTER IV: Discussion 86
CHAPTER IV: Conclusion and future work 96
References: 98

LIST OF TABLES

Table 1.1: Chitosan available Mw ranges. Adaptd from (113).....31

Table 1.2: Summary of the physicochemical modifications on Ct by microwave treatment. Table adapted from my review Paper (130) 36

Table 2.1: Optimization of microwave treatment conditions 46

Table 2.2: Nanoparticles optimization trials:.....49

Table 3.1: Elemental analysis of control and microwave treated Ct 64

Table 3.2: Flow time (Viscosity) of control and microwave treated chitosan.....65

Table 3.3: Carbon nitrogen elemental analysis of Control Ct, CURC and CCC.....73

Table 3.4: NPs optimization trials results:.....77

Table 3.5: Zeta potential of of Control Ct & CCC at RT (A) and 4°C (B), and 300W Ct & CCC at RT (C) and 4°C (D).....82

LIST OF FIGURES

Figure 1.1:Anatomy, mucosa and musculature of the large intestine. 3

Figure 1.2: composition of the colon layers. 5

Figure 1.3: Stages of colon cancer. 8

Figure 1.4: Schematic representation of ionic gelation method using STPP as a crosslinker and chitosan as a polymeric drug carrier. 14

Figure 1.5: Chemical structure, bioactivity and health benefits of curcumin. 15

Figure 1.6: Keto enol form of CURC. From (66) 16

Figure 1.7: Curcumin color changes in different pHs. 17

Figure 1.8: Chemical structure of CURC (A) DMC (B) and BDMC. 18

Figure 1.9: Compounds of thermal degradation of CURC. 19

Figure 1.10: Cancers against which curcumin has a prevention / treatment potential. 21

Figure 1.11: Curcumin mechanism of action against CoC. Adapted from (76). 23

Figure 1.12: methods of improving CURC properties 25

Figure 1.13: Chitosan chemical structure. 29

Figure 1.14: Illustration of the modes of the cellular uptake of chitosan particles. 31

Figure 1.15: Microwave irradiation impat on Ct NPs molecular size, Mw, and polydispersity. 35

Figure 1.16: Illustration of microwave mechanism in chitosan depolymerization 42

Figure 2.1: Schematic of Ct depolymerization via microwave irradiation 46

Figure 2.2: Schematic illustration of the developed CURC-Ct conjugation process. 48

Figure 3.1: Graphical illustration of CCC NPs formulation 59

Figure 3.2: UV-Vis spectrum of control and microwave treated Ct 61

Figure 3.3: FTIR spectrum of control Ct and microwave treated Ct 62

Figure 3.4: X-Ray diffraction analysis (XRD) patterns of control Ct and microwave treated Ct 63
Figure 3.5: Flow time (Viscosity) of control and microwave treated Ct. 65
Figure 3.6: differential scanning calorimetry (DSC) of microwave treated and untreated Ct. 67
Figure 3.7: A) Control and microwave Ct solubility intervals for 2h, and B) Solubility after 5 mins. 68
Figure 3.8: FTIR spectrum of Control Ct, CCC and CURC.....69
Figure 3.9: X-Ray diffraction patterns of Control Ct, CURC and CCC.....70
Figure 3.10: differential scanning calorimetry (DSC) of Control Ct, CURC and CCC 72
Figure 3.11: Calibration curves of different CURC concentrations (in mg/ml) using HPLC. 74
Figure 3.12: Trial of different solvents A) HAc 1%, B) Ethanol, and C) distilled water to dissolve CCC at a concentration of 1 mg/ml. 75
Figure 3.13: Stability of CCC at different pHs: A) 1.98, B) 12, and C) 6.5.....76
Figure 3.14: AFM analysis of the nanoparticles of A) Control Ct, B) 300W Ct, C) Control CCC, D) 300W CCC.....79
Figure 3.15: TEM Images of A) Control Ct, B) 300W Ct, C) Control CCC, D) 300W CCC.80
Figure 3.16: Changes in size and PDI of Control Ct & CCC at RT (A) and 4°C (B), and 300W Ct & CCC at RT (C) and 4°C (D) for days to 28. 81
Figure 3.17: In vitro profiles of CURC release from A) control CCC and B) 300W CCC over 96 hours at pH 6.7. 83
Figure 3.18: Cell viability of A) HCT-116 and B) LoVo cell lines treated after 48h. 85

LIST OF ABBREVIATIONS

5-FU: 5-fluorouracil

APC: Adenomatous polyposis coli

API: Active Pharmaceutical Ingredient

BDMC: bis-demethoxycurcumin

BRAF: v-raf murine sarcoma viral oncogene homolog B1

CCC NPs: Curcumin-chitosan conjugates nanoparticles

CCC: Curcumin-chitosan conjugates

CIMP: CpG island methylator phenotype

CIN: Chromosomal instability

CoC: Colon cancer

CoRC: Colorectal cancer

COX-2: Cyclooxygenase

CpG: Cytosine and guanine linked by phosphate group

Ct: Chitosan

CURC: Curcumin

DD: degree of deacetylation

DMC: demethoxycurcumin

DMSO: dimethyl sulfoxide

EMR: Endoscopic mucosal resection

ESD: Endoscopic submucosal dissection

FAP: Familial adenomatous polyposis

FBS: Fetal bovine serum

FTIR: Fourier Transform Infrared Spectroscopy

h MLH1: Human MutL homolog 1

HAc: acetic acid

HCl: hydrochloric acid

hPMS1: Human postmeiotic segregation1 gene

KRAS:

LMWC: low molecular weight chitosan

MLH1: MutL protein homolog 1

MSI: Microsatellite instability

MTT: 3-[4,5-dimethylthiazol-2-yl]-2,5 diphenyl tetrazolium bromide assay

MUTYH: MutY DNA Glycosylase

Mw: molecular weight

NPs: Nanoparticles

PBS: Phosphate buffered saline

PDI: polydispersity index

PLGA: Poly Lactide-Glycolide

PPAR: Peroxisome proliferator–activating receptor

RPMI: Roswell Park Memorial Institute

RT: room temperature

UV-Vis spectroscopy: Ultraviolet-visible spectroscopy

W: Watt

ZP: Zeta potential

CHAPTER I: INTRODUCTION

1.1 Colon cancer (CoC) and Colorectal cancer (CoRC): Overview:

The term colorectal cancer (CoRC) is a broader term used interchangeably with the term colon cancer (CoC) or rectal cancer, depending on the location of cancer manifestation. This is due to the fact that they present identical pathological features (1). CoRC is a prevalent malignancy that can affect the colon or rectum and can be fatal. In 2023, CoRC was ranked third among the most commonly diagnosed cancers, and ranked second among the deadliest cancers in both sexes worldwide (2, 3). CoRC predominantly occurs in individuals aged 50 years or older and accounts for 10% of all cancer cases (2). In the State of Qatar, there is an expected increase in gastrointestinal cancers burden by more than 50% by the year 2030, from 18 to 34 cases per hundred thousand people. A 28% mortality rate in CoRC was reported among Qatari patients as reported in the National Cancer Registry (4). Symptoms of CoRC are usually observed during the later stages of the disease and include constipation or diarrhea, abdominal pain, bloody stool, fatigue, unexplained weight loss and reduction in blood iron levels (2). Despite the sporadic nature of most CoRC cases, crude estimates indicate that more than 20% of all cases are due to genetic predispositions, where the incidence of CoRC in two or more first degree relatives is observed (5). The occurrence of CoRC can be due to two main types of risk factors, modifiable and unmodifiable. Factors such as personal demographics, medical history and family history are unmodifiable, whilst lifestyle and personal habits are within the realm of modifiable risk factors. Personal demographics and medical history include the sex, race, age, history of diseases such as inflammatory bowel disease (IBD), adenomatous polyps, Lynch syndrome, Crohn's diseases or ulcerative colitis for eight years or above (5, 6). Most CoRCs were found to develop in patients aged 50 years old and above, with males being more susceptible than females, at average ages of 68 and 72 years old in men and women, respectively (6). Family history is

associated with early-onset CoRC, and the risk is highest in individuals with a first-degree relative diagnosed with the disease (6). Diet and lifestyle are examples of modifiable risk factors that may contribute to developing the disease. Physical inactivity, high body mass index (BMI), regular alcohol consumption, cigarette smoking, consumption of red or processed meat are all within the modifiable risk factors that were reported to be associated with elevated CoRC risk (6, 7).

1.1.1 Anatomy and histology of colon

1.1.1.1 Anatomy

The colon is a large hollow organ derived from hindguts and the primitive midguts (8). The hindgut in particular, evolves into the upper portion of the anal canal, the rectum, the sigmoid colon, the descending colon and the third distal transverse colon (9), whilst the midgut comprises of the proximal half of the transverse colon, the ascending colon, the cecum, the ileum, the jejunum and the distal half of the duodenum (10). The colon is a continuous structure extending from the ileocecal valve, where it originates, to the anus. The first part of the colon is the cecum, which is ovoid-shaped and located posteriorly at the right iliac fossa. The cecal cavity accounts for a generous proportion of the colon compared to other portions. The appendix originates in the cecum and appears as a blind-ending outpouching. The ascending part of the colon continues anteriorly and cephalad from the cecum to the hepatic flexure (just inferior to the liver) is called the ascending colon. After the ascending colon, comes the transverse colon, which travels distally from the hepatic flexure to the splenic flexure, then posteriorly until it reaches the sigmoid colon. The sigmoid colon has a narrow, tortuous, S-shaped peritoneal structure. Finally, following the sacral curve, the rectum arises at the peritoneal reflection and leads to the anal canal (Figure 1.1) (11). The pH of the colon changes noticeably throughout the different sections of the colon. It rises rapidly

from the stomach (highly acidic, 1.5 to 2) to a pH of around 6 in the duodenum. Then, it gradually starts increasing in the small intestine until it reaches around 7.4 in the terminal ileum. In the cecum region, the pH decreases to 5.7, while in the rectum region it increases to 6.7 (12).

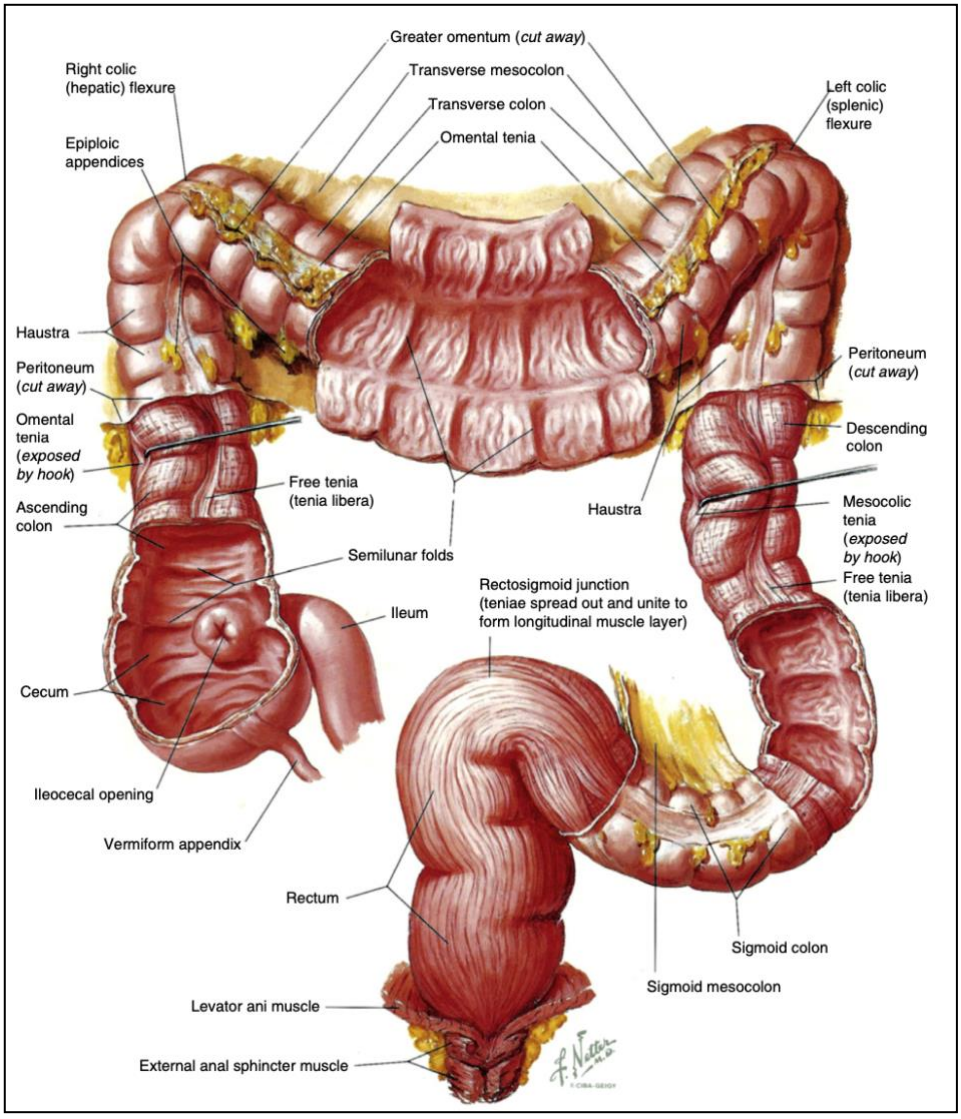

Figure 1.1:Anatomy, mucosa and musculature of the large intestine.

Adapted from (11).

1.1.1.2 Histology

The colon wall is divided cross-sectionally into four layers. The outermost part comprises of a monolayer of mesothelial cells called the serosa. Then the muscularis externa follows. These muscular layers comprise of an internal circular layer and an external longitudinal layer, and the Auerbach's (myenteric) plexus lies in between the two layers. The next is the submucosa, a layer comprising of a rich admixture of cells, connective tissues, fibroblasts, immune cells such as eosinophils, plasma cells, lymphocytes, macrophages and mast cells, as well as vascular tissues and lymphatics. The deeper submucosa is separated from the mucosa by a thin smooth muscle sheet called muscularis mucosa. Interior to this layer, the lamina propria runs. The lamina propria layer (part of the mucosa) comprises of connective tissues located underneath the epithelium, and is occupied by specialized immune cells such as IgA-secreting B lymphocytes, antigen presenting cells, and T lymphocytes. (11, 13). The luminal epithelium lines the lamina propria. The epithelium of the intestine comprises of a tight monolayer of cells that absorb liquids, nutrients, electrolytes and secretes mucus and fluids. The intestinal epithelium is also interspersed with numerous crypts that include enteroendocrine cells, epithelial precursor cells, Paneth cells, other undifferentiated and the mucin secreting goblet cells (Figure 1.2). However, charged species cannot traverse due to the hydrophobic lipid bilayer of the intestinal epithelium. Charged molecules may traverse the intestinal epithelium via carrier proteins, protein transporters and through narrow channels. Colonocytes have an average lifetime of three to six days (11).

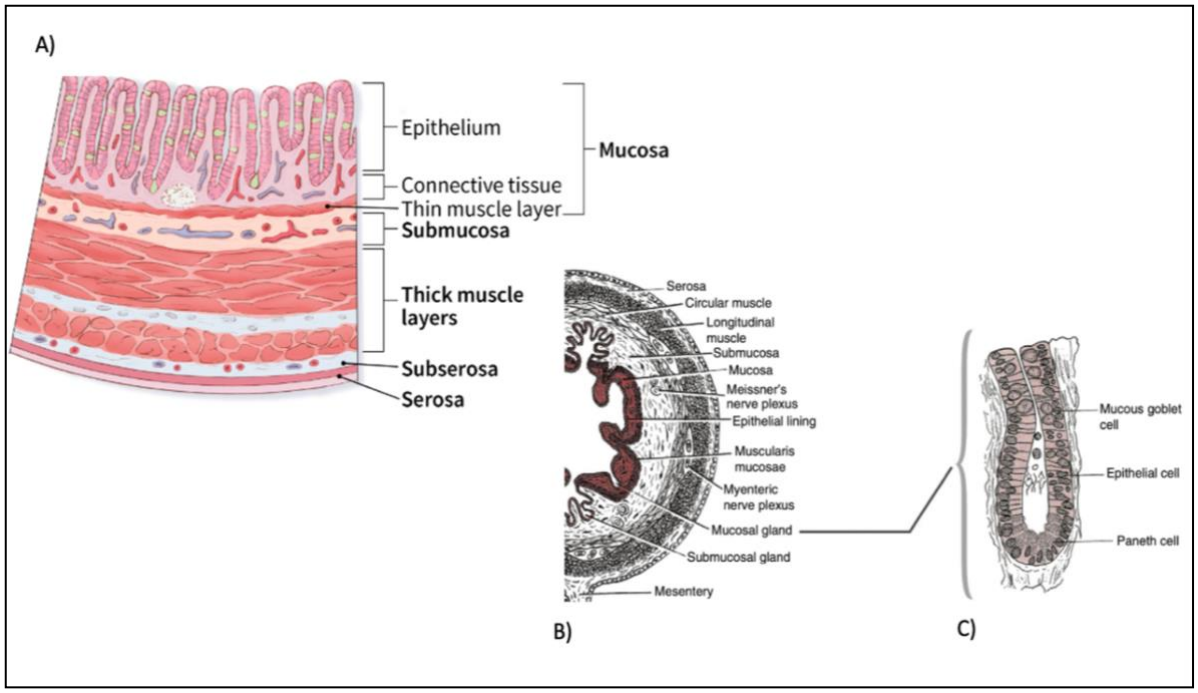

Figure 1.2: composition of the colon layers.
Adapted from (1) and (11).

1.1.2 Pathophysiology and Stages

1.1.2.1 Pathophysiology

Location wise, the most frequent colon site affected with CoC is the sigmoid colon (55%). Comes after that the ascending colon, transverse colon, descending colon, and the cecum at 23.3%, 8.5%, 8.1% and 8.0%, respectively (14). CoRC originates as adenomatous polyps, which are benign growths with the potential of maturing into cancer cells. The most common type of polyps with potential of developing into cancer is the adenomatous polyps, whilst current evidence shows that other polyps such as serrated and hamartomatous polyps could also lead to CoRC (3, 15). These polyps can progressively grow into the rectum or colon wall. As described in section 1.1.1, the colon comprises of multiple layers that differ in terms of anatomy and physiology. CoRC hence initiates in the mucosa, the innermost layer of the colon, and subsequently, expands outward to the deeper layers (Figure 1.2) (1). The transformation of normal colonic epithelium into an adenoma (precancerous lesion) and eventually to an invasive carcinoma is predisposed by accumulated genetic mutations that are

either germline (inherited) or somatic (acquired) (3). The pathophysiology of CoC suggests that clonal mutation evolution in the colon gives the advantage of cell survival-immortality to the affected cells, and hence, paves the way for further mutations with cancer hallmarks, rendering them capable of proliferation invasion and metastasis (16). The process of CoRC development usually takes 10-15 years of acquired dysplastic changes of the polyp to ultimately develop into invasive carcinoma (3, 17).

CoRC is mainly linked to three molecular pathways, which are mismatch repair, chromosomal instability and hypermethylation. Deficiency of DNA mismatch repair (dMMR) can make cells unable to repair errors within the genome, leading to accumulation of genetic errors. This accumulation leads to an increased level of microsatellite instability (MSI-H). MSI, in turn, has correlation with the mutations in genes responsible for the replication or repair of the DNA, and is a hallmark of the inherited type of cancer Lynch Syndrome (also known as hereditary non-polyposis colorectal cancer (HNPCC) (3, 18, 19). The chromosomal instability is represented by the possession of mutations that cause imbalances in the equilibrium of tumor suppressors and oncogenes. One example is the mutations seen in the adenomatous polyposis coli (APC) genes, which are inherited tumor suppressor genes secondary to autosomal dominant pattern (20). APC is a feature of the classic familial adenomatous polyposis (FAP) (3). On the other hand, CpG hypermethylation of the DNA can contribute to the silencing or activation of specific genes such as MLH1 and BRAF, respectively. Other mutations implicated in CoRC include RAS mutations, which were found with the most clinical relevance and in half of CoRC sporadic cases. It is also noteworthy that 15% of sporadic CoRC cases leading to Lynch-like syndrome with MSI-H were found to be related to MMR genes mutations that can arise in hPMS1, hPMS2, hMSH2, hMLH1, hMLH3 and hMSH6, hMLH3 genes. Mutations in MutY DNA Glycosylase (MUTYH) repair genes can also lead to autosomal recessive FAP. The defects in this gene

have a recessive inheritance pattern that requires conjunction with mutations in APC gene or bi-allelic second hit. Reports have also indicated the implication of PPAR and COX-2 in the carcinogenesis of CoRC, and they are currently under investigation (3).

1.1.2.2 Stages

CoC has four stages of development similar to other cancers, including : initiation, promotion, progression, and metastasis. Another categorizion is stage 0 (In situ carcinoma), stage I, stage II, stage III and stage IV (21). The stages of CoC cancer initiate with the hyperproliferation of epithelial cells, secondary to a series of epigenetic or genetic aberrations (22). Cells start to grow rapidly leading to the formation of a benign adenoma, which advances later to a cancerous tumor and further metastasize to other body organs through certain pathways (Figure 1.3). These pathways include microsatellite instability (MSI), serrated neoplasia, and chromosomal instability (CIN, followed by the majority of CoRC cases) (6, 23). Cancer progression is described by the term adenoma-carcinoma, as it begins as an amiable small adenoma, that continues to grow with time into a gigantic adenoma, and eventually, cancer (6). MSI-high status, CpG island methylator phenotype (CIMP)-positive (an inflammation pathway), and CIN, are the molecular aberrations that are involved during tumorigenesis of CoRC and found in 15%, 20% and 85% of sporadic CoRC cases, respectively (24). Tumorigenesis mostly starts with a normal cell developing into a hyperplastic polyp, then sessile serrated adenomas, and ending up with cancer. This pathway is also responsible for developing (CIMP)-high subtype, which is an inflammation developing route. After inflammation is initiated, the prolonged inflammation with time will lead to the development of indeterminate dysplasia cells, which will progress to low grade and then high grade dysplasia, and eventually, develop cancer. The moment an adenocarcinoma turns invasive, cancerous cells become capable of spreading via lymphatic

system or blood to other body organs and become metastatic. Common metastatic sites of CoRC are the liver (most common), followed by the lung and the bone (6).

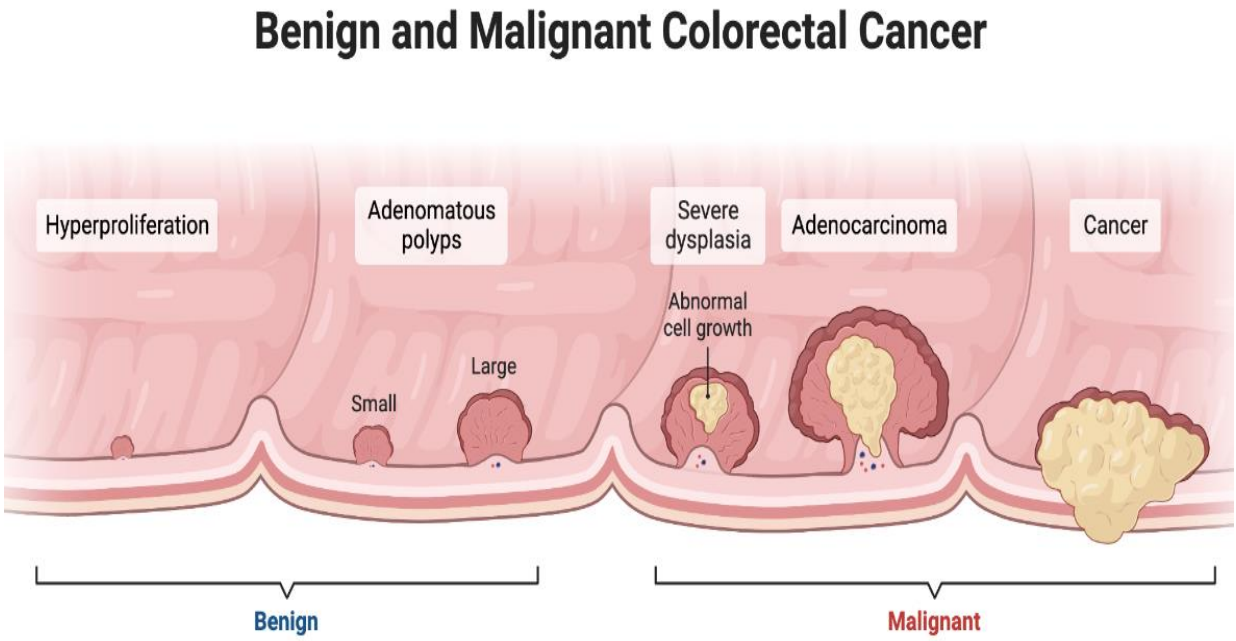

Figure 1.3: Stages of colon cancer.

1.1.3 Treatment modalities and constraints

Consistent endeavors have been aimed at eradicating or attenuating the threat of CoC worldwide. The mainstay of CoC treatment remains as surgery-based comprehensive treatments for patients with non-metastatic localized stage, optimized comorbidities and acceptable performance status, regardless of their age (3). CoC in early stages can be treated with the resection of tumor through trans-anal endoscopic microsurgery. This procedure has the advantage of preserving organ function and reducing surgical complications (25). Reduction in tumor stage, distant metastasis occurrence and local recurrence, as well as prolonged survival and improved quality of life was reported in patients receiving neoadjuvant chemotherapy or radiotherapy before surgery (26, 27). More advanced stages

might require palliative tumor excision when removal of all oncologic tumors is no longer possible. Stent insertion, or removal of metastasized tumors can also ameliorate clinical symptoms in patients. Although immunotherapy has emerged recently, it is now the fourth most popular CoC treatment of choice (25).

1.1.3.1 Endoscopic resection:

Endoscopy, or more specifically, colonoscopy can be a vital tool in the diagnosis and treatment of CoC and its precursors at early stages. The procedure utilizes endoscopy/colonoscopy to locate and perform local tumor excisions for the cancer confined in the mucosa (endoscopic mucosal resection (EMR)), or in the superficial submucosa (endoscopic submucosal dissection (ESD)) (3, 28). This procedure has a high success and low recurrence rates (90.3% and 13.8%, respectively), owing to the fact that cancer is treated at early stages. However, it remains an invasive procedure, that is inconvenient to patient and associated with the complications of bleeding and perforations (3).

1.1.3.2 Surgical resection:

The preferred modality is either laparoscopic colectomy, which should be performed by experienced and high-profile surgeons, or the conventional open colectomy. The procedure is usually done with the goal of complete tumor removal, as it is considered the only curative treatment by far for localized CoC (stage I disease). However, for patients with advanced stages, the 5-year survival estimate decreases with surgery alone, requiring adjuvant therapy (3). The surgical resection involves the removal of the tumor, the lymphatic drainage basin (at least twelve or more lymph nodes), and the vascular ligation of major vascular pedicles (3, 29). Internal bypass procedures, primary anastomosis, and diverting colostomy are examples of other potential palliative surgical procedures in case of

unresectable CoC (3). Although colorectal surgeries can be useful means in eradicating CoC, they are still invasive techniques and associated with several concerns such as increased costs, prolonged operative durations, and increased complications rates (30).

1.1.3.3 radiotherapy:

Radiotherapy utilizes high energy radiation (x-rays) to destroy cancerous cells, causing cells to undergo mitotic catastrophe and hence impede or prohibit their growth and multiplication (31). This approach can be used for both primary and advanced tumors, alone, or adjuvant to other treatments. It also assists in shrinking tumor size to facilitate excision, reducing pain and discomfort, and relieving other symptoms (32). Despite its potential usefulness in CoC, adjuvant radiotherapy is generally not recommended due to distant spread patterns and difficulty remotely targeting cancer tissue, as well as the limited provision of tumoricidal dose to that avoids affecting proximal tissue (33).

1.1.3.4 systemic therapy

Chemotherapy

Chemotherapy in CoC treatment is either pre-operative (neoadjuvant) or post-operative (adjuvant chemotherapy). Treatment should be individualized based on the patient characteristics. However, the standard of care treatment for patients with advanced stage III CoC is a combination of oxaliplatin-based or fluoropyrimidine-based chemotherapy, mainly CAPOX (capecitabine and oxaliplatin) or FOLFOX (fluorouracil, oxaliplatin, and leucovorin) regimens (34, 35). According to the American Society of Colon and Rectal Surgeons, neoadjuvant CoC therapy is recommended in cases of locally advanced or unresectable CoC with liver metastasis, whereby, shrinkage of size of the tumor is done to facilitate subsequent surgical excision. Adjuvant CoC therapy in general is recommended to

be initiated within eight weeks of surgical resection (32). The usual duration of therapy is six months, but can be lowered to 3 months based on the regimen and other patient's factors, including risk of recurrence. The shorter duration has the advantage of posing lower cumulative toxicity risk (e.g. sensitive neuropathy) (34). Although chemotherapy is still considered the foundation stone for the treatment of advanced cancer stages, it has the disadvantages of its high costs, toxicity, inconvenience, and in some cases, fatal side effects, which encompass gastrointestinal toxicity, neuropathy, leukopenia, and increase in all-cause mortality (36).

Biologic agents and monoclonal antibodies (mAbs):

The establishment of mAbs and biologic agents has enhanced systemic anticancer therapy. These agents are approved for the treatment of metastatic CoRC and can target proteins and molecular abnormalities involved in cancer progression and angiogenesis, such as the epidermal growth factor and vascular endothelial growth factors (37). Prolonged and improved overall survival rates have been observed with the use of of mAbs (e.g. bevacizumab and ziv-aflibercept) in combination with CoRC chemotherapy. Other mAbs (e.g. panitumumab) have been designed to specifically target mutations such as KRAS and NRAS wild-type mutations, which are associated with poor CoC prognosis, to further ameliorate the efficacy of chemotherapy (38). Despite the merits of mAbs, their exquisite specificity, and fewer side effects compared to conventional chemotherapy, they are associated with some limitations. These include the price, induction of human immune response, which can lead to the prompt elimination and reduced targeting capabilities of the drug, as well as the dependance of treatment efficacy on the molecular heterogeneity of the tumor, the affinity of antibody, the accessibility and metabolism of antigens (37).

1.2 Nanotechnology in cancer treatment:

In the last few decades, nanotechnology has earned a great deal of attention as a formidable tool in the fabrication of nanoparticulate (NP) drug delivery system for therapeutic agents, in both pharmaceutical and biomedical fields. Especially, biodegradable polymeric nanoparticles, utilizing polymers such as chitosan, carrageenan and alginate, because they are non-toxic, fully biodegradable, and have the capability of deploying targeted antitumor agents by virtue of the small hydrodynamic diameter they can be constructed into (39, 40). The small diameter of nanoparticles and propensity for phagocytosis by epithelia favors their permeability through tumor vasculature and subsequent accumulation in tumor. This is because tumor vessels are immature, with poor smooth muscle cells content, anomalous basement membrane, disjointed endothelial cell lining, and impaired blood flow. All these characteristics lead to disturbances in osmotic equilibrium, resulting in elevated interstitial fluid pressure and accumulated vascular contents, which eventually leads to impaired blood flow and leakiness (41). Overall, these abnormalities grant the NPs their exceptional enhanced permeability and retention effect (EPR effect), which allows them to passively target solid tumors, and hence, accumulate within tumor area and thus, have reduced systemic drug toxicity (39, 42). NPs additionally have the ability to improve drugs utility and display controlled drug release patterns, due to their prolonged circulation time (43). Furthermore, various biological phenomena such as clearance patterns, extravasation through vessels, and half-lives are driven by the size of the NPs, which necessitates careful optimization of NP size to ensure optimal passive tumor targeting (42). As previously reported, the recommended hydrodynamic diameter for optimal passive tumor targeting is 100-400 nm. In other resources, it is 50-300 nm (44, 45). This is because NPs need to be large enough to circumvent prompt leakage into blood capillaries, but also sufficiently small to avoid being capture by macrophages (39, 42).

1.2.1 Nanoparticles preparation and parameters optimization:

Methods of preparing polymeric nanoparticles include ionic gelation, de-solvation, nanoprecipitation, dialysis, salting out, solvent evaporation, supercritical fluid, emulsification, solvent diffusion, microemulsion, and spray drying (39, 46). One of the most common and convenient method, especially for polymeric materials is ionic gelation, a chemical method firstly discovered in 1997 by Calvo and co-workers (47). This method requires an aqueous media and different counterions pairs and utilizes the interaction between the different charges of ions to generate electrostatic forces. For instance, the positively charge amino groups in chitosan can interact and cross link in the presence of the negatively charged polyanion, such sodium tripolyphosphate (STPP). With constant stirring of the mixture and in certain concentration ranges, these electrostatic forces lead to the self-assembly of particles into either nanoparticles or microparticles depending on several parameters and factors (Figure 4) (39, 48). The factors affecting the size of the nanoparticles should be optimized based on the desired size and future application of the NPs. The parameters that can be modified for this purpose include the ratios and concentrations of initial components, pH of the media, time and speed of stirring, rate of STPP addition, and time of reaction (49). Examples of polymeric species that can be used in the same method include alginate, fibrin, gellan gum, hyaluronic acid, gelatin, collagen, dextran, carboxymethyl cellulose and pectin (50).

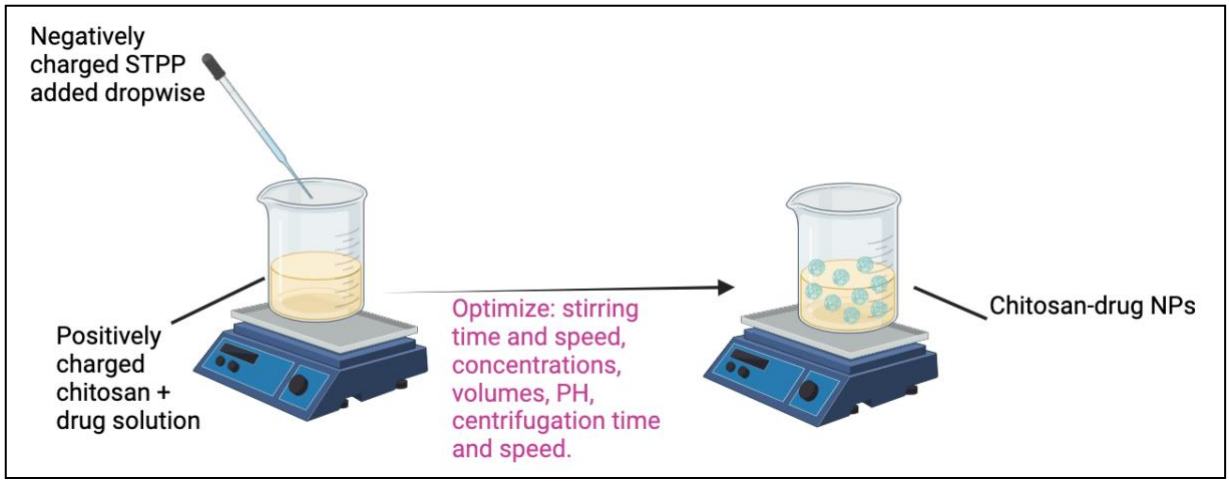

Figure 1.4: Schematic representation of ionic gelation method using STPP as a crosslinker and chitosan as a polymeric drug carrier.

1.2.2 Factors affecting the stability of NPs:

Ionic gelation method can produce NPs in aqueous dispersions, that can also be dried to powder. The stability of NP relies on several aspects such as solution pH, electrostatic charge of surface, ionic strength, concentrations of reagents, ratio of the anionic–cationic species. To improve the stability of the size and zeta potential for long-term storage, some techniques such the use of freeze-drying or nonionic stabilizers are recommended. However, drug or polymer resistance to freeze-drying should be taken into consideration and it may require the use of cryoprotectants to retain the surface charge of the NP (51). The storage temperature of 4°C is recommended over room temperature in case of polymeric NPs in dispersions. This is due to the fact that some polymers possess thermo-responsive properties and can hence exhibit pH variation at 25°C. This variation can result in a reduced stability and loss of polymer properties, e.g. antibacterial effect. If NPs are stored in powder form, additional caution should be allocated to environmental humidity (50). This can be minimized by optimizing the storage conditions and temperature, using moisture proof packaging and adjusting the formulation using appropriate stabilizers.

1.3 Curcumin:

As discussed in section 2.3, chemotherapy offers a rational approach to treating colon cancer, but the side effects associated with these agents have to be contended with by the patient. Consequently, there is a growing interest in the utilization of anticancer agents that manifest lesser side effects and yet potent. For example, curcumin has been found to possess anti-cancer properties. Curcumin is extracted from the rhizome of the condiment turmeric (Curcuma longa), from the family Zingiberaceae first by Vogel and Pelletier in 1842 (52, 53, 54). Turmeric since time immemorial has been well-known for its culinary (as a spice) and medicinal (as a pharmaceutical agent) advantages (55). In the last few decades, it has gained attention due to its exceptional biomedical features, which include anticancer (56), antimicrobial (57), antioxidant and anti-inflammatory properties (58). In addition it contributes in alleviating arthritis, metabolic syndromes, hyperlipidemia, and anxiety (52). All these features, together with its non-toxic nature made it a promising active pharmaceutical ingredient, especially in cancer treatment (59, 60).

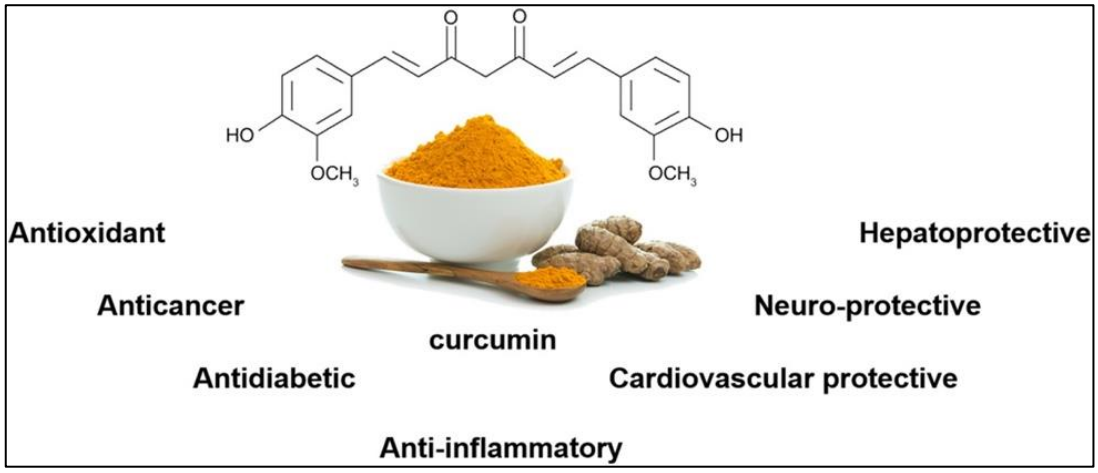

Figure 1.5: Chemical structure, bioactivity and health benefits of curcumin.
From: (61)

1.3.1 Physicochemical properties

Curcumin is present as orange-yellow needles, and was first described as a 'yellow coloring-matter' (53). Chemically, it is diferuloylmethane or (1,7-bis(4-hydroxy-3-methoxyphenyl)-1,6-heptadiene-3,5-dione) (52), with a chemical formula of $C_{21}H_{20}O_6$, molecular weight of 368.4 g/mol and a melting point of 356 to 361°F (62). It has two pk_a values: pk_a1=9.08 and pk_a2=-4.4 (63). Curcumin is very poorly soluble in water (0.00575 mg/mL) and acidic media, however, it is readily soluble in organic solvents like ethanol, dimethyl sulfoxide (DMSO), and acetone (63, 64). Depending on solution pH, CURC displays keto-enol tautomerism. In neutral and acidic environment, keto-form (responsible for the antioxidant effect) predominates. On the other hand, in alkaline environment, CURC decomposes and the enol form becomes dominant. The enol form is less stable and prone to degradation, which favors the maintenance of CURC in its keto form (58, 65).

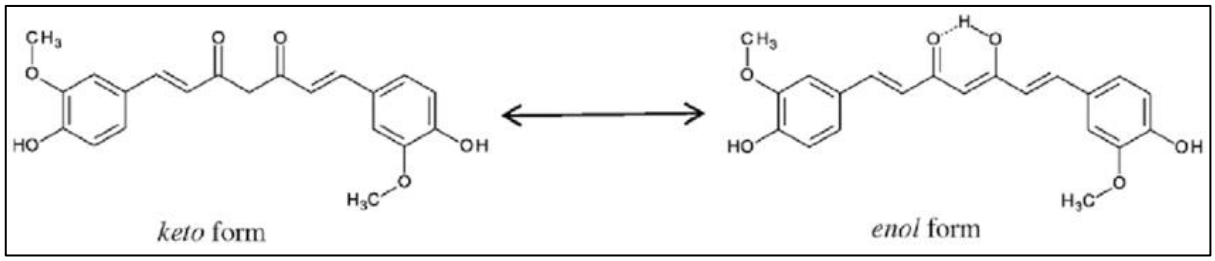

Figure 1.6: Keto enol form of CURC. From (66)

The aqueous stability of CURC is highly dependent on pH, as indicated by the changes in its color. In acidic media with a pH below 1, the color turns into red as an indication of the protonated state, while in a pH range of 1 to 7, the majority of CURC molecules are in neutral form and the solution remains yellow. At pH above 7.5, the color changes to orange red (58).

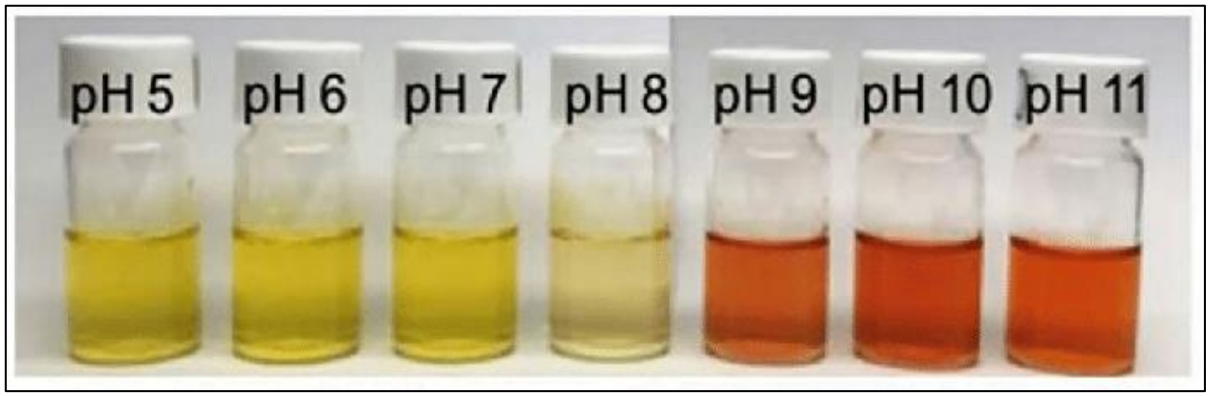

Figure 1.7: Curcumin color changes in different pHs.
From (67).

The bioactivities of turmeric are mainly confined to the three phenolic compounds, which are CURC, bisdemethoxycurcumin (BDMC), and demethoxycurcumin (DMC). These compounds are collectively named as curcuminoids, and are shown to be synergistic in the activity of turmeric (68). However, although it is reported that BDMC and DMC can have biological activities similar to or higher than CURC, CURC remains the most extensively studied curcuminoid and is considered the main constituent responsible for many of turmeric bioactivities, including cancer (69, 70). Figure 8 illustrates the three major curcuminoids of turmeric.

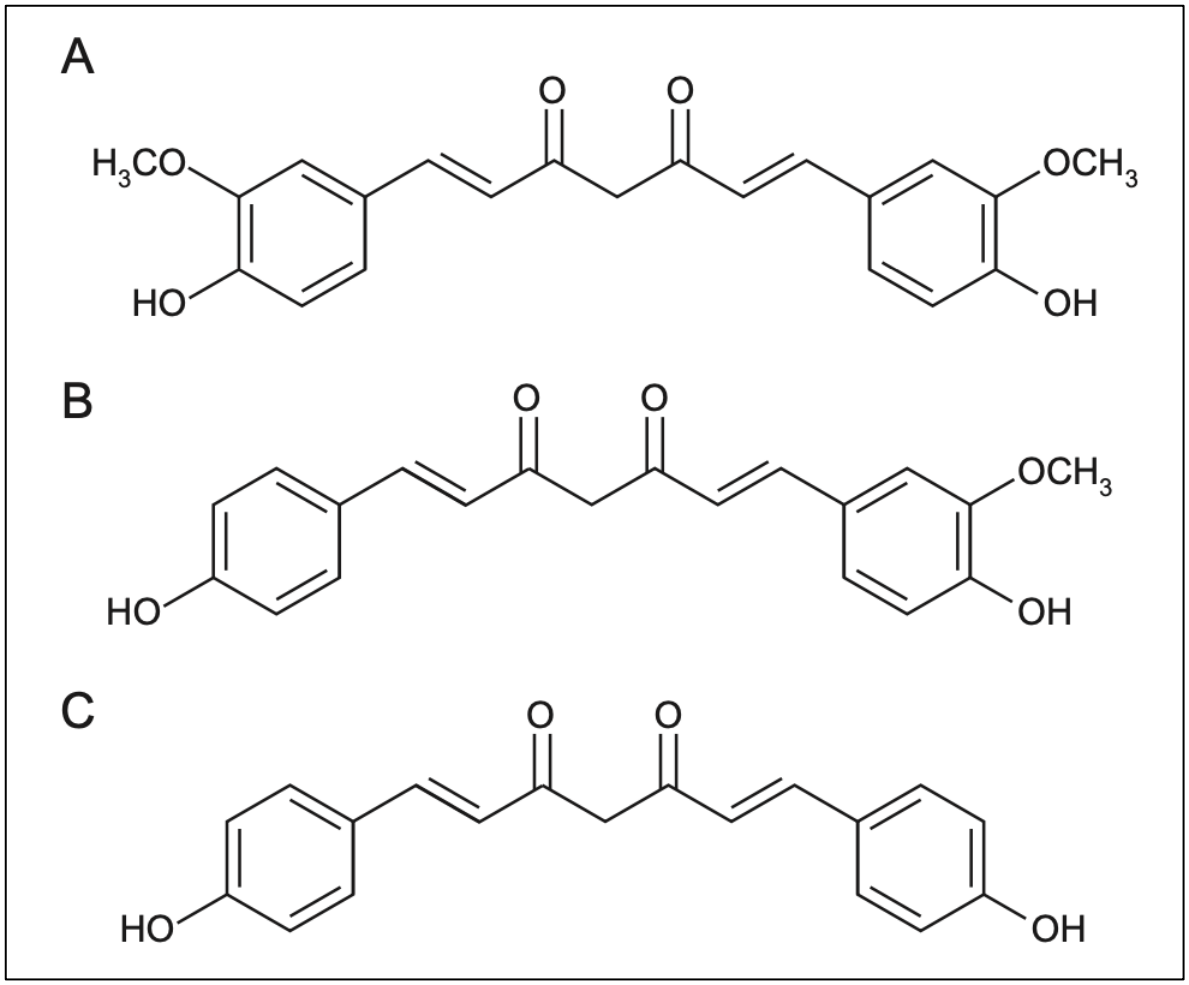

Figure 1.8: Chemical structure of CURC (A) DMC (B) and BDMC.
Adapted from (58)

1.3.2 Thermal and photo stability

In general, curcuminoids are considered heat stable, albeit this is depending on the degree of temperature to which they are exposed, and the heating duration. CURC remains stable up to 80 to 85°C (69, 71). Thereafter, (100°C), the vulnerability of β-diketone linkage in CURC to thermal degradation increases (Figure 9) (69). Generally, it is recommended to store CURC at lower temperatures to reduce the risk of decomposition and improve its physicochemical stability (72).

CURC photodegrades in sunlight, especially when dissolved in organic media (73). Methanolic or ethanolic CURC solutions showed CURC degradation when directly exposed to sunlight. The photodegradation of curcumin was found to be following first-order kinetics, and the reported resultant degradation products included p-hydroxybenzaldehyde, vanillin, p-hydroxybenzoic acid, ferulic aldehyde, ferulic acid, 4-vinylguaiacol, vanillic acid and feruloylmethane (58).

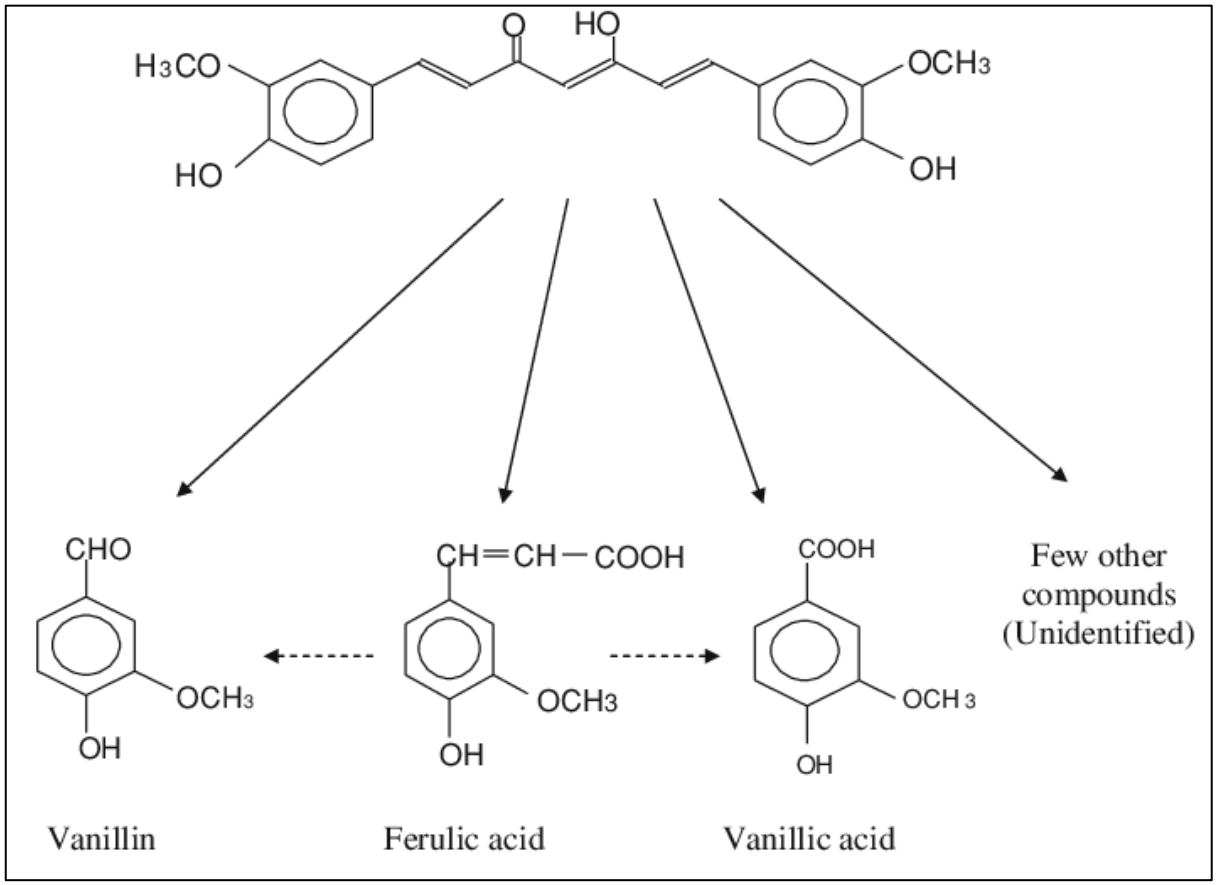

Figure 1.9: Compounds of thermal degradation of CURC.
Adapted from (74).

1.3.3 Effect on colon cancer

The anti CoC mechanism of CURC has been an area of intense investigation (75). It was reported to have a promising antitumor effect in a variety of cancers, such as breast, gastrointestinal, head & neck, genitourinary, thoracic, hematological, bone and brain tumors (Figure 10) (60). It scavenges oxygen species such as singlet oxygen, superoxide anions and hydroxyl radicals. It also inhibits peroxide-induced DNA damage as well as lipid peroxidation. Furthermore, through modulation of several signaling molecules, curcumin can mediate vigorous anti-carcinogenic and anti-inflammatory activities. For instance, it can suppress various signaling transduction pathways associated with the growth, progression and malignancy of tumors. Curcumin was also found to inhibit the expression of cyclooxygenase (COX)-2 enzymes, protein kinases, prostaglandin biosynthesis, and c-Jun/AP-1 activation in in-vitro studies (63).

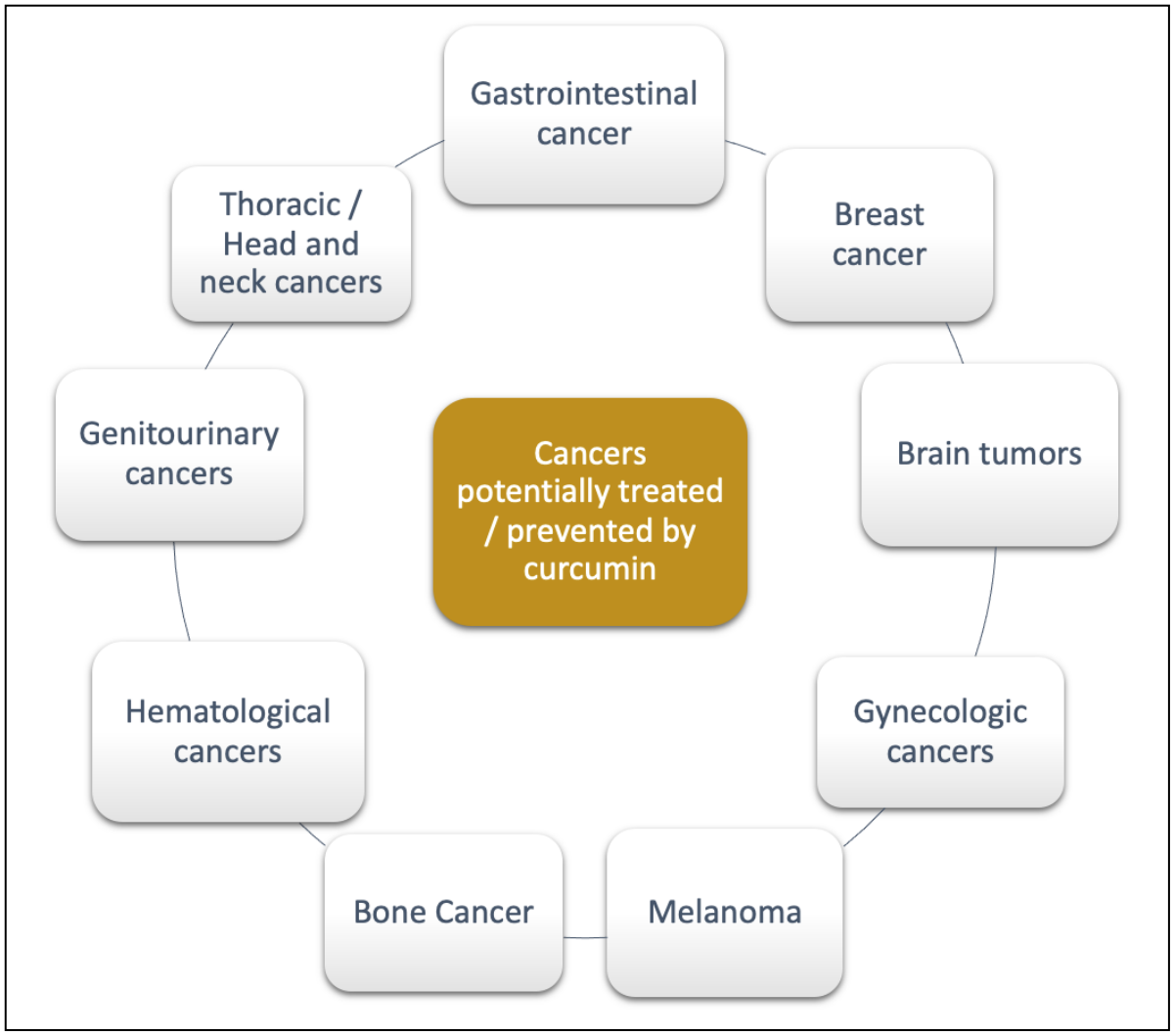

Figure 1.10: Cancers against which curcumin has a prevention / treatment potential.

The anti-CoC effect of curcumin is nowadays more evident by virtue of the numerous recent investigations. Some evidence suggest that there is a role of the transcriptional activity of constitutive nuclear factor-kappa B (NF-κB), p38 mitogen activated kinase (MAPK), as well as c-jun N-terminal kinase (JNK) in apoptosis (76). The exposure to a concentration of 35 μM of curcumin resulted in NF-κB inhibition, p38 activation and sustained JNK activation. This eventually lead to apoptosis in HCT116 colorectal carcinoma cell line (77), while in another study, the induction of 100 μM curcumin demonstrated an increase in ceramide generation (a messenger involved in the activation of apoptosis) (78). These findings imply that curcumin potentially induces apoptosis through the downstream

activation of JNK, production of reactive oxygen species (ROS), and the increase in ceramide generation to a lesser extent. This leads to the mitochondrial membranes lysis and induces oxidative reactions in the cancer cells (76, 79). In another in vitro study, curcumin anticancer activity was evaluated using colon cancer cell lines (HCT116 and SW480), whereby, DNA damage was detected in HCT cell lines when exposed to a concentration of 10 μM of curcumin. Authors attributed the damage to DNA double-strand breakage (80). HCT-116 cells along with human LoVo colorectal cancer cells showed accumulation in G2/M phase in the cell cycle, indicating cell cycle arrest and prevention of cells from going to the next cycle (76). In another in vitro study done on SW480 and SW620 colon cancer cell lines, curcumin activated caspases 3, 8 and 9 (81). It was also found that curcumin elevated the expression of DNA damage and growth arrest gene (GADD153). This gene is involved in the process of apoptosis, potentially by modulating protein kinase C (PKC) (76). Figure 11 summarizes other potential pathways by which curcumin acts against cancer.

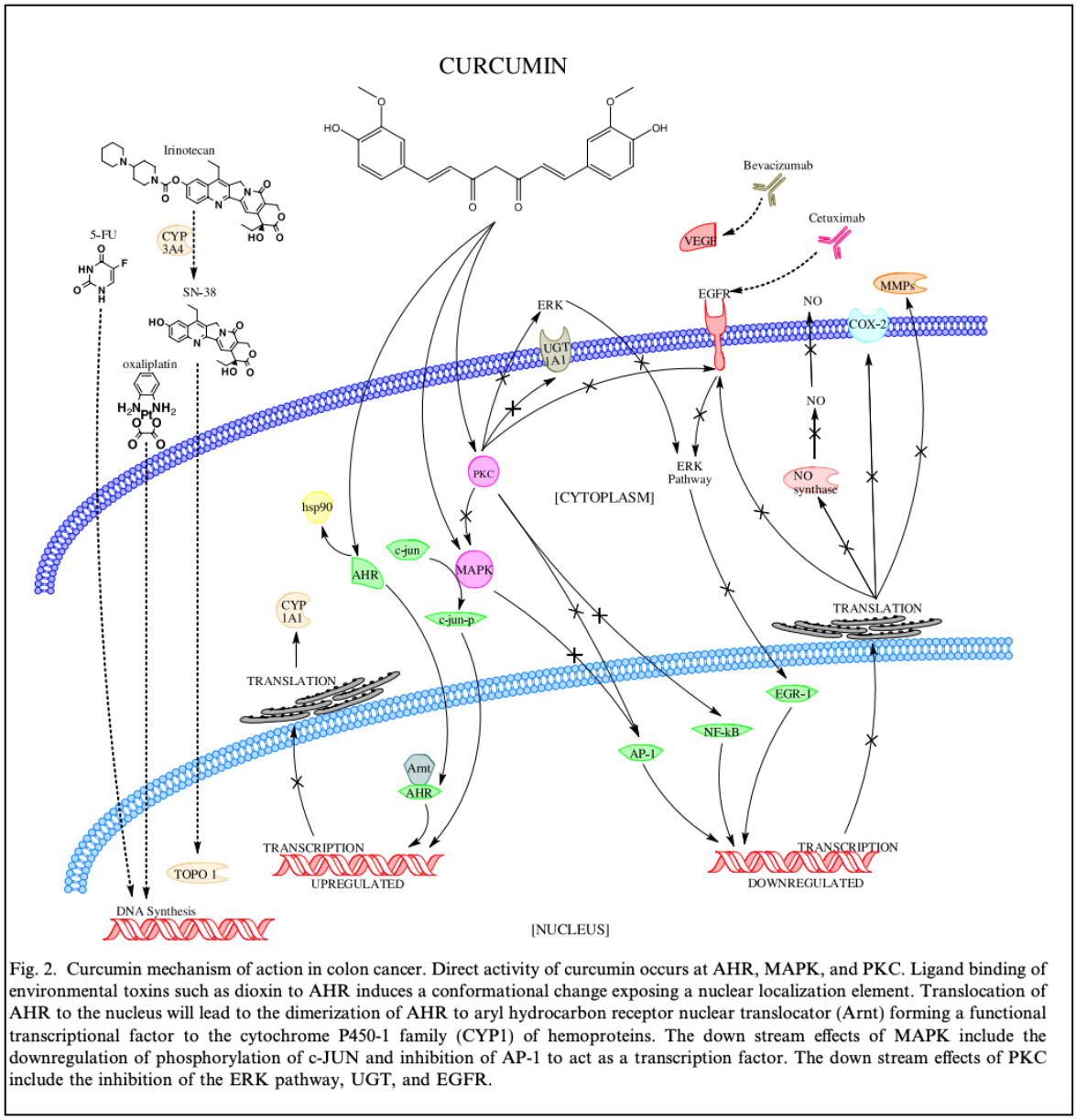

Fig. 2. Curcumin mechanism of action in colon cancer. Direct activity of curcumin occurs at AHR, MAPK, and PKC. Ligand binding of environmental toxins such as dioxin to AHR induces a conformational change exposing a nuclear localization element. Translocation of AHR to the nucleus will lead to the dimerization of AHR to aryl hydrocarbon receptor nuclear translocator (Arnt) forming a functional transcriptional factor to the cytochrome P450-1 family (CYP1) of hemoproteins. The down stream effects of MAPK include the downregulation of phosphorylation of c-JUN and inhibition of AP-1 to act as a transcription factor. The down stream effects of PKC include the inhibition of the ERK pathway, UGT, and EGFR.

Figure 1.11: Curcumin mechanism of action against CoC. Adapted from (76).

1.3.4 Limitations of pure curcumin use

Despite the verity of well-established anti-colon cancer properties attributable to curcumin, there remain several limitations hampering its effective use as an anticancer agent. One pivotal constraint is its very poor solubility in neutral or acidic aqueous media, as stated in section 1.3.1, with the high risk of decomposition in basic media, which renders curcumin less clinically effective (55). Although it shows better stability in acidic conditions at a pH lower than 7 (72), its low water solubility (~ 0.6 µg/mL) highly affects it bioavailability, with

a meagre approximately 60 nM serum level. Besides, its low bioavailability is also compounded by its hydrophobic nature of curcumin molecule, inactivation through liver metabolism, and the rapid elimination from the body (40, 43). The low stability of curcumin is considered another main issue restricting its efficient use (82). Curcumin is sensitive towards light and undergoes photodegradation especially when dissolved in an organic solvent (73).

1.3.5 Methods to improve curcumin solubility/bioavailability:

The huge potential held by curcumin in treating cancer has remained the motivation to several scientist who have dedicated their research in finding ways to modify the physicochemical properties of CURC towards achieving improved bioavailability and hence better anticancer treatment outcomes. Methods used to enhance the bioavailability of CURC include chemical or formulation methods. Chemical modifications of CURC into analogues capable of addressing the above constraints and additionally enhance its therapeutic propensity is one valid option. For instance, monocarbonyl analogs (namely, (1E, 4E)-1-(5-(2-methoxyphenoxy)-3-methyl-1-phenyl-1H-pyrazol-4-yl)-5-(3,4,5-trimethoxyphenyl)penta-1,4-dien-3-one and 1,5-bis(4-hydroxy-3-methoxyphenyl)-1,4-pentadiene-3-one) of CURC synthesized and tested against SW620 and SW620 human colon cancer cell lines displayed significant antiproliferative activity and remarkable selectivity in comparison to free CURC (83, 84). Formulation strategies include the formation of amorphous solid dispersions (ASD) of curcumin or encapsulation approaches. In ASD, the solubility of CURC is improved by the distortion of its crystalline domains using a suitable polymer or surfactant combinations, whereby, the bioactivity, bioavailability, and physicochemical properties of CURC are significantly improved. (84). Improvement of CURC solubility via encapsulation in suitable polymers appears to be more favored. In this regard, nanoformulations have proved

formidable in deploying encapsulated CURC in tumors. Other formulation methods include, complexation with water soluble polymers, formation of curcumin cocrystals or the formation of amorphous solid dispersions of curcumin (40). In the present research, my focus is on the adoption of polymeric nanoformulation methods, and typically ionic gelation of polymers into NPs.

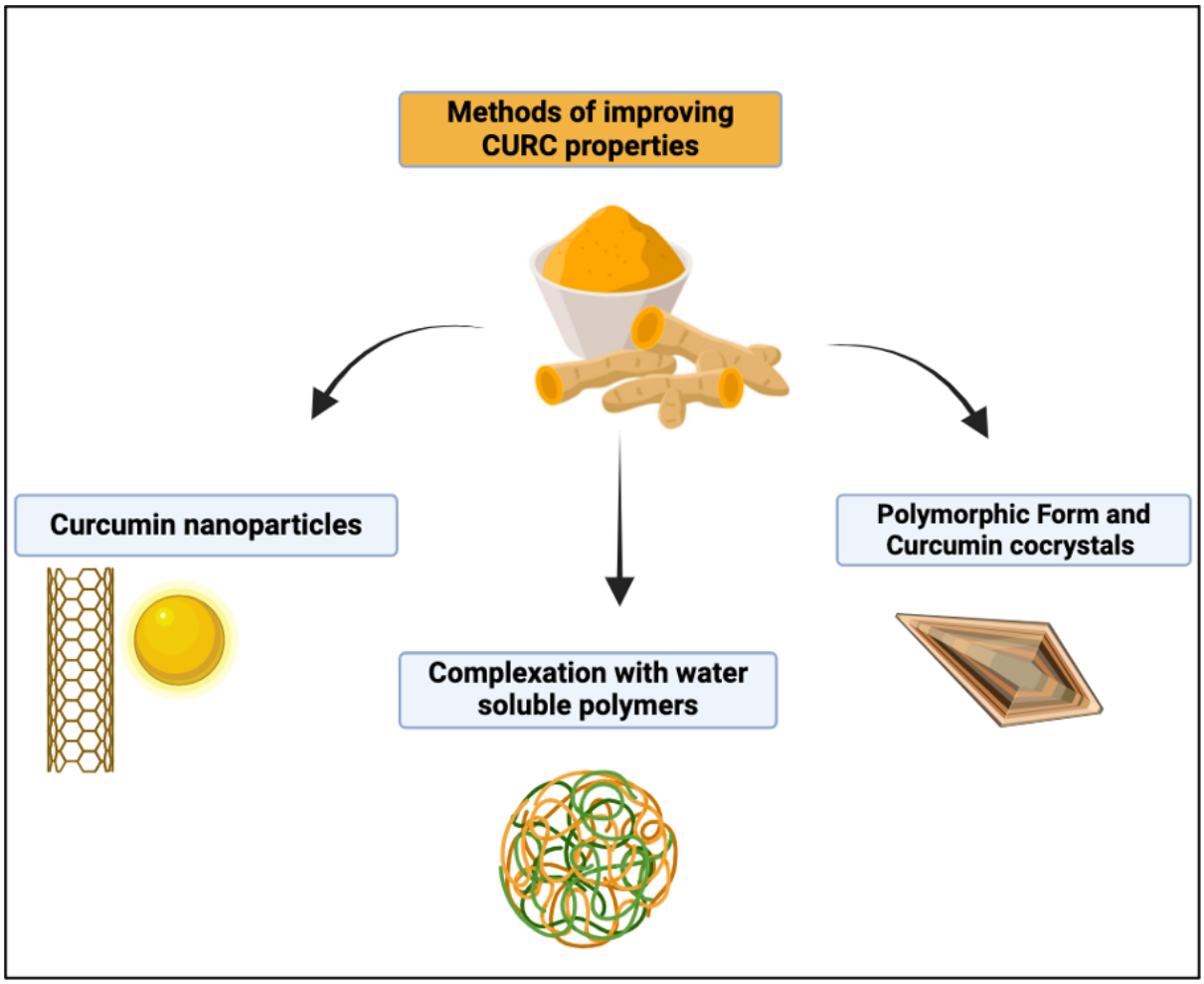

Figure 1.12: methods of improving CURC properties.

1.3.5.1 Co-crystallization of curcumin

One of the means to enhance the bioavailability of curcumin is by transforming it to CURC cocrystals. This can be done using a Supercritical Solvent technique such as a fluid mixture of acetone and CO_2, or by co-crystallization from 4-hydroxypyridine in ethanol (40,

85). CURC co-crystallization process is an effective approach used to adjust the stability, and solubility of the compound. This process introduces a co-component within the curcumin lattice in a manner that results in a weaker lattice framework compared to the parent. The two molecules (API and co-component) are connected with weak hydrogen bonds that break in aqueous media in a brief period (1 minute to few hours)(40). Consequently, such cocrystals have improved solubility profiles and can hence be used to improve the bioavailability of curcumin by 2-4 folds (80). Co-crystallization also has the added advantage of extending the elimination half-life (86).

1.3.5.2 Complexation of CURC with water-soluble polymers

The solubility of CURC can also be improved via complexation with water soluble polymers. For example, successful complexation with curcumin was achieved with a pH sensitive cationic copolymer poly(butyl-methacrylate-co-(2-dimethylaminoethyl) methacrylate-co-methyl-methacrylate) (81). The complex was an amorphous solid with enhanced drug loading (around 280 μg/ml), and solubility (> 2 mg/ml). When tested in mice, the formulation showed increase in the bioavailability and peak plasma concentration of CURC by 20 and 6 folds, respectively (87). CURC-polymeric complexes can also be formed by utilizing the carbonyl group in CURC to form imine linkages with amine group in relevant polymers via Schiff base reaction. This reaction was first described by Hugo Schiff in the year 1864 (88), and is featured by the ease of synthesis and purification. The reaction involves condensation of carbonyl compounds with primary amines at a specific pH to give rise to Schiff bases (also known as azomethines, or imines) (89, 90). Such Schiff bases have been shown to manifest various biological properties, including antibacterial, antifungal, antiproliferative, antimalarial, anti-inflammatory, antipyretic and antiviral properties, that qualify them as excellent candidates for pharmaceutical and industrial applications (91, 92).

Schiff bases have also been reported to aid photo-stabilization of polymers such as poly (vinyl chloride) and polystyrene, where better stability against UV radiation and photodegradation is achieved (89). Another important property of Schiff bases is that they are pH sensitive, which enables them to provide more controlled, acid-triggered drug release and become employed successfully in polymeric nanomedicine (93).

1.3.5.3 Nanoparticles formation

Improvement of API bioavailability via formulation of nanoparticles has emerged as an indispensable approach for the deployment of poorly soluble/absorbable drugs, such as CURC (40). By careful choice of appropriate encapsulation material, we can impart biocompatibility or biodegradability to drug delivery systems that ensure that they are safe for use in human. For example, it is reported that the encapsulation of CURC in chitosan nanoparticles resulted in an increase in solubility from 0.6 μg/mL up to a concentration of 180 mg/ml. Up to 95% CURC was released in phosphate buffered saline (PBS) pH of 7.4 (94). Other nanostructures used to encapsulate CURC include silica nanoparticles, poly lactide-glycolide (PLGA) nanoparticles, and single-walled carbon nanotubes (40). CURC encapsulated silica nanoparticles can be easily synthesized, with a hydrophilic surface that is nontoxic and biocompatible. The hydrophilic surface permits prolonged curcumin release of CURC which improves bioavailability (95). PLGA NPs yielded an increase in solubility compared to free CURC, with rapid release and 9-fold increases in bioavailability (96). CURC nanosuspensions prepared by high-pressure the technique of homogenization using soy lecithin and sodium deoxycholate as stabilizers. This yielded a faster dissolution (10-fold higher) and higher solubility (600-fold higher). The nanosuspension showed an acceptable safety profile during intravenous delivery for cancer treatment, with a low thrombocyte hemolysis index, and no local irritations (97). It is noteworthy that single-walled carbon

nanotubes have offered another effective approach in improving the solubility, stability and bioavailability of CURC. They are artificial nanomaterials made from graphene sheets coiled up to form thin tubes. These nanomaterials have exceptional properties, including ease of uptake and internalization by cells. They also can be used in the ablation of cancer cells due to their photothermal properties (98), so when used in conjunction with CURC, an enhanced therapeutic profile is expected.

1.4 Chitosan (Ct):

In view of the above discussion, it is imperative to utilize carrier systems that display biocompatible and/or biodegradable characteristics, in addition to being able to modify the physicochemical properties of the drug payload in favor of improved solubility. One such polymer, that has received significant attention by formulation scientist is chitosan (Ct), which is the subject of the present investigation. It is a cationic, aminated, semisynthetic copolymer consisting of D-glucosamine and N-acetyl-D-glucosamine subunits linked via β-,4 glycosidic bonds (99). It is obtained from various natural resources such as exoskeletons of crustaceans, eggshells and insects, and is extracted by deacetylation process from chitin, the only cationic polysaccharide available in nature (100, 101, 102, 103). Ct has attracted researchers' interest due to its multifaceted properties and versatility, which made it a candidate for use in many pharmaceutical and biomedical applications (99). This is by virtue of the antihyperglycemic, antioxidant, wound healing, antitumor, antimicrobial, antifungal and antitumor effects it was shown to exhibit (104).

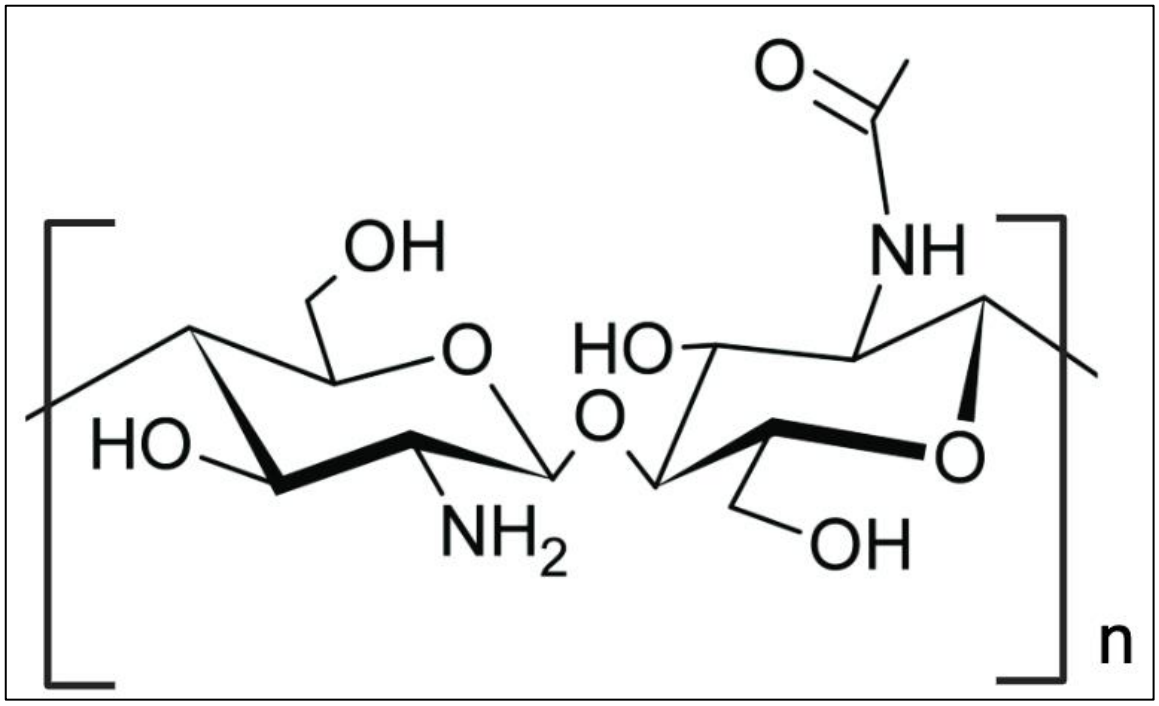

Figure 1.13: Chitosan chemical structure.

1.4.1 Physical and chemical properties of Ct

Chitosan appears as an off-white to white, coarse odorless ground flaky powder with a melting point of 102.5°C. It is generally stable, but incompatible with oxidizing agents. Recommended storage temperature is 2-8°C. Ct has a log(P) of approximately 11, which means that it is preferentially soluble in aqueous media, more specifically, in dilute aqueous acidic solutions (pH >6.5) (105). Thus, it dissolves in 1% dilute acidic solutions including, acetic acid (HAc), hydrochloric acid (HCl), formic acid, L-ascorbic acid, L-glutamic acid, lactic acid, succinic acid, malic acid, maleic acid and phosphorus acid (106). The primary and secondary hydroxyl (-OH) groups at positions C-6, C-3 and the amine ($-NH_2$) group at position C-2 allows for functionalization with other chemical moieties that may impart relevant physicochemical or biological properties to Ct (104). Other properties of Ct such as

the degree of deacetylation (DD) and molecular weight (Mw) also have a significant role in the functionality of Ct, including solubility, biodegradability, conjugation propensity (107).

1.4.2 Degree of deacetylation (DD)

The DD of Ct identifies the amount of d-glucosamine units containing free amino groups in the copolymer containing both n-acetyl-glucosamine and d-glucosamine subunits. It is an important factor affecting the versatility in the applications of Ct (108). The DD is directly associated with the hydrophilicity of Ct, and hence its solubility. Ct with DD of 70% is not very soluble in HAc (109). 55-70% DD is known as 'low DD of chitosan', 85%-95% is 'high DD' and reflects good water solubility, while 95%-100% DD is 'ultra-high' but is difficult to attain (110). At the biological level, the DD was also shown to have an impact on Ct cellular uptake of formulated NPs. This is due to the fact that an increase in DD and NH_2 groups generate higher positive charge within NP surface. This positive charge promotes the drawing of Ct particles into the plasma membranes which possess a net negative charge due to their sialic acid moieties (111, 112). The higher DD additionally prohibits endosomal opsonization of Ct and promotes uptake by varied pathways, which include phagocytosis, clathrin-mediated uptake, cadherin-mediated uptake or caveolin-mediated uptake (figure 14) (112).

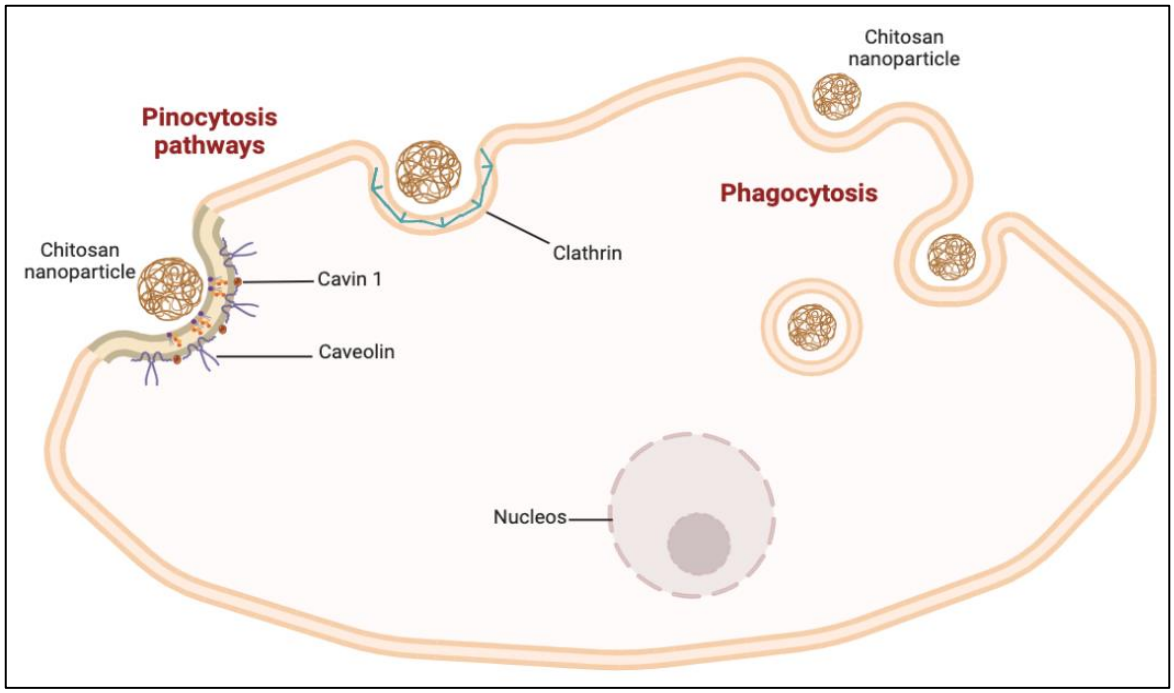

Figure 1.14: Illustration of the modes of the cellular uptake of chitosan particles.

1.4.3 Molecular weight (Mw) and methods of chitosan depolymerization

Ct is available in the market in variant molecular weights; thus it is classified based on its Mw as oligochitosan, low molecular weight chitosan (LMWC), medium molecular weight chitosan (MMWC), or high molecular weight chitosan (HMWC) (Table 1.1). The Mw varies depending on the method of Ct depolymerization and the properties desired. The production of different Mw of Ct depends mainly on the preparation method and the source from which raw chitin was obtained (102).

Table 1.1: Chitosan available Mw ranges. Adaptd from (113).

Type of Chitosan	Mw
Oligochitosan	~ 4.7 kDa ~ 10 kDa 22 kDa 120 kDa 13 kDa

	4.8 kDa
	3.69 kDa
Low molecular weight chitosan (LMWC)	50-90 kDa
	50-190 kDa
Medium molecular weight chitosan (MMWC)	250 kDa
	190-310 kDa
High molecular weight chitosan (HMWC)	64.8-170 kDa
	340 kDa
	310-375 kDa

One of the key requirements of Ct formulated delivery systems, especially as NPs, is their propensity to traverse cellular membranes. In this regard, the smaller the size of the NP, the better its uptake by cells. There is a direct correlation between the size of NP produces and the polymer molecular weight. Therefore, it is preferable to utilize polymers with low molecular weight when formulating NP. For the same reason, it is also desirable to utilize depolymerized entities in the construction of NP. There are various techniques that have been employed in Ct depolymerization to achieve lower molecular weight, including chemical treatment including sodium nitrite (114), hydrogen peroxide (115), and acid hydrolysis (116). However, chemical methods have drawbacks, including higher energy consumption , requiring high temperatures and pressure, both of which can degrade Ct to irregular fragments and produce d-glucosamine subunits instead (116, 117). Hydrogen peroxidation is more environmentally friendly, but poses the risk of ring opening, carboxylation, or deamination of Ct (115, 118). Other methods such as the enzymatic degradation employ specific (e.g. chitosanase) or non-specific (e.g. proteases, chitinases, cellulases and lysozyme) enzymes. Although such systems are beneficial in terms of the specificity by certain enzymes, they are costly and time consuming due to the difficulty in isolating and purifying the enzymes (116).

On the other hand, physical methods are comparably favorable compared to chemical methods in terms of reproducibility, amenability for scale-up, production of better quality oligomers and most importantly, environmentally friendly. They involve electromagnetic

radiation (e.g. microwave, gamma, UV irradiation), conventional heating, ultra-sonication, hydrodynamic cavitation, milling, ultrasound (116). Conventional heating can lead to deamination, decomposition and dehydration of the polymer (119). Ultrasonic cavitation was reported to be time consuming and offers no significant increase in DD in comparison to microwave irradiation. A recommended approach is to use a combination of physical methods to have improved outcomes. In the present research endeavor, I opted for the use of microwave depolymerization of Ct due to the aforementioned advantages of physical methods.

1.4.4 Effect of Microwave depolymerization on chitosan

Microwave irradiation specifically was reported to have the highest yield of degraded Ct products, in comparison to other thermo-chemical and physical methods. It produced 90-95% Mw reduction. Furthermore, microwave increases the DD of Ct, especially, with the aid of hydrogen peroxide (H_2O_2) or in alkaline conditions (116). The impact of microwave irradiation on the physiochemical properties of Ct constitute a core aspect of my investigation. The use of microwave was found to significantly reduce the Mw of Ct depending on some factors such as the duration of exposure, time and synergy with other depolymerization agents (most commonly H_2O_2) (115, 120). microwave was also reported to affect other parameters such as the DD, rheological and morphological properties of Ct. However, with regards to the chemical structure, in most microwave irradiation investigation, the main Ct chain remained unchanged which is an indication of the safety (118, 121, 122), except in some instances where microwave used in conjunction with other depolymerization methods such as H_2O_2, resulted in the production of carboxylate ions and aldehyde (123, 124). There is a direct correlation between molecular weight and the intrinsic viscosity of the polymer's solution (Table 1.2) (104), thus, the viscosity is expected to decrease after depolymerization. The rheological behavior of Ct is also affected by the polymer

concentration and ionic strength of solvent in addition to the molecular weight (103, 120). Furthermore, improvement in Ct solubility is observed with microwave irradiation as reported previously (118, 125, 126). Improved solubility can be attributed to increase in DD, which subsequently leads to an increase in the primary amines and a reduction in acetyl functional groups. The lone pair in the primary amines here plays an important role in enhancing the solubility, by its ability to generate affinity to water molecules and attract adjacent protons. This eventually forms the ammonium cation that creates a positive charge density in the microwave treated Ct, and subsequently leads to formation of more intermolecular reactions with water (127). Such positive charge is retained when these oligomers are constructed into NP, a useful feature due to the possibility of interaction with negative charge within the cell membrane (Section 4.2). Table 1.2 summarizes the changes in Ct properties secondary to microwave irradiation based on literature review. Herein, depolymerization of chitosan by microwave was used to reduce the Mw of chitosan, increase the positive charge and formulate Ct NPs (127, 128, 129). Basit et al. for example were successful in decreasing the viscosity and Mw of Ct chitosan using microwave irradiation, which facilitated the production of smaller nano-sized particles with higher positive charge (+46 mV), and sizes ranging around 170.7±2.9 and 223.7±9.3 nm. Another trial by Kocak et al. proved that microwave-assisted ionic gelation produced perfectly round small 25 nm sized NPs in a much shorter reaction time (only 1 min). The treatment also demonstrated homogenous Ct NPs dispersion, without significantly affecting the zeta potential (128). Figure 15 demonstrates the added advantage of microwave irradiation on chitosan nanoparticles in terms of size, Mw, PDI, and charge.

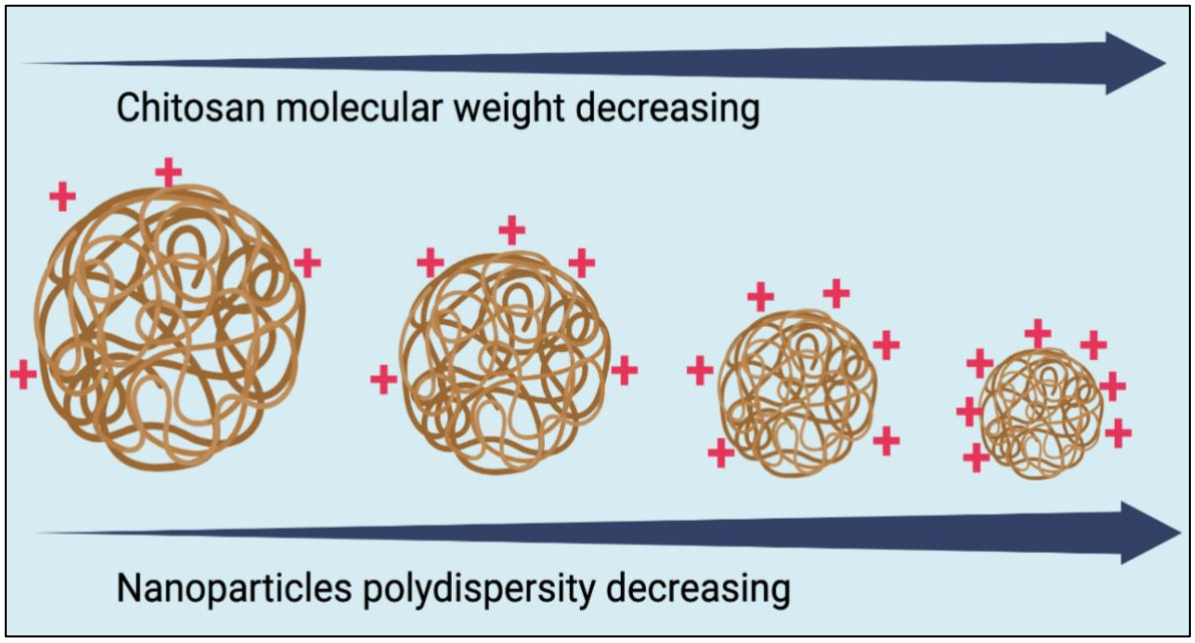

Figure 1.15: Microwave irradiation impat on Ct NPs molecular size, Mw, and polydispersity.

Table 1.2: Summary of the physicochemical modifications on Ct by microwave treatment. Table adapted from my review Paper (130)

Clinical trials/year(s) approved	Method used in addition to microwave irradiation	Microwave power	Microwave reaction time (minutes)	Molecular weight (Mw) reduction	Effect on DD%	Effect on viscosity	Chemical/ structural changes
Cheng et al. 2020	None. Only compared microwave to water bath (WB) method)	Equivalent to 90 °C	0 – 240 mins	Increased first then decreased. Final Mw after 240 mins ≈ $3x10^5$ Da	Increased within 60 mins from ≈ 60% to 73.86% After 240 mins = 79.15%	Viscosity reduced with the increase in microwave exposure.	No significant changes
Basit et al. 2020	0.9% NaCl	800 W	5 and 8 mins	Significantly reduced from 30,665 ± 245 Da to 15,223 ± 182 Da within 9 mins	Increased from 81.29 ± 6.9% to 91.41 ± 8.2%	Significantly lower solution viscosity within 9 mins (from 13.466 ± 2.690 to 2.009 ± 0.0164).	NR
Mecwan et al. 2011	None.	700 W	6, 18, and 30 mins	Decreased significantly from $4.40x10^5$ Da to $2.38x10^5$ Da after 30 mins.	No significant change (from 87.74% to a range of 87.58 to 88.18%)	Decreased by 45.78% after 30 mins treatment	NR

Clinical trials/year(s) approved	Method used in addition to microwave irradiation	Microwave power	Microwave reaction time (minutes)	Molecular weight (Mw) reduction	Effect on DD%	Effect on viscosity	Chemical/ structural changes
Journot et al. 2020	None	Equivalent to 100 °C	19 mins	Reduced from 90,000 kDa to 12.6 ± 0.6 kDa.	No change (85%)	NR	No degradation side products
Wasikiewicz et al. 2013	None. compared microwave to WB at 89 °C	100 W (2.46 GHz)	80 mins	Reduced from $219.40x10^3$ g/mol at time 0, to 31.36 g/mol	No significant change	NR	No alteration
Mahdy Samar et al. 2013	NaOH ((30%, 40% and 50%) solution.	1400 W	10 mins	Ranged from 866.03 to 4467.05 KDa	Highest was 95.19% (using NaOH 50%)	NR	NR
Jafari et al. 2021	1% H_2O_2	400, 600, 800 and 1000 W at 80 °C	20 mins	From 50–190 kDa to 1-3 KDa, 3-5 KDa, and 4-8 KDa.	No significant difference (from 89.6% to 88.9, 88.8, and 88.6)	Chitosan showed non-newton flow. Viscosity was influenced by the differences in microwave.	Chitosan skeleton remained unaffected

Clinical trials/year(s) approved	Method used in addition to microwave irradiation	Microwave power	Microwave reaction time (minutes)	Molecular weight (Mw) reduction	Effect on DD%	Effect on viscosity	Chemical/ structural changes
Li et al. 2012	0.3% H_2O_2. Compared microwave to WB	100, 200, 400, 600, 800, and 1000 W at 70 °C	20 mins	Significant reduction with the increase in reaction time (From ≈ $2.3x10^4$ to $1.5x10^4$	NR	Lower viscosity with the increase in microwave exposure.	No significant change in chitosan backbone
He et al. 2016	30% H_2O_2	600 W at 70 °C	5-240 mins	degraded to 1000 to 10,000 g/mol.	≥90% (deacetylated using alkali solution)	NR	No changes despite H_2O_2 use.
Zhang et al. 2017	1-3% H_2O_2, 40% NaOH	2450 MHz and 650 W	30-120s	Reduced from 8712.25 kDa to 124.25 kDa	Increased from 52.14% to 90.58	NR	Structural changes attributed to H_2O_2 use with microwave.

Clinical trials/year(s) approved	Method used in addition to microwave irradiation	Microwave power	Microwave reaction time (minutes)	Molecular weight (Mw) reduction	Effect on DD%	Effect on viscosity	Chemical/ structural changes
Li et al. 2021	None	2.45 GHz	10-70 mins	Reduced from 540 KDa to ≤ 10 KDa	Increased from 97.45% to 99.71 with the increase in degradation time.	With the increase in degradation time, viscosity continued to decrease. After 30 mins, e viscosity slowly decreased.	No significant change
Sun et al. 2006	30% H_2O_2	NR	15–54 mins	Reduced to ~ 2880 Da	NR	NR	Oxidation of C–O in chitosan oligomers formed aldehyde group (CHO)
Xing et al. 2005	NaCl, KCl, and $CaCl_2$ salts	480–800 W	0.5–25 min	Reduced from 560 KDa to ~$10x10^4$ under microwave alone, and to ~ $3x10^4$ under microwave + inorganic salts.	85% initially. Change in DD% was NR	Decreased with time under microwave irradiation + salts	NR

Clinical trials/year(s) approved	Method used in addition to microwave irradiation	Microwave power	Microwave reaction time (minutes)	Molecular weight (Mw) reduction	Effect on DD%	Effect on viscosity	Chemical/ structural changes
Shao et al. 2003	15% H_2O_2	700W	4 mins	Reduced from $2.2x10^5$ to 900-1000 g/mol	91.2% initially. Change in DD% was NR.	NR	No structural changes
Sun et al. 2007	30% H_2O_2	800 W	4–14 mins	Reduced to 1130, 2430 and 4350 Da	NR	NR	COO group produced from the oxidation by H_2O_2

'NR': not reported; 'mins': minutes; 'GHz': Gigahertz; 'MHz': Megahertz; 'NaCl': sodium chloride; 'KCl': potassium chloride, '$CaCl_2$': calcium chloride

1.4.5 Proposed mechanisms by which microwave depolymerizes Ct

There are several proposals that explain the mechanism of Ct degradation by microwave energy. In one proposal the splitting of the polymer chain occurs in two stages. First an initiation of a mechanical induction by the microwave electromagnetic field, which then induces vibrational and oscillatory motion of the molecules. Secondly, the oscillations aid in the generation of shear forces sufficient to split the polymer chain. In another proposal it is assumed that the molecular oscillation generates sufficient heat that induce hydrolysis, however, this is contributes to a lesser extent to the depolymerization (119). Another more in-depth explanation points to the possibility of cleavage occurring via dielectric heating produced by microwave heating. This leads to the formation of electric migration and rotational movements between the charged molecules and causes temporal polarization. The rapid reversals in polarization within the particles generate frictional heat within the molecules. Subsequently, the synchrony between the molecular rotational energies of the polar Ct moieties and the microwave energy causes a transfer of energy which is rapidly absorbed by polar bonds (115, 131). Hence, the location of cleavage in Ct is suggested to be between the glycosidic bonds (-C-O-C-). Furthermore, the acetyl density in Ct polymer decreases, which supports the claim that microwave increases the production of primary amino groups and thus increases the DD of Ct (125, 127). Figure 16 illustrates the proposed locations of Ct cleavage using microwave irradiation.

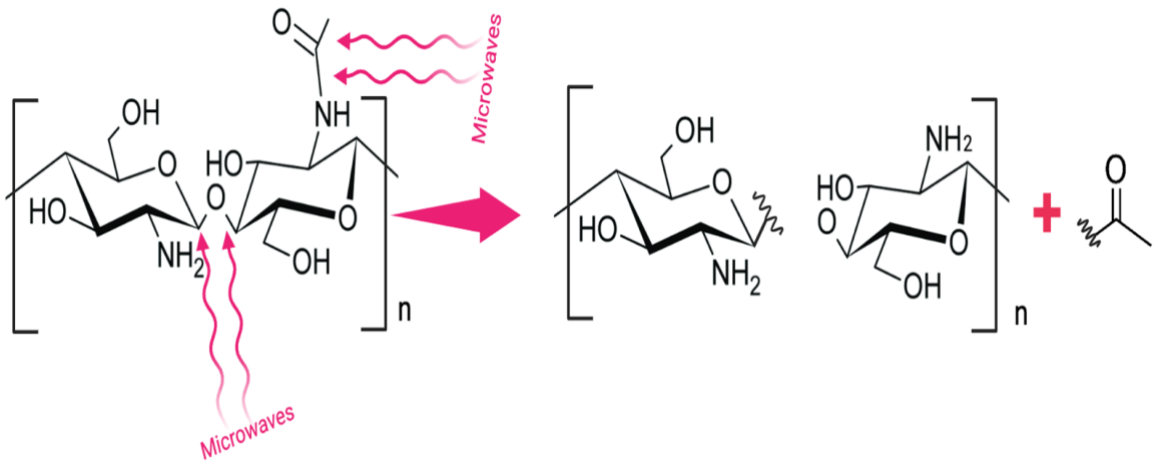

Figure 1.16: Illustration of microwave mechanism in chitosan depolymerization

1.5 Research gaps and study rationale

The poor stability and solubility and low bioavailability of CURC are severe obstacles to its effective therapeutic use. As explained previously, CURC also has low photo-stability when dissolved in organic media, and decomposes in alkaline media, which renders it arduous to maintain in such conditions. CURC is also known to exhibit better stability and antioxidant effect when dissolved in acidic media (Section 3.1). Furthermore, the acid milieu within tumor cells (132, 133), as opposed to normal tissue, makes it possible to selectively deploy NPs that trigger the release of the payload within the cells. In this regard, there is the possibility of also exploiting the increased solubility of CURC due to the acidic milieu, and hence improved anticancer effect. Furthermore, Ct favorably dissolves in acidic media (Section 4.1), making it ideal for the deployment of CURC to tumor cells in a selective manner.

These pointers form part of the core premise of my research endeavor whereby I aim to improve the uptake of CURC in colon cancer cells. Furthermore, the side effects and complications akin with conventional CoC chemotherapeutic treatment modalities discussed

in Section 2.3 demand effective and safer CoC treatment. Crucially, the propensity for NP uptake by cancer cells is increased with decreased size of the NP. Indeed, the use of polymeric materials for fabricating NP has become contingent on the utilization of low molecular weight versions due to its proportional relationship with size of formulated NP. microwave depolymerization of chitosan into the lowest possible configuration, ideally, oligomers, will permit its construction into very small NP. Whilst this may be ideal in deploying loaded CURC into tumors, it is important to note that, when present as a physical guest, CURC is prone to expulsion. Thus, I decided to conjugate CURC to the microwave depolymerized Ct (curcumin-chitosan) by a novel approach utilizing the principles of Schiff base reaction. This conjugation is expected to produce higher curcumin yield and loading capacity than the conventional encapsulation method. Furthermore, when constructed into NP, there is less chance of expulsion of CURC . In addition to the fact that the formulation relies on the use of affordable, handy, environmentally friendly and non-toxic materials. To the best of my knowledge, this approach has not been reported in the literature. Moreover, the effect of curcumin-chitosan conjugates nanoparticles (CCC NPs) on colon cancer was not tested before according to the literature.

1.6 Aims of research

Based on the research gaps and rationale for the study, I composed the following research question/hypothesis: Will depolymerization of Ct by microwave irradiation followed by conjugation to CURC and subsequent formulation as nanoparticles achieve the following?:

- Smaller sized NP compared to those derived from non-depolymerized Ct,
- Prevent CURC expulsion from NP, and
- Improve cellular uptake and hence cytotoxicity in colon cancer cells.

To address the above hypothesis, the following specific aims of the research was constructed:

1- **To degrade Ct into oligomeric form via microwave treatment, and evaluate the physicochemical characteristics.**
2- **To synthesize CURC-Ct conjugates from both the microwave treated and untreated Ct by means of Schiff base reaction and characterize the properties.**
3- **To formulate nanoparticles from the resultant chitosan-curcumin conjugates and characterize the properties.**
4- **To finally test the new formulation on colon cancer cell lines.**

CHAPTER II: MATERIALS AND METHODOLOGY

2.1 Materials

Low molecular weight chitosan (molecular weight 50,000 to 190,000 Da, degree of deacetylation: 75%-85%, Sigma Aldrich, St. Luis, USA), acetic acid glacial (≥99%, Fisher Chemical, Loughborough, LE11 5RG, UK), CURC, molecular weight: 368.38 g/mol, (Sigma Aldrich, St. Louis, USA), sodium hydroxide pellets (≥ 97%, Fisher Scientific, Loughborough, LE11 5RG, UK), ethanol (99-99.5%, Research-Lab Fine Chem Industries, Mumbai, India), NaCl (BDH, Poole, BH151TD, England), sodium carbonate anhydrous (Fluka, Charlotte, North Carolina, USA) , sodium tripolyphosphate (STPP granular, Alfa Aesar, Thermo Fisher Scientific, Ward Hill, USA), Poly ethylene-alt-maleic anhydride) (PEAMA, Mw 100,000 – 500,000, Sigma Aldrich, Steinheim, Germany), DMF, diethyl ether (≥99.0%, Honeywell, Seelze, Germany), CCK8 kit (Dojindo Molecular Technologies, Inc., Japan), DMSO (Sigma Aldrich, USA), Roswell Park Memorial Institute (RPMI) cell culture media (gibco, UK), fetal bovine serum (FBS), trypsin (Sigma Aldrich, USA), distilled and MilliQ water as needed.

2.2 Microwave treatment of Ct:

A concentration of 2% acetic acid (HAc) was prepared from 99% glacial acetic acid into which was dissolved 0.4% of LMWC and stirred overnight till complete dissolution of chitosan. For microwave treatment, a domestic microwave oven (Panasonic, NN-CD87KS) equipped with a variable power option was used at 300W (low power) or 800W (high power). For this treatment, 100 ml of the above chitosan solution was transferred to 500ml or 600ml beakers for the 300 and 800W respectively. 0.9% NaCl added to the solutions to facilitate energy conduction (127). The beaker was covered with aluminum foil with tiny perforations to control the pressure buildup during exposure to microwave energy and placed at an off-center position of the turntable in the microwave oven in order to achieve a uniform energy

distribution. Specific microwave treatment conditions are presented in Table 2.1. After the microwave treatment, 3 M NaOH solution was added dropwise to the content until precipitation of Ct (approximately pH 7), which was collected after centrifugation at 4000 rpm for 3 min. The precipitate was washed thrice with distilled water and then freeze-dried (SP Scientific freeze dryer, VirTis, USA) at -50 C and 53 mTorr, until a dry powder was produced.

Table 2.3: Optimization of microwave treatment conditions

Formulation	Power	Total Exposure time (mins)	Exposure intervals (mins)	NaCl conc. (w/v%)
Control	0 W	0	0	0
Ct1	300 W	30	2	0.9
Ct2	800 W	30	1	0.9
Ct3	300 W	30	2	0

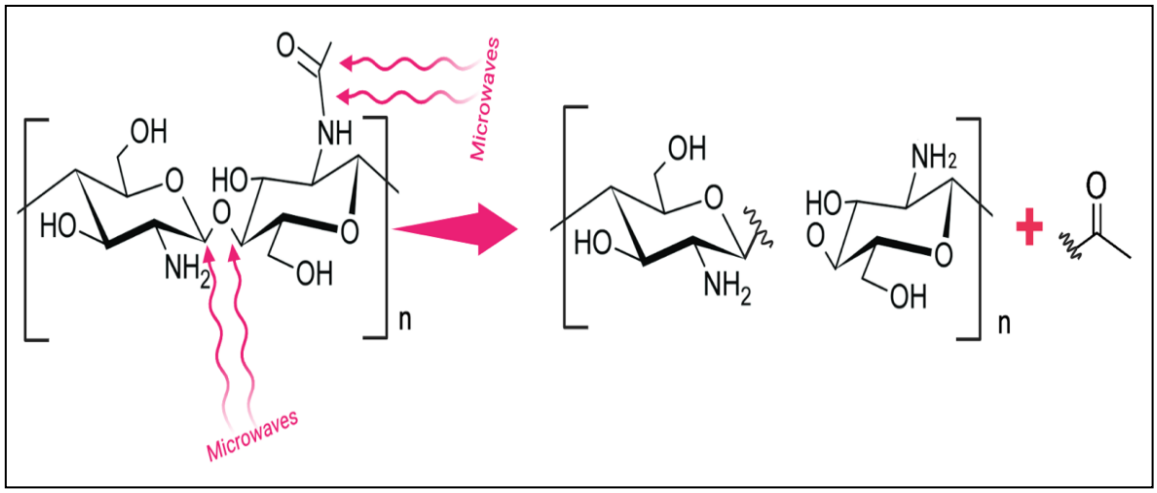

Figure 2.17: Schematic of Ct depolymerization via microwave irradiation

2.3 Conjugation of CURC to Ct

Conjugation of CURC to Ct was executed using four different schemes, in order to assess the best conjugation yield. Each of the scheme is described below.

2.3.1 Scheme 1: Microwave assisted conjugation of CURC to Ct (134):

184 mg of CURC was dissolved in 15 ml of absolute ethanol (99.5%), followed by the addition of 64 ml (255 mg) of Ct solution (Section 2.2). The two solutions were mixed in a 150ml beaker at 800 rpm for 30 mins and then transferred to the domestic microwave operated at 100W power for 10 mins. The product was freeze-dried and stored at 4^{o}C until analyzed.

2.3.2 Scheme 2: Conjugation of CURC to Ct using poly(ethylene-alt-maleic anhydride) PEAMA as a crosslinker:

Method 2.A: Conjugation using poly(ethylene-alt-maleic anhydride) PEAMA as a crosslinker

CURC (184mg) was completely dissolved in 20 ml of dimethylformamide (DMF). Separately, 50 mg of polyethylene-alt-maleic anhydride (PEAMA) was dissolved in 5ml of DMF to form PEAMA solution and 225mg of Ct was dissolved in 64ml of 2% HAc. Under continuous stirring, the Ct solution was first mixed with the PEAMA solution, which led to precipitation of the conjugate. The mixture was stirred for 2h at 300 rpm. Subsequently, CURC solution was added to the Ct-PEAMA conjugate and the mixture was stirred for another 2h. Afterwards, diethyl ether was added to wash the product from unreacted materials. Centrifugation at 4000 rpm for 3 mins was then done, the supernatant including diethyl ether was discarded, the precipitate was washed with distilled water thrice and then freeze-dried.

Method 2.B: Conjugation using poly(ethylene-alt-maleic anhydride) PEAMA as a crosslinker

In this scheme, CURC (184mg) was dissolved in 20 ml of (DMF) and 50 mg of PEAMA separately dissolved in 5ml of DMF. CURC was reacted with PEAMA by

continuous stirring at 80 - 100°C for 1 hour until a homogenous mixture was obtained. This reaction preceded under anhydrous conditions. To this reaction mixture was then added dry 255mg of Ct and the mixture stirred at 80 - 100°C for another 1 hour. The product was then washed with diethyl ether and a sticky material was produced. The product was covered with aluminum foils perforated with holes to allowed to air dry for 48hr in a fume hood.

2.3.3 Scheme 3: Conjugation by Schiff base formation between CURC and Ct

The idea of Schiff base formation out of CURC and Ct is inspired from Saranya et al (134). Chitosan solution 16 ml (64mg) was transferred to a 150 ml beaker and the pH raised to 6 - 6.5 using 3 M NaOH (Checked using a pH meter) with continuous stirring at 300 rpm, ensuring that Ct did not precipitate out of solution. Under dark conditions, CURC solution (92 mg dissolved in 30 ml ethanol) was added dropwise to the Ct solution and stirred for 6h at 300 rpm. The product was then exposed to microwave power of 100W (with pauses when solution begins to boil) until precipitates was formed. This took about 20 mins. The conjugate was cooled down to room temperature and centrifuged in 15 ml Falcon tubes at 4500 rpm for 15 mins, the supernatant was then discarded and the precipitate was washed thrice with absolute ethanol (with each wash, it was centrifuged at 4500 rpm for 5 mins). Next, the product was freeze-dried at -53^{o} C and a pressure of 78 mTorr until dry.

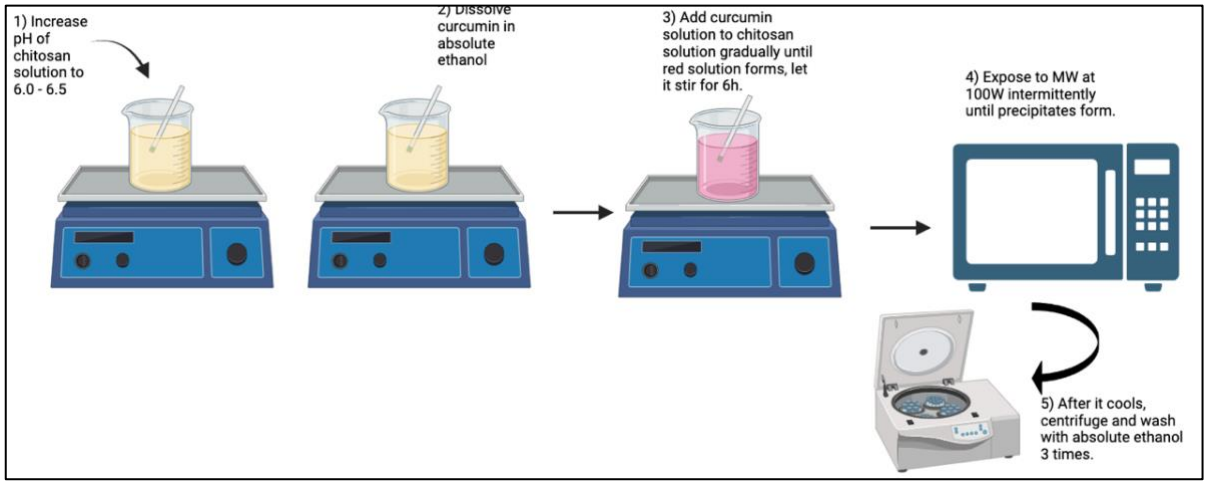

Figure 2.18: Schematic illustration of the developed CURC-Ct conjugation process.

2.4 Preparation of Ct and CURC-Ct conjugate nanoparticles (CCC NPs)

Nanoparticles were formulated by ionic gelation which results via differences in ionic charges between Ct (positive) and sodium tripolyphosphate (STPP, negative) that spontaneously promote their self-assembly into small spherical nanoparticles. The method was adopted from (135) and (128) with modifications, briefly described as follows. First, 50 mg of STPP was dissolved in 50 ml milli-Q water to a concentration of 1 mg/ml, and Ct was dissolved in 2% acetic acid (HAc) to achieve 1 mg/ml. Two milliliters of the Ct solution was transferred to a 10 ml beaker and stirred at 900 rpm, followed by the addition of 500 µL of STPP solution dropwise at a rate of approximately 1 drop/5 seconds (drops being added in different positions each time). After that, 1.2 ml of the resulting NPs was transferred using a micropipette to 2 ml Eppendorf tube, centrifuged using a Thermoscientific centrifuge (SORVALL LEGEND MICRO 21R, Germany) at a speed of 4,000 XG for 15 mins. From the supernatant, 1 ml was then taken, diluted with 500 µL of milli-Q water and vortex mixed at a speed of 1000 for 2 mins before analyses. The formulation was carried out at room temperature. In case of CURC-Ct conjugate (CCC) NPs, the same procedure described above was used with the exceptions that 1% HAc was used to dissolve CCC, and the centrifugation was at a speed of 10,000 XG for 15 mins without dilution with milliQ water. Optimization of the procedure was carried out based on variation of the various parameters shown in Table 2.2. Parameters that gave the most desirable attributes were adopted for further work.

Table 2.4: Nanoparticles optimization trials:

Trial no.	Ct : STPP ratio	Stirring speed (rpm)	Stirring time	Centrifugation speed – time	Vortex mixing
1	10:1	1000 rpm	60 secs	No	No
2	1:1	800 rpm	30 mins	No	At 1800 for 25 secs
3	5:1	700 rpm	60 mins	4000 ×g – 30 mins	No

4	5:1 (pH raised to 5 using NaOH)	900	15 mins	4000 ×g – 15 mins	At 1000 for 5 mins
5	5:1 (pH raised to 5 using NaOH)	900	60 mins	4000 ×g – 15 mins	At 1000 for 5 mins
6	20:1	4000 ×g	30	4000 ×g – 15 mins	At 1000 for 5 mins
7A (Ct NPs)	4:1	900 rpm	30	4000 ×g – 15 mins	At 1000 for 2 mins
7B (CCC NPs)	4:1	900 rpm	30	1000 ×g – 15 mins	At 1000 for 2 mins

2.5 Physical characterization of the microwave treated Ct and CCC

2.5.1 UV-Vis spectra of microwave treated and untreated Ct

UV-Visible absorption spectra of microwave treated Ct were recorded on a UV-Vis spectrometer (JENWAY, Model number 7205, UK). Approximately, 3 ml of fresh microwave treated and untreated Ct was transferred to a standard cuvette and the absorption read over a wavelength range of 200 to 500 nm.

2.5.2 Ascertaining the presence of relevant chemical moieties in Ct after microwave treatment

The presence of relevant chemical moieties, and the changes in the chemical groups before and after microwave treatment of Ct was recorded between 400 to 4000 cm^{-1} using a Fourier transform infrared (FTIR) spectrometer (Jacso, model FT/IR-4200, Japan) equipped with a TGS detector at a resolution of 16 cm^{-1}.

2.5.3 Assessment of the crystalline nature of Ct after microwave treatment

Assessment of the crystalline nature of Ct before and after microwave treatment was carried out on an X-ray diffractometer (PANalytical X-ray Diffractometers, model

EMPYREAN, Netherlands) at scan angle range for 2θ between 5° and 80°. The diffractometer was equipped with a Cu anode and a κ-alpha1 and κ-alpha2 wavelengths were 1.540 and 1.544, respectively. Divergence slit was fixed and no monochromator was used. Generator voltage was 45 kV with a tube current of 40mA. Scan type was continuous with a scan step size of 0.0131 and a scan range of 4.99.

2.5.4 Carbon-nitrogen (CN) elemental analyses

The elemental analysis for carbon and nitrogen was performed using CHNS % Organic Elemental Analyzer, (Thermo Fisher, model Flash 2000, United Kingdom) to estimate the weight percentage of each element in treated and untreated Ct, CURC or CCC. 1-3 mg of the sample was mounted on the CHNS analyzer and the percentage of carbon and nitrogen in each sample was recorded. C/N ratio was then used to determine the DD% of Ct using the following reported equation:

$$DD\% = \left(\frac{9600}{(364x29.06+2400)}\right)x100\% \ (136) \quad \ldots\ldots\ldots\ldots\ldots\ldots\ldots(1)$$

2.5.5 Flow time (viscosity) of microwave treated and untreated Ct

The flow times (viscosity) of unmodified and microwave treated Ct solutions prepared at a concentration of 0.4% (w/v) in a 2% HAc solution were measured using a Cannon-Fenske capillary viscometer. The process involves the aspiration of polymer solutions to the upper mark above the bulb and noting the time it takes to flow down by gravity to the lower mark below the bulb. In addition, the changes in viscosity can provide insight into the molecular weight. Polymer solutions with lower molecular weights have lower viscosity (137).

2.5.6 Thermal profile of microwave treated and untreated Ct

The thermal profile of treated Ct was evaluated using a differential scanning calorimeter (DSC) (PerkinElmer, model Jade DSC, India). About 3 mg of each sample was placed in a DSC aluminum pan, covered and crimped. The reference pan was without any sample. The sample was heated at a flow rate of 10 ^{o}C/min between 0 to 350°C under a gentle stream of nitrogen gas of 40 ml/min. The thermal profile during the heating episode was recorded.

2.5.7 Solubility studies of microwave treated Ct

UV-Vis absorbances of untreated and treated (300 and 800W) Ct solutions were used to construct three separate calibration curves at 0.25, 0.5, 1, 2, 3 mg/ml from UV-Vis absorbances at a wavelength of 200 to 500 nm. The absorbance of solutions made from 45 mg of each of the microwave treated Ct preparations in 15 ml of 2% HAc stirred (700 rpm) in a 50 ml beaker at 0, 5, 30, 60, and 120 mins was used to estimate their solubility values as a function of time. The solubility values were determined by withdrawing 3 ml samples into Eppendorf tubes and centrifuged at 10000 rpm for 10 mins. The supernatant was obtained and analyzed by UV-Vis spectroscopy.

2.5.8 Percent yield and drug loading capacity

The CCC product yield and drug loading capacity was calculated after the conjugation, purification and freeze-drying of the samples using the following equations:

$$\text{Percent yield (\%)} = \frac{\text{actual yield}}{\text{theoretical yield}} \times 100 \quad \text{.....(1)}$$

And the drug loading efficiency was calculated as:

$$\text{Drug loading capacity (\%)} = \frac{\text{mass of the drug in the final product}}{\text{Total mass of the final product}} \times 100 \quad \text{.....(2)}$$

2.5.9 CURC quantification by high-performance liquid chromatography (HPLC)

Quantification of CURC in CCC was carried out using an HPLC System (Agilent, series 1260 quaternary pump, USA). The mobile phase was 0.1% trifluoroacetic acid (TFA): acetonitrile (ACN) (50:50, v/v) and elution through a C18 reversed phase stationary phase (SUPELCO Analytical, Discovery® HS, 7.5cm x 2.1 mm, 3µm) at a flow rate of 0.2ml/min at room temperature. The HPLC system was equipped with a UV/Vis detector set at 425 nm. After the conjugation reaction was complete and after washing with ethanol, the supernatant was collected. Then, 1 ml of the supernatant was freeze dried and redissolved in absolute ethanol. Afterwards, 50 µL of the samples was diluted in 950 µL ethanol, filtered, and then injected in the HPLC device for analysis. All data are presented as an average of three independent runs (mean ± SD (n=3)).

2.5.10 Solubility and stability studies on CCC in different pHs of CCC:

To assess the solubility of the new CCC compound, 10 mg of it was weighed and dissolved in 10 ml of aqueous (water, HAc 2%) and organic solvents (Ethanol). Subsequently, the CCC samples were left to dissolve overnight at a speed of 900 rpm. For the assessment of the stability of CCC in different pH media, three beakers of 10 ml, 2% HAc were prepared, and the pH was adjusted in two beaker using 3M NaOH to either 6.5 or 12. The conjugates were then left to dissolve overnight at a speed of 900 rpm. Afterwards, an aliquot of each pH solution was freeze-dried and analyzed using FTIR for any changes in the chemical groups and the structure.

2.6 Physical properties of nanoparticles

2.6.1 Size and zeta potential analysis

A Nano series Zeta sizer (Malvern Instruments, model ZEN3600, UK) was used for determining the size and surface charge of the nanoparticles. The polydispersity index (PDI) was also measured using the same device to determine the size distribution of the sample. Fresh samples were placed in the cuvette and the reading was recorded on three runs.

2.6.2 Morphological studies using Atomic Force Microscopy (AFM) and Transmission electron microscopy (TEM)

The topography and roughness analysis of the formulated nanoparticles was carried out using an Atomic Force Microscope (AFM) (Asylum Research, Model MFP 3D, UK). The samples were first prepared by placing two drops of each NPs suspension on a microscope glass slide, ensuring that the drop was uniformly distributed on the slide. The slide was left to dry overnight at room temperature. The AFM analysis was done on samples fixed on a platform with a double-sided adhesive. The cantilever was operated at a force constant of 0.7 $N.m^{-1}$, resonance frequency of 150 kHz and scan area of 5x5µm. The internal structural morphology was done on a transmission electron microscope (FEI, Thermo Fisher) Transmission Electron Microscope (Model Tecnai G2 S Twin FEG 200kV) was used. Few drops of each sample were loaded onto thin support grids and left to dry overnight. The analysis was done by transmitting a beam of electrons through an ultra-thin specimen. The image was then magnified and focused onto an imaging device or detected by a sensor.

2.6.3 Stability studies of Ct NPs

The size, polydispersity index and zeta potential of the control nanoparticles, nanoparticles made from unmodified Ct, 300W, 800W Ct and CCC nanoparticles were recorded at room temperature and 4°C on day 1, 7, 14, 21 and 28 to assess the changes in these parameters as a function of time, and to determine the appropriate storage temperature.

2.7 In vitro studies

2.7.1 In vitro drug release studies

The in vitro assessment of CURC release from the new nanoparticle drug carrying system was assessed following the method from (135) and (138), with adjustments. Briefly, the pH of 50 ml PBS (release medium) was adjusted to 6.7 to mimic the colonic medium using 0.1% HCl, to mimic the gastric acid in humans. 1ml of the PBS was then distributed in 2 ml Eppendorf® tubes and 0.5 ml of either Control or 300W CCC NPs suspension was added to each tube to obtain a ratio of 2:1 (v/v) release medium: NPs suspension. The tubes were then placed in an incubated shaker. The temperature in the closed incubated shaker system was set to 37°C, and the shaking was set to 150 rpm. The time intervals were 0.5, 1, 2, 6, 24, 48, 72, and 96 hours. At each time point, one Eppendorf® tube was removed, 100 µL of the released CURC was withdrawn, redissolved in 400 µL absolute ethanol and filtered using (13m/0.45 mcm) HPLC syringe filters. The amount of CURC at each time point was then quantified using HPLC following the prespecified method in section 2.5.9. The amount of CURC at each time point was represented without subtraction from the previous point. The data was obtained in a form of a mean of three independent runs (n=3). The drug release was calculated using the following equation:

$$\% \text{ Release} = \frac{\text{amount of CURC released}}{\text{amount of CURC inside NPs}} \times 100$$

2.7.2 Cell thawing and incubation

Human LoVo and HCT-116 CoRC cell lines (passage 14) were thawed in a 37°C water bath, centrifuged at 1000 rpm for 5 mins and then the supernatant was discarded and the cells pellet was obtained. The pellet was then diluted with 5 ml of a prewarmed Roswell Park Memorial Institute (RPMI) growth medium supplemented with 5% activated fetal bovine

serum (FBS) and 1% antibiotic penicillin-streptomycin in a T-25 flask. Subsequently, the cells were observed under the microscope at 10x magnification, and then kept in the incubator at 37°C with 5% CO_2. The procedure of observing cells under the microscope was repeatedly done daily to check on cells' adhesion, morphology and health state.

2.7.3 Cell subculturing

After confluency, the cells were sub-cultured in a T-75 tissue culture flask (Thermo Fisher Scientific, USA). The media was first discarded and the cells were washed with phosphate buffered saline (PBS). 1 ml of Trypsin was added to the cells and placed in the incubator for 2 mins to allow them to completely detach from the flask. Subsequently, the detachment was confirmed by gently tapping the flask and observing under the microscope, then, 2 ml of the prespecified media was quickly added and distributed evenly on the entire flask surface to deactivate trypsin. The mixture was then transferred to a 15 ml Falcon tube and centrifuged at 1000 rpm for 5 mins to obtain the cells pellet and the supernatant discarded. The cells were resuspended in 2 ml media, and transferred to a new T-75 flask. The flask was observed under microscope and cells were afterwards kept in the incubator.

2.7.4 Cell counting using a hemocytometer

10 µL of the resuspended cells was withdrawn and mixed with 10 µL of trypan blue solution (0.4%, sigma Aldrich, USA). Then the mixture was added to the hemocytometer after cleaning the cover slip and chamber with alcohol. Following that, the chamber was placed under the microscope at 10x magnification. Phase-contrast was used to distinguish the viable cells, and dead cells (stained with blue color) were excluded from counting. The

calculated number was then multiplied by the dilution factor (2 in our case), then by 10^4 to determine the number of cells per 1 ml.

2.7.5 Cell cytotoxicity using CCK8 assay

The cytotoxic effect of the Control CCC NPs, 300W CCC NPs in comparison to free curcumin and 5-FU as a positive control was assessed in both HCT-116 and LoVo human colon cancer cell lines. HCT it is an aggressive cell line that has mutations present in 80% of CoRC patients (KRAS and BRAF mutations). KRAS mutation by itself is associated with thirty to sixty percent of sporadic CoRCs (139), while BRAF mutations are present in ten percent of them (140). After counting the cells, they were distributed evenly in a 96-well plate to achieve a number of 5000 cells/well. Next, the plate was kept in the incubator for the next 24 hours. Three stock solutions of the each of the four formulations were prepared at concentrations of 12.5, 25, 50 and 50 uM for the test. In the next day, the cells were checked under the microscope and treated with the formulations in a total volume of 100 μL for each plate. The plate was then covered with aluminum foil and incubated at 37°C with 5% CO_2. After 24 hours of incubation, the plate was analyzed using Cell Counting Kit 8 (CCK8) assay (Dojindo Molecular Technologies, Inc.). Briefly, each well was treated with 10 μL of the CCK-8 reagent. The plates were then incubated at 37°C, 5% CO2, for 40 minutes. Subsequently, the absorbance for each well was read by a microplate spectrophotometer system (Tecan, Magellan Spark, USA). The optical density (OD) /absorbance was read at 450 nm and cell viability was calculated as follows:

$$\text{Cell viability \%} = \frac{\text{OD of the experimental group cells}}{\text{OD of the Control group cells}} \text{ x } 100\%$$

2.8 Statistical analyses

Descriptive statistics (mean ± SD) were done using Microsoft Office Excel (Version 16.77.1) and statistical significance was determined using GraphPad Prism statistics software (Version 10.2.1). P-value of ≤ 0.05 was considered statistically significant (**** P-value ≤ 0.0001; *** P-value ≤ 0.001; ** P-value ≤ 0.01; * P-value ≤ 0.05; ns $P > 0.05$). One-way Anova test with multiple comparisons was used for ascertaining significant statistical differences between experimental groups. Unpaired t-test was used for determining the statistical significance between two microwave treated groups. Two-way Anova test was used to determine statistically significant differences between experimental groups and the concentrations of treatments on cell viability.

CHAPTER III: RESULTS

This Chapter is dedicated to the formulation of a CURC chitosan nanoparticle delivery system. As opposed to the incorporation of CURC in chitosan NPs, the aim here is to conjugate CURC to Ct and then use this conjugate to construct NPs. Briefly Ct was first treated with microwave irradiation to obtain depolymerized Ct, which was subsequently conjugated to CURC through utilizing the concept of Schiff base reaction and the formation of imine linkage. Finally, NPs of the above CCC compound were formulated by ionic gelation.

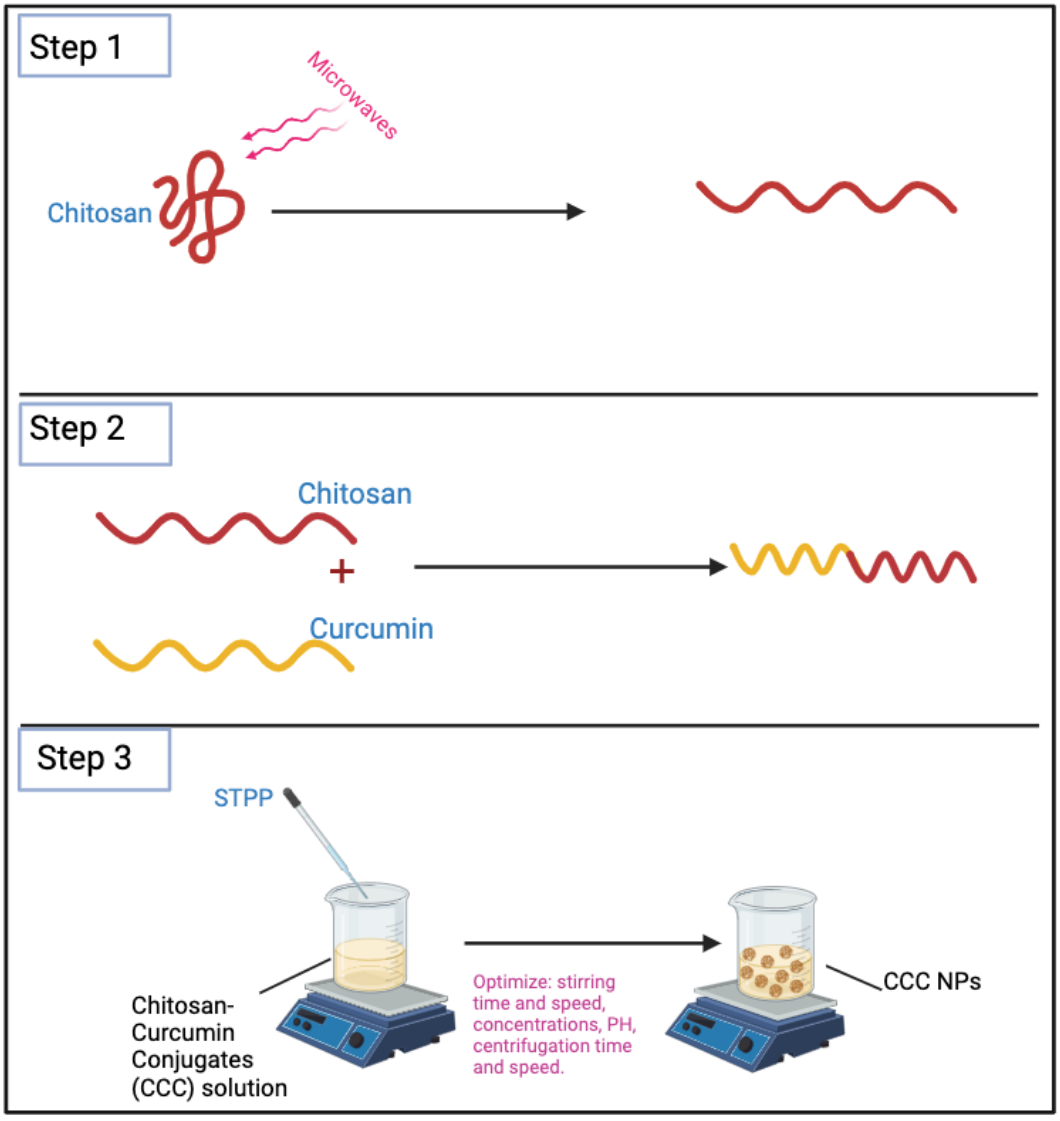

Figure 3.19: Graphical illustration of CCC NPs formulation

3.1 Physicochemical Characterization of Microwave Treated Ct:

3.1.1 Characterization Using Ultraviolet-visible (UV-Vis) Spectroscopy

Figure 3.2 shows the UV-Vis absorbance spectra of Ct solutions without and after microwave treatment. The characteristic peaks of chitosan at wavelengths 230 nm and 290 nm are evident in all Ct samples. The 230nm peak is ascribed to the n-σ* transition of the amino group, in addition to the π-π* of either carboxylic or carbonyl groups, while the peak around 290 nm is referred to the carbonyl/carboxyl groups n-π* transition (141). In addition, a trend of an increase in the absorbance with the increase in microwave exposure power can be seen clearly from the spectra, with control Ct having the lowest absorbance, followed by 300W and 800W, respectively. This aligns with the fact that the UV-Vis absorbance and the molecular weight of chitosan are inversely related, which can be explained by the elevating 230nm and 290nm peaks. This can indicate the formation of carbon–oxygen double bond groups (carbonyl containing groups) after the scission of the main Ct chain (118). It is important to mention that there is a potential impact of the background on the absorbance. This is because slight differences in the absorbance of the background are seen with the different formulations, which can be due to the presence of small undissolved particles.

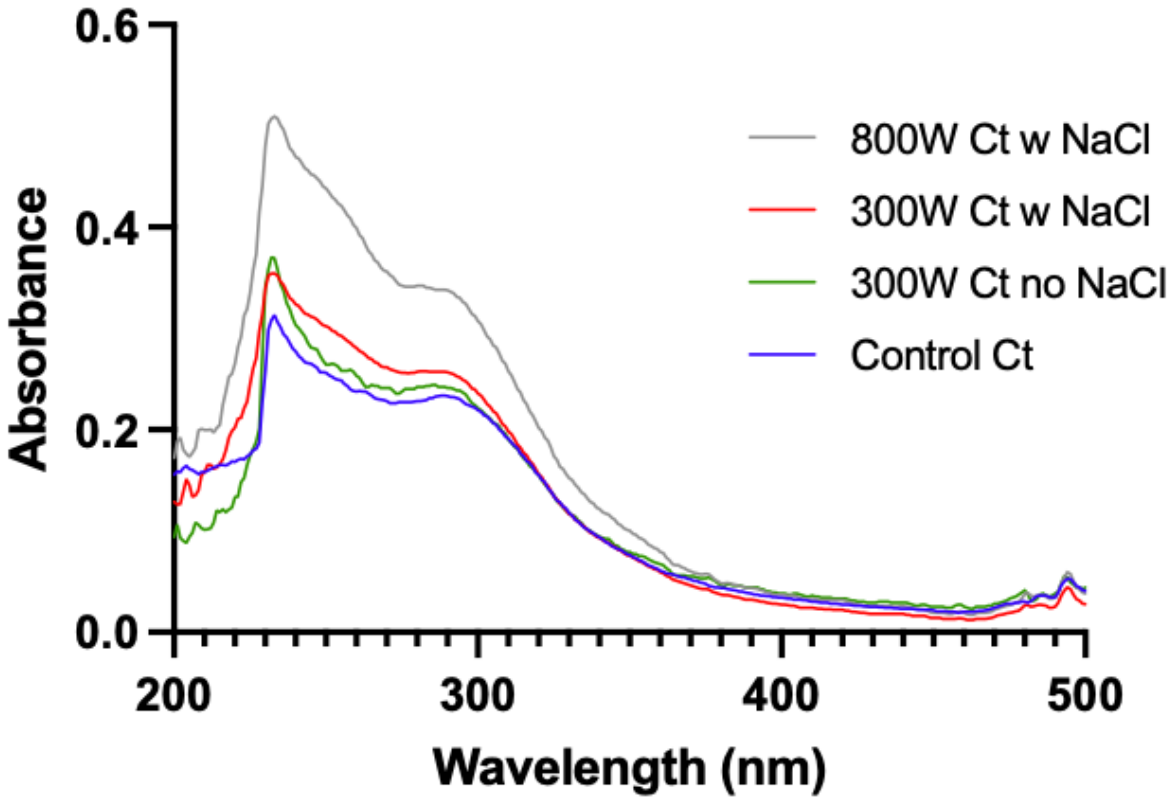

Figure 3.20: UV-Vis spectrum of control and microwave treated Ct

3.1.2 Characterization Using Fourier Transform Infrared (FTIR) Spectroscopy

Although microwave irradiation alone was reported to be an efficient mean of Ct depolymerization without causing significant chemical changes (see chapter 1 section 1.4.4.). The FTIR analysis remains a necessary step to monitor the changes in the structure and functional groups of Ct after microwave irradiation. It additionally gives insights on the purity and the quality of the sample. FTIR spectra of microwave treated chitosan in general disclose no significant change in Ct core chain. For instance, the main Ct characteristic peaks (i.e. the amide I band at around 1650 cm^{-1} stretching, amide II band at 1450-1550 cm^{-1}, small amide III peak at 1310 cm^{-1}, NH_2 bending at 1599, C-O stretching in the range 1000-1200 cm^{-1}, O-H stretching at 3200-3500 cm^{-1}, and the bands present at 1158–895 cm^{-1} are ascribed to the polysaccharide structure characteristics) (125). Also, the absence of O-H stretching of carboxylic groups in the region 2500-300 cm^{-1} is a good indication that no ring opening or

formation of carboxylic groups occurred. However, there appears some slight changes in the side groups of Ct such as the stretching of the primary amino groups (-NH_2) in the region 3200 cm^{-1} and 3500 cm^{-1}, which appears more prominent in case of 300W treated Ct without NaCl. In addition to the shortening of the amide III band at 1310 cm^{-1}, this can indicate further removal of the unwanted acetyl groups and an increase in the degree of deacetylation as compared to the microwave Ct treated with NaCl.

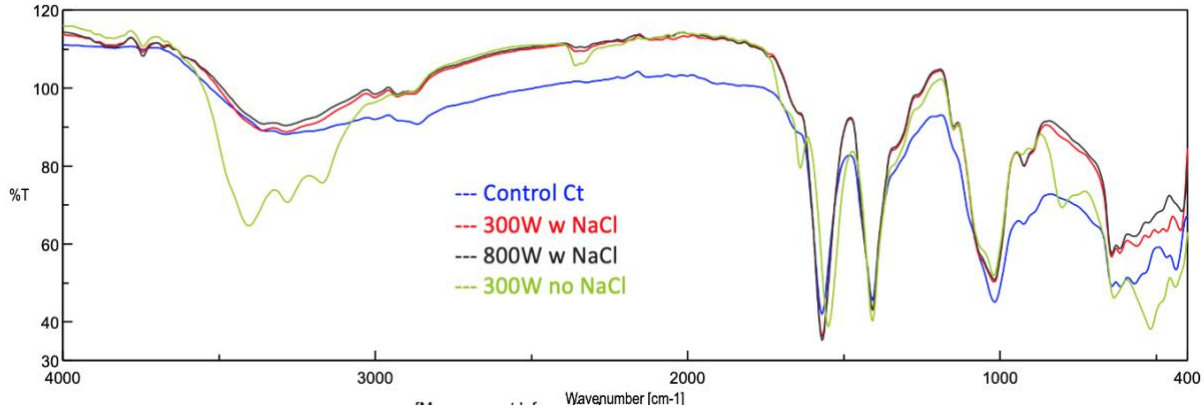

Figure 3.21: FTIR spectrum of control Ct and microwave treated Ct

3.1.3 Assessment of the crystalline nature of Ct after microwave treatment

The x-ray diffraction patterns of each of the control and microwave treated Ct are presented in Figure 3.4. Chitosan is semi-crystalline in nature and has characteristic XRD peak at around 2-theta angle 10° and 20.1°, which in the case of this pattern can be seen present in 2-theta angle of 8.8-8.95° and 20.2°, respectively, albeit with changes in their intensity that can be attributable to microwave exposure. The presence of these peaks is consistent with other Ct XRD patterns reported in literature (125, 142, 143). The changes of intensity are attributable to the microwave treatment with different exposure powers and intervals. The lowest intensity (lowest crystallinity) was seen with the 300W treated Ct with NaCl with an intensity of 1443 at 2-θ angle of 8.86°, followed by 300W without NaCl (8.9°, 2210), 800W w NaCl (8.95, 2511), and the highest was the untreated control Ct (8.85°,

2673). A possible explanation of the unexpectedly higher crystallinity with the higher power (800W) can be referred to the behavior of the microwaves. microwave treatment was reported to preferentially degrade the amorphous portion of chitosan first, leading to an initial increase in the crystallinity. This is due to the finding that Ct main chains are constrained in the beginning of depolymerization by the hydrogen bonds in its structure and the disordered side chains that have more rotational freedom than Ct main chain. However, with further degradation (recall that the exposure intervals in the 300W Ct were double the exposure time in the 800W Ct), microwave succeeds to destruct the crystalline structure of Ct and decrease its crystallinity (118). The more amorphous the Ct is the more soluble, as further surface area will be exposed to interactions with the solvent.

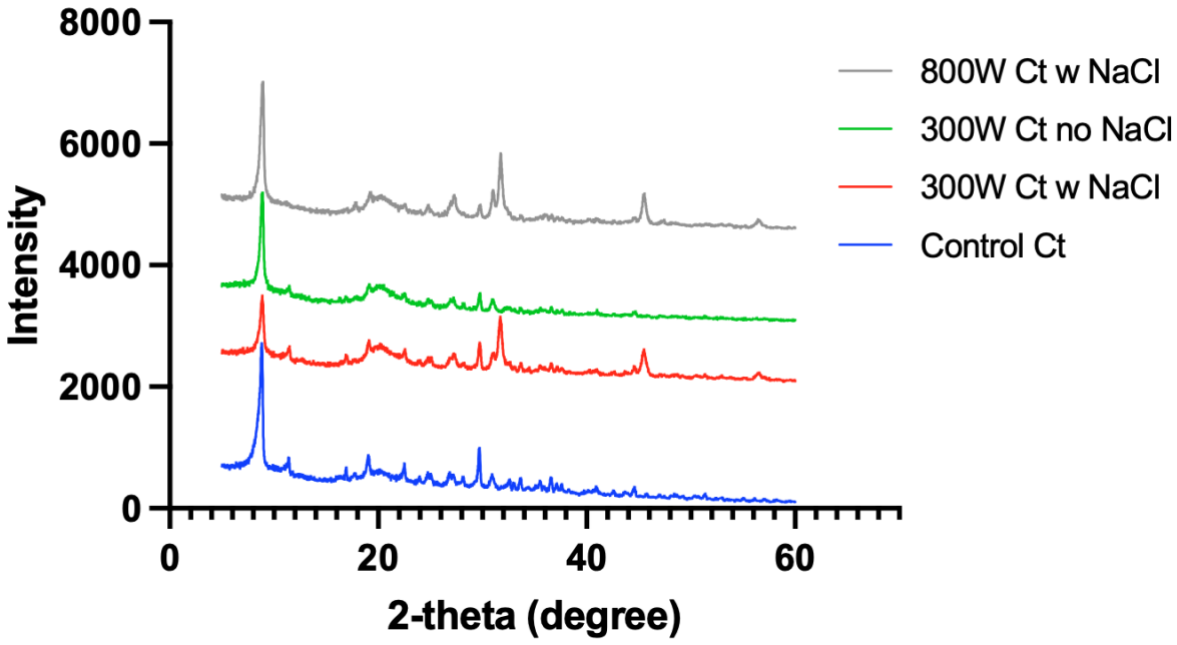

Figure 3.22: X-Ray diffraction analysis (XRD) patterns of control Ct and microwave treated Ct

3.1.4 Carbon-nitrogen (CN) elemental Analyses

The Carbon nitrogen elemental analysis was done to determine the composition and weight percentage of both carbon and nitrogen elements as products of combustion. The CN

ratio can then give insight on the degree of deacetylation. The higher the CN ratio indicates higher deacetylation degree and more free amino groups in the chitosan. Table 3.1 demonstrated the carbon and nitrogen content in the control and microwave treated chitosan. The higher the nitrogen content (seen in 300W Ct with no NaCl) is important that it can allow for enhanced solubility. That is because the amine group lone pair of electrons increases the interaction of the polymer with water by attracting adjacent protons and forming intermolecular bonds with water molecules (127, 130). However, the DD% of the 300W no NaCl was found to be the lowest, and the reason should be further investigated.

Table 3.5: Elemental analysis of control and microwave treated Ct

Sample Name	N% w	C% w	C/N ratio	DD%
Control Ct	3.48	29.06	8.35	73.97
300W Ct w NaCl)	3.91	31.91	8.16	68.49
800W Ct w NaCl)	3.71	31.66	8.53	68.94
300W Ct no NaCl)	4.61	35.42	7.68	62.77

3.1.5 Flow time (viscosity) of microwave treated and untreated Ct

The flow time analysis of each of the Ct preparation was investigated with the purpose of determining the changes in chitosan solution viscosity. The flow time of the diluted solution can be indicative of its viscosity, and accordingly, the changes in viscosity are relatable to the changes in the molecular weight. Solutions of polymers with lower molecular weights exhibit lower viscosity (137). As can be seen from table 3.2 and figure 3.5, the longest flow time, as expected, was seen with the control unmodified Ct after three independent runs and taking the average, followed by a statistically significant decrease in the flow time of all Ct preparations treated with microwave ($P < 0.0001$). However, it is noteworthy that the flow time in the microwave Ct with NaCl was significantly higher than the one without NaCl ($P < 0.0001$), supporting by this the claim that NaCl increases solution conductivity (127),

resulting in higher Ct degradation, albeit, microwave irradiation alone (as can be seen from 300W no NaCl) can also produce significantly lower viscosity than the untreated Ct and hence, lower Mw. The highest reduction in Mw was seen with the 800W Ct with NaCl.

Table 3.6: Flow time (Viscosity) of control and microwave treated chitosan

	Flow time (min: sec) (Net flow time)			Flow time (min: sec) ± SD	Average net flow time (min: sec) ± SD
Sample	Flow 1	Flow 2	Flow 3	Average	
Solvent (2% HAc)	1:09	1:08	1:08	1:08 ± 0.0004	NA
Solvent (2%Hac + 0.9% NaCl)	1:12	1:12	1:12	1:12 ± 0.000	NA
Control Chito	12:53 (11.75)	12:59 (11.85)	13:01 (11.88)	12:57 ± 0.001	11:49 ± 0.001
300 W w NaCl	3:56 (2.73)	3:59 (2.78)	3:59 (2.78)	03:58 ± 0.001	02:46± 0.001
800 W w NaCl	2:41 (1.48)	2:47 (1.58)	2:48 (1.6)	02:45 ± 0.0005	01:33± 0.0005
300 W no NaCl	4:43 (3.58)	4:43 (3.58)	4:43 (3.58)	4:43 (3.58)	3:35 ± 0.00

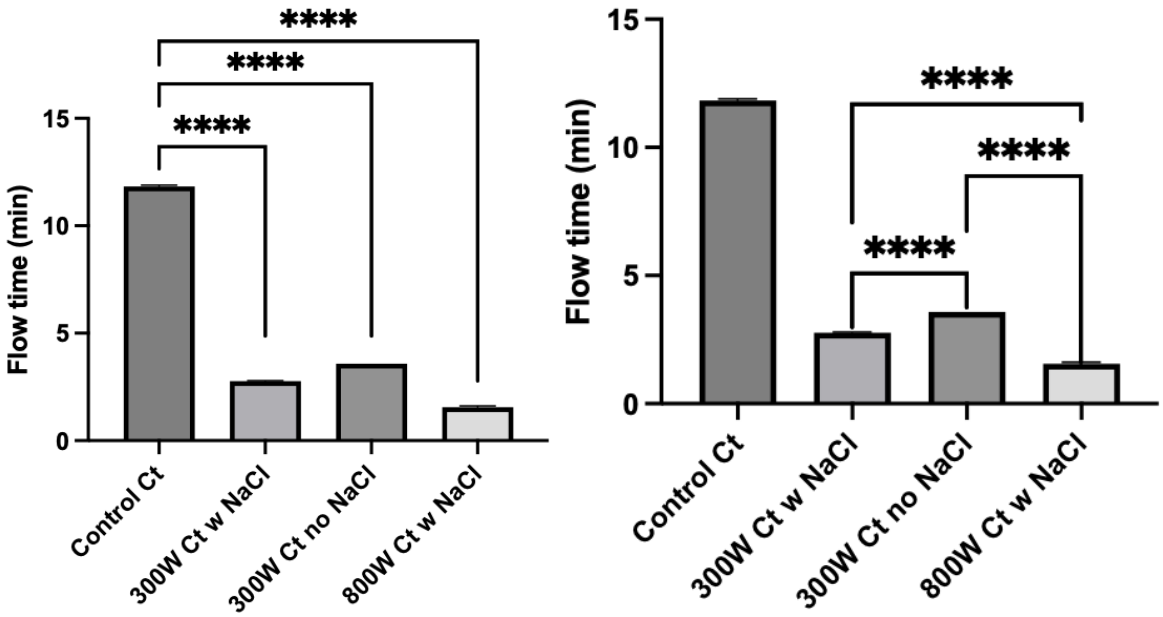

Figure 3.23: Flow time (Viscosity) of control and microwave treated Ct.
Statistical significance was determined using One-way Anova test (****= statistically significant with P-value < 0.0001).

3.1.6 Thermal profile of microwave treated and untreated Ct (DSC)

Figure 3.6 illustrates the thermal profile using differential scanning calorimetry for the microwave treated and untreated Ct. From the DSC thermogram of control Ct, can be seen a characteristic endothermic peak of chitosan at around 85-118°C, and an exothermic peak at around 308°C. The endothermic peak is assigned to the water loss within Ct hydrophilic groups and is called 'dehydration temperature (T_D)'. The exothermic peak can be ascribed to Ct thermal degradation and glycosidic bond cleavage (monomer dehydration and deacetylated units). These findings are comparable to what is reported in the literature (144, 145). Regarding the microwave treated Ct, it is noted that the exothermic peak was lost, the endothermic peak is becoming broader and less prominent, especially in the 300W no NaCl Ct, and longer phase transition was required. This suggests the occurrence of physical changes which include a decrease in the crystallinity of the polymer. In case of the Microwaved Ct with NaCl, eutectic impurities can be seen in their DSC thermogram at around 60°C, which can be attributed to the use of NaCl. The absence of the peak at 308°C can indicate that microwave treated Ct started decomposing after a temperature of 300°C.

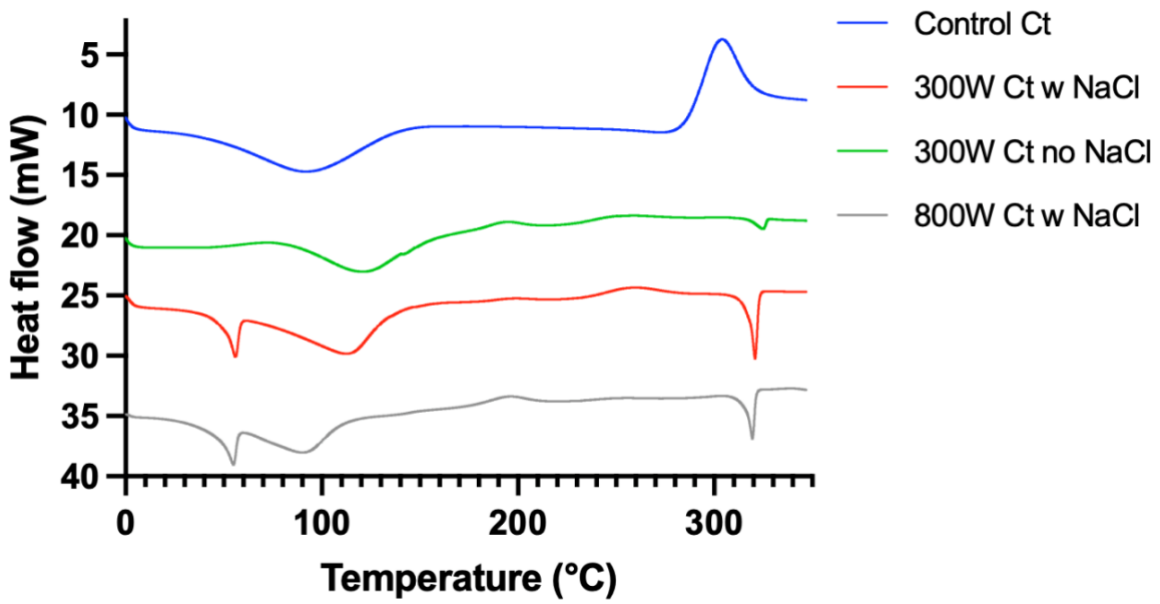

Figure 3.24: differential scanning calorimetry (DSC) of microwave treated and untreated Ct.

3.1.7. Solubility studies of microwave treated Ct

Four calibration curves were made for control, 300W and 800W Ct with NaCl, and 300W no NaCl for the concentrations 0.25, 0.5, 1, 2, 3 mg/ml. The solubility was assessed in 2% HAc solution at room temperature (Figure 3.7). From the graph, it can be seen that, in general, the microwave treated Ct preparations showed an improved solubility in a total period of 2h (120 mins) in comparison to the control Ct. 300W Ct in particular, either with or without NaCl, outperformed each of the control Ct ($P < 0.0001$) and 800W Ct ($P < 0.0005$), by being able to reach the concentration threshold (3 mg/ml) after only 5 mins compared to 2h in both cases. These findings are in alignment with the XRD analysis, as the 300W showed lower crystallinity than both control Ct and 800W due to the reasons mention in section 3.1.3, and hence, more amorphous Ct preparation is expected to show better solubility due to the higher availability of surface area that can interact with the solvent.

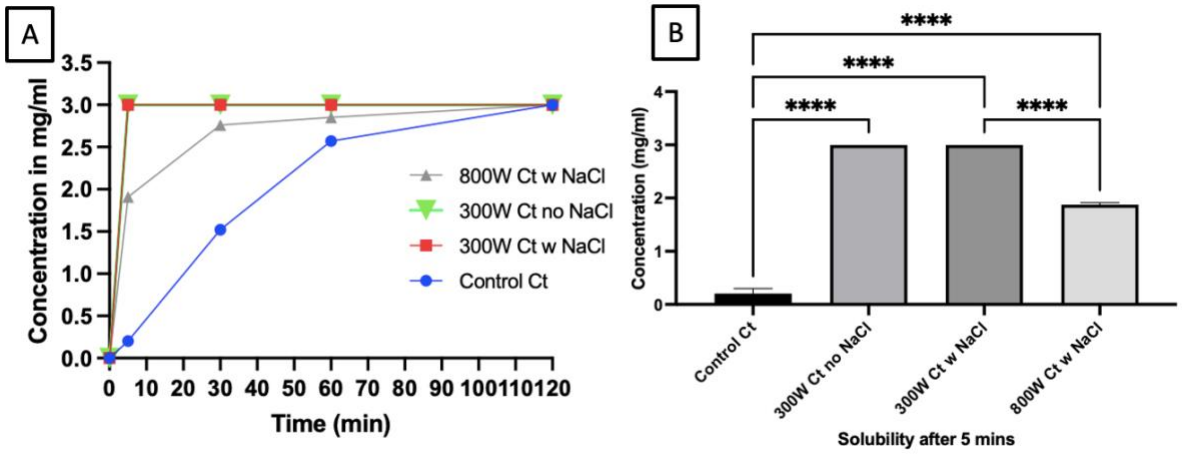

Figure 3.25: A) Control and microwave Ct solubility intervals for 2h, and B) Solubility after 5 mins. Statistical significance was determined using One-way Anova test (****= statistically significant and $P < 0.0001$).

3.2 Physicochemical Characterization of Chitosan-Curcumin Conjugates (CCC):

For proceeding with conjugation, the Ct preparation chosen for conjugation with CURC was 300W Ct not treated with NaCl in addition to the control Ct, for the reasons mentioned in Chapter IV.

3.2.1 Characterization Using Fourier Transform Infrared (FTIR) Spectroscopy

The FTIR spectrum in figure 3.8 supports the formation of CURC-Ct conjugates by showing the characteristic peak of the imine link (C=N stretching vibration) within the expected range of 1640-1690 cm^{-1}. This is a strong piece of evidence and a classic characteristic of a Schiff base, supporting the formation of a conjugate between CURC's aldehyde group and Ct's amine group, especially, because the imine peak is not present in the spectra of both individual components. Furthermore, Ct amide I, II and III characteristic bands (regions 1650, 1550, and 1310 cm^{-1}, respectively) are present in the CCC spectrum. The N-H bending in the amide I and II peaks is noticeably shortened in the CCC spectrum compared with Ct alone, suggesting that that the -NH2 group in CCC is now occupied by the carbonyl group of CURC, and hence converted to the N=H of the imine, as evident from the

new imine peak in CCC spectrum. On the other hand, the fingerprint stretching of CURC is apparent in the CCC spectrum in the region 400-700 cm^{-1}. In addition, the O-H stretching seen in 3000-3500 cm^{-1} is broader and more prominent in the CCC conjugate compared with Ct alone, suggesting that the O-H groups in CURC are incorporated into the CCC conjugate. All these observations suggest a successful conjugation between CURC and Ct, and a combination of both CURC and Ct components in the newly formed CCC conjugate.

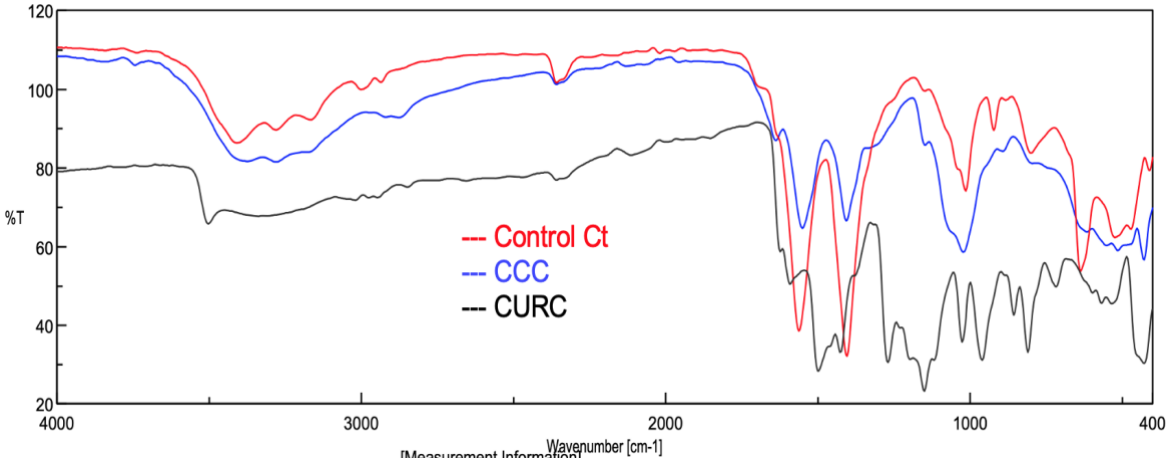

Figure 3.26: FTIR spectrum of Control Ct, CCC and CURC

3.2.2 X-Ray diffraction analysis (XRD) and assessment of the crystalline nature

Figure 3.9 illustrates the X-Ray diffraction patterns of each of Ct, CURC and CCC. Chitosan typically shows broad peaks due to its semi-crystalline nature, with amorphous regions from the polysaccharide chains. Curcumin exhibits sharp and intense peaks, indicating a highly crystalline structure. These peaks correspond to the specific crystallographic planes of curcumin's crystal lattice. XRD analyses of CCC suggest the formation of a new compound. The spectrum for CCC that differs from both Ct and CURC, having intensity higher than Ct spectrum but lower than the crystalline CURC spectrum is an indicator of a new phase or altered crystalline structure, which align with the creation of a new conjugated material. This change in the XRD pattern can result from the Schiff base

linkage altering the molecular arrangement, leading to a new crystalline or amorphous structure. Furthermore, there are mutual peaks between CCC spectrum with Ct at (2-theta 11.54° and 29.79°), CURC (2-theta 17.17°, 19.23°, 20.52°, 22.71°, 26.98°) and both of Ct and CURC (2-theta 8.87°, 16.98°, 22.71°, 31.26°). Moreover, the conjugation process is suggested to disrupt the orderly crystal lattice of curcumin by introducing more amorphous characteristics from chitosan, rendering the resulting spectrum exhibit broader peaks or less defined crystalline patterns. The differences in crystallinity and the presence of new diffraction patterns in the CCC sample are indicative of structural changes at the molecular level, likely due to the formation of new covalent bonds between curcumin and chitosan. This aligns with the expectation of a Schiff base reaction altering the material's physical properties, including its crystalline structure.

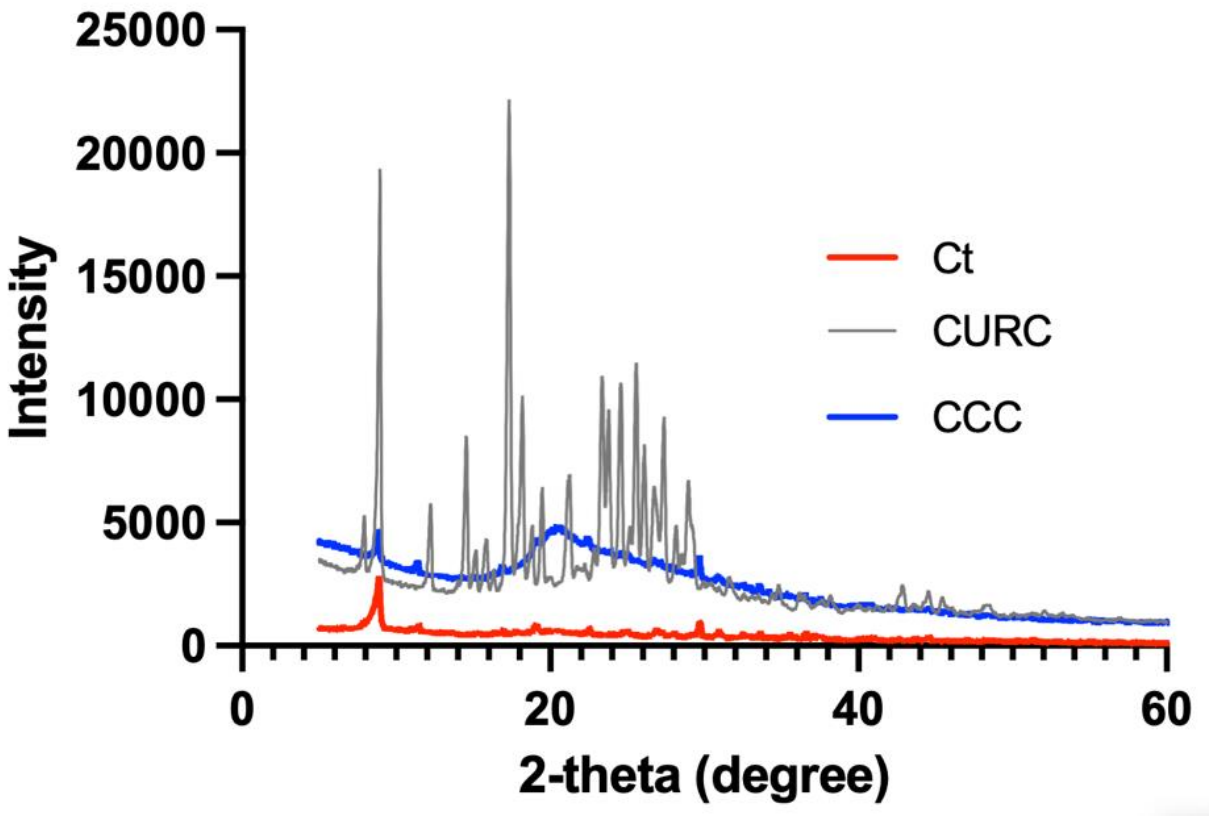

Figure 3.27: X-Ray diffraction patterns of Control Ct, CURC and CCC

3.2.3 Thermal profiles and differential scanning calorimetry (DSC)

Figure 3.10 illustrates the distinct thermal profiles of Ct, CURC and CCC. Curcumin typically shows a sharp melting endothermic peak at 176.3°C (CURC's melting point T_m=175 (146)), which is followed by a decomposition peak at higher temperatures. This sharp peak indicates that the substance is crystalline, given the abrupt drop in endothermic peak that appeared where the melting point is expected. In case of Ct curve, due to the size distribution of the crystallites, partially crystalline polymers like Ct produce broad melting peaks. The same observation is seen with the broad peaks of CCC conjugate. Moreover, The CCC curve lacks the sharp CURC peak at around 176.3°C and shows a typical Ct curve with slight changes, such as the shift in the exothermic peak from 308°C in Ct alone to 277°C in CCC. This alludes to potential changes in the thermal stability and behavior due to the conjugation. In addition, a new small endothermic peak in CCC curve at 328°C which can indicate weightlessness as a result of CCC decomposition after this temperature. In conclusion, the DSC analysis indicates distinct thermal transitions that do not align with the known properties of either CURC or Ct alone, in support of the formation of a new substance.

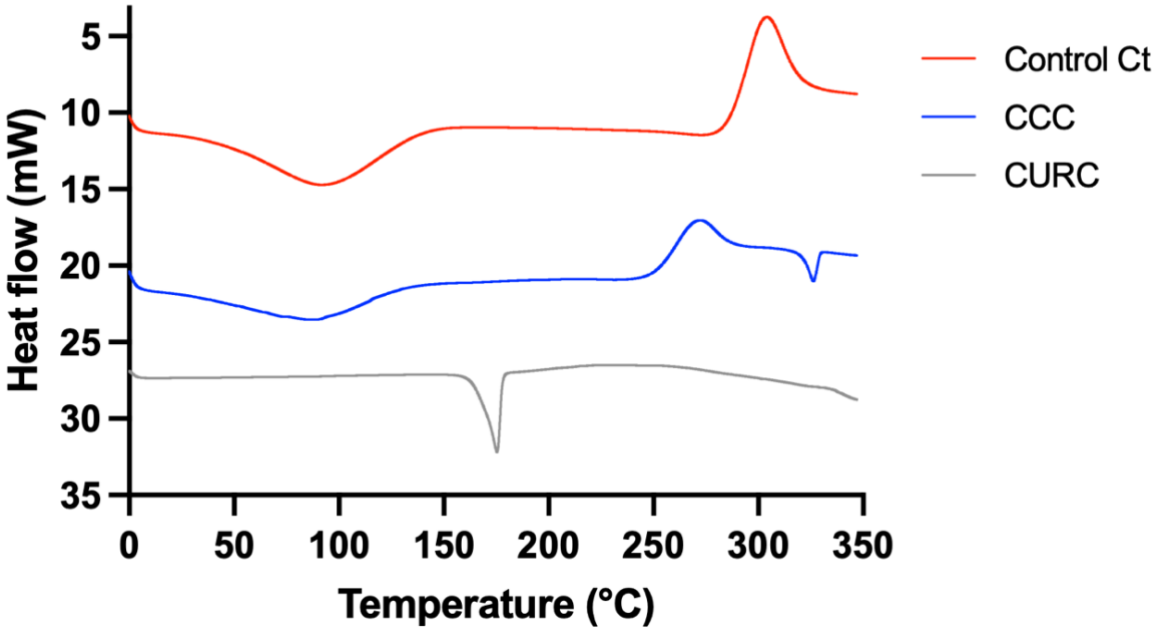

Figure 3.28: differential scanning calorimetry (DSC) of Control Ct, CURC and CCC

3.2.4 Carbon-nitrogen (CN) elemental Analyses

As can be inferred from table 3.3, the CN analysis data indicates an increase in nitrogen content in the CCC compared to the control chitosan sample, which is consistent with the introduction of the aldehyde group reacting with the amine group of chitosan. The absence of nitrogen (%N = 0) in the curcumin sample is expected, as CURC does not contain nitrogen in its molecular structure. The high carbon content (%C = 68.004) aligns with the aromatic and extensive conjugated system in CURC.

With regards to Ct, the presence of nitrogen (%N = 4.083) is consistent with chitosan's structure, which includes amino groups (-NH_2) along the polysaccharide chain. In case of CCC, the increase in both nitrogen (%N = 6.226) and carbon (%C = 38.992) content in the CCC sample compared to Ct alone suggests a successful conjugation. The higher nitrogen content could be due to the introduction of additional nitrogen from the CURC carbonyl groups reacting with the Ct's amine groups, possibly through Schiff base formation or other types of conjugation such as amidation or esterification. It can also suggest that more than

one Ct molecule containing nitrogen (from the amino groups in Ct) reacted with one molecule of CURC in more than on position, knowing that CURC has more than one carbonyl groups in its structure (Section 1.3, Figure 1.5). By this, the availability of more than one carbonyl group in CURC to react with Ct makes reasonable explanation of the increase in nitrogen content seen with the CCC conjugate in comparison to Ct alone.

Table 3.7: Carbon nitrogen elemental analysis of Control Ct, CURC and CCC

Sample Name	N%w	C%w
Control Ct	4.083	24.279
CURC	0	68.004
CCC	6.226	38.992

3.2.5 Percent yield and drug loading efficiency

After preparing the CCC conjugates by reacting Ct with CURC, the percent yield was recorded as follows:

- Control CCC:
    - Yield: $\frac{127.3 \text{ mg CCC}}{64 \text{ mg Ct} + 92 \text{ mg CURC}} \text{ x } 100 = 81.60\%$
- 300W CCC:
    - Yield: $\frac{126.6 \text{ mg CCC}}{64 \text{ mg Ct} + 92 \text{ mg CURC}} \text{ x } 100 = 81.15\%$

For determining the loading capacity, the supernatant after washing was collected, and the following calibration curve (Figure 3.9) was created using HPLC based on the method described in section 2.5.8, for the concentrations 0.001, 0.002, 0.005, 0.01, 0.015, 0.02, 0.03, 0.05, and 0.1 mg/ml. Then, the amount of curcumin in CCC was subtracted from the amount of in the supernatant and was found to be 43.68 ± 0.26 and 32.4 ± 0.25 for Control CCC and 300W CCC, respectively, and hence the loading capacity was calculated to be 47.48 ± 0.29 mg and 35.27 ± 0.28 mg for Control CCC and 300W CCC respectively.

Curcumin in 1mg of control CCC and 300W CCC was found to be 0.343mg/mg and 0.213mg/mg (w/w), respectively.

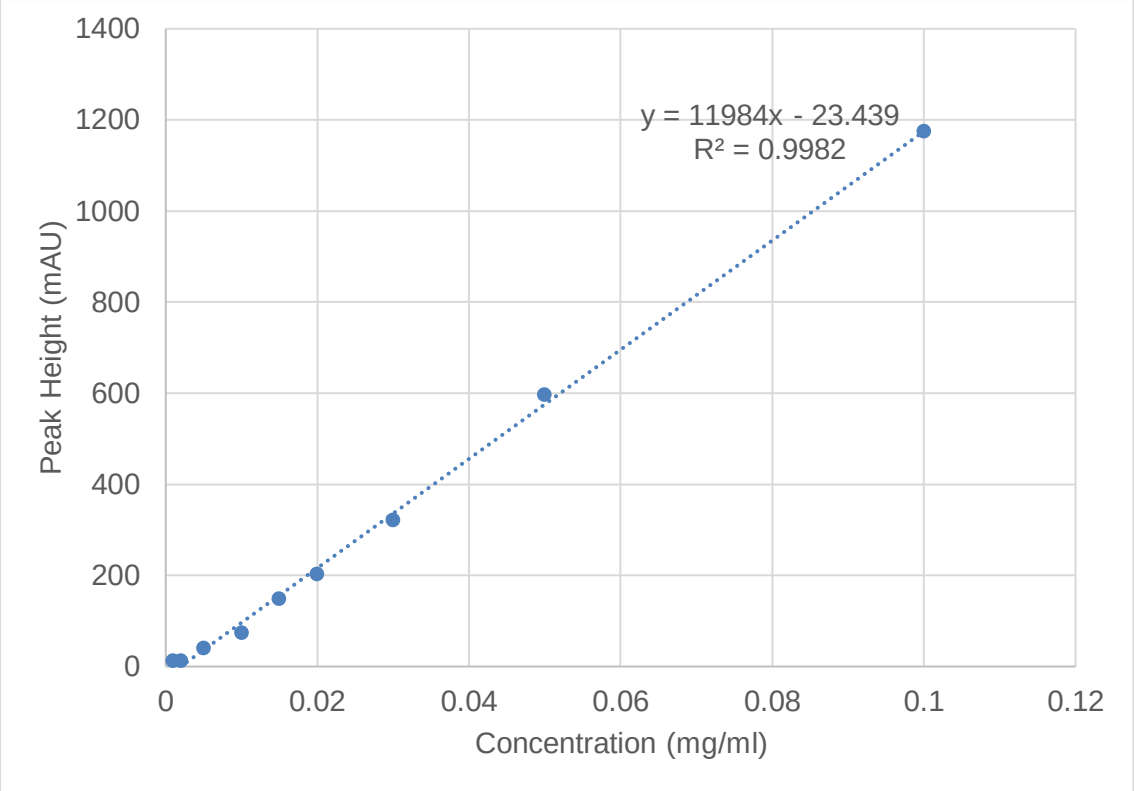

Figure 3.29: Calibration curve of different CURC concentrations (in mg/ml) using HPLC.

3.2.6 Solubility and stability studies of CCC in different solvents and pHs:

3.2.6.1 Solubility of CCC in different solvents:

Trials of dissolving the new CCC conjugate in various aqueous and organic solvents were done for 24h. Ethanol, water and HAc have been investigated as possible solvent relying on the fact that Ct dissolves in diluted HAc and CURC dissolves in ethanol. As can be seen from Figure 3.12, CCC did not dissolve in either ethanol or water in a concentration of 1mg/ml, although kept for overnight stirring. On the other hand, it completely dissolved in 1% HAc solution in less than 15 min. This suggests that changes in CURC physicochemical properties arose, making it more influenced with the properties of Ct and more soluble in aqueous acidic media.

A B C

Figure 3.30: Trial of different solvents A) HAc 1%, B) Ethanol, and C) distilled water to dissolve CCC at a concentration of 1 mg/ml.

3.2.6.2 Stability of CCC compound at different pHs:

The stability of CCC compound was examined in different pH media: acidic (pH=1.98), slightly acidic-neutral (pH=6.5), and alkaline (pH=12). The FTIR spectrum of each is shown in figure 3.13. The three spectra reveal that the most appropriate pH for CCC conjugates was the acidic media, as it did not cause significant chemical changes in the functional groups in CCC, in addition to the fact that it allowed it to completely dissolve. Only slight elongation in the amide I and II bands are notices, which can indicate partial dissociation of the imine linkage. Whereas, in the other 2 media, the CCC spectrum is almost distorted with obvious changes in the intensities and shapes of the peaks, and appearance of new peaks in new positions, suggesting that the basic media catalyzed the hydrolysis of the imine bond and caused complete dissociation of the imine linkage, or formation of new side products.

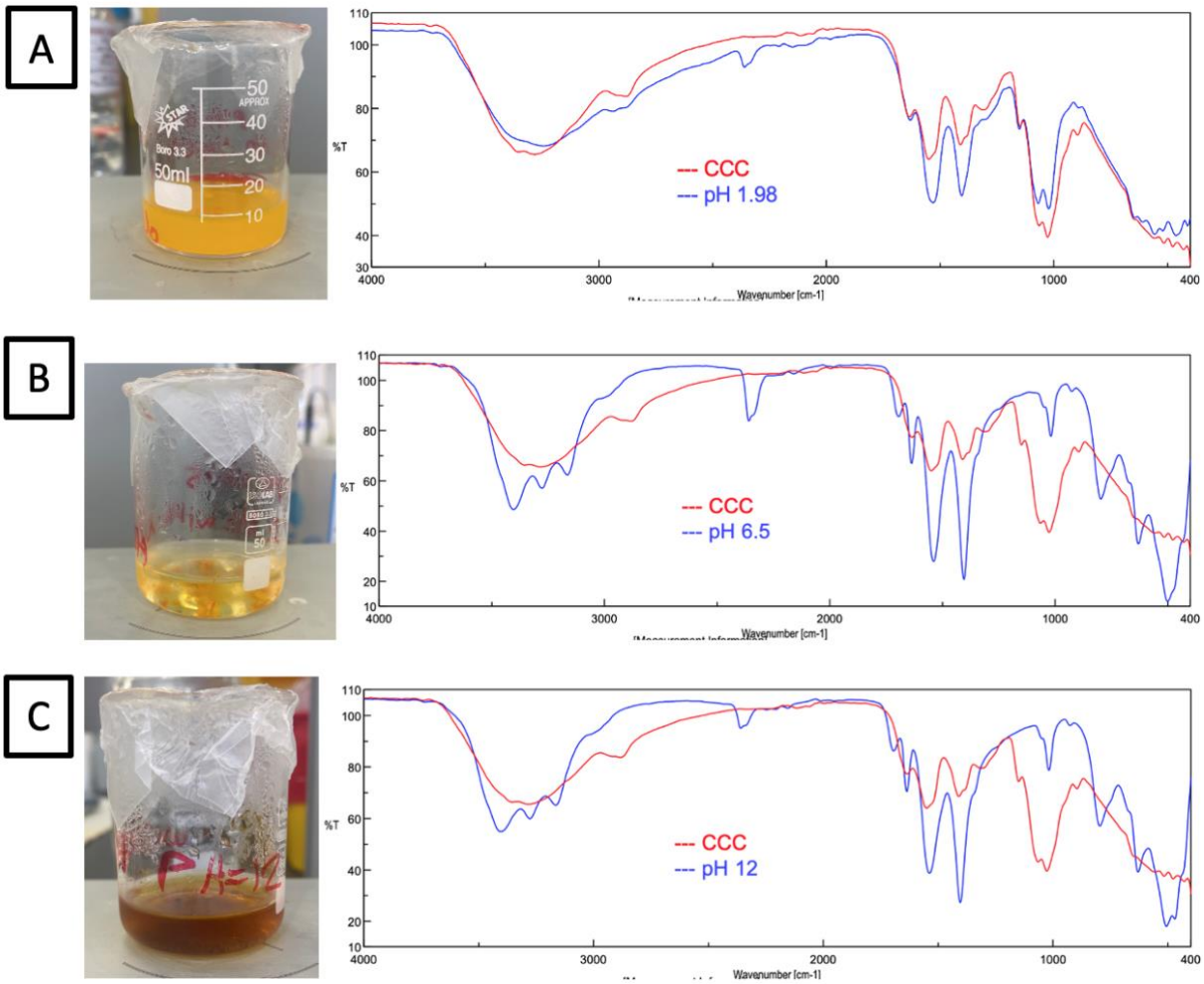

Figure 3.31: Stability of CCC at different pHs: A) 1.98, B) 12, and C) 6.5

3.3 Physicochemical Characterization of Chitosan-Curcumin Conjugates Nanoparticles (CCC NPs):

3.3.1 Size, polydispersity (PDI) and zeta potential (ZP) analysis

The purpose was to determine the hydrodynamic diameter of the formulated nanoparticles, their surface charge, which is represented by the zeta potential, in addition to the polydispersity index (PDI). The PDI is a reflection of the quality of the particles within a sample in terms of their size distribution. The closer it is to 0 is the narrower the size distribution and the more uniform the particles are (147). The optimization of the size, PDI and ZP was attained after various trials of changing different parameters (Table 3.4) Control Ct NPs had an average size, PDI and ZP of 131.5±5.21 nm, 0.487±0.1 and 40.8±1.04 mV,

respectively. 300W Ct had an average size PDI and ZP of 80.77±1.08 nm, 0.481 ± 0.03, and 38.3±5.17 mV, respectively. The size of the microwaved Ct NPs has noticeably decreased in comparison to the normal chitosan as an indication of the success of microwave in reducing the molecular weight of Ct. Regarding the NPs containing CURC, Control CCC showed an average size, PDI, and ZP of 95.31±0.17 nm, 0.467±0.07, and 29 mV± 1.21, respectively, and 300W CCC showed an average size, PDI and ZP of 71.19 ± 0.52 nm, 0.382 ± 0.01, and 26.2 ± 0.93 mV, respectively. The positive ZP is important for cellular uptake. This is because of the negatively charged sialic acid moiety in the cellular membrane that will attract the positively charged NPs and thus facilitate cellular uptake and allow CURC to penetrate the mucosal layers of the colon (112, 148). The decrease in the ZP of the control CCC and 300W CCC NPs is strong evidence that CURC is incorporated inside the NPs, because curcumin typically has a negative ZP. However, and despite CURC integration, the ZP remained high (above +20 mV) for better repulsion between the NPs and better attraction to the negatively charged cellular membrane as mentioned before. The smaller size seen in the NPs containing CURC compared to the empty Ct NPs is another indication of the successful formation of nanoparticles from the conjugates of both Ct and CURC. This is due to the fact that CURC has a Mw of 368.38 g/mol and Ct polymer has much higher Mw ranging from 50,000 to 190-000 g/mol. Hence, the Ct polymer containing portions of CURC that has a low Mw will be expected to show smaller NPs, because the molecular weight is directly proportional to the nanoparticle size (130).

Table 3.8: NPs optimization trials results:

Trial no.	Z-Average Size (nm)	PDI	Zeta Potential (mV)
1	3823.3	0.537	23.2
2	248.1	0.583	19.1
3	248.2	0.583	19.1
4	130.9	0.224	17.2
5	133.2	0.212	17.5

6	422.6	0.576	24.5
7A (Ct NPs)	131.5	0.487	40.8
7B (CCC NPs)	95.3	0.467	29

3.3.2 Morphological studies using Atomic Force Microscopy (AFM) and Transmission electron microscopy (TEM)

The morphology and surface topography of Ct and CCC nanoparticles was investigated using Atomic Force Microscopy (AFM) and Transmission electron microscopy (TEM). The AFM (figure 3.14) illustrates both two-dimensional and three-dimensional shapes of the control Ct, 300W Ct, control CCC and 300W CCC NPs. The surface roughness was measured by AFM's average surface roughness parameter. It ranged for control Ct from -100 nm to 131.87 nm (skewness=0.36), for 300W Ct it was -235.726 nm to 266.262 (skewness=0.382). For control CCC it was -163.52 nm to 182.49 nm (skewness= 0.456) and finally, for 300W CCC it was -130.215 nm to 142.301 nm (Skewness= 0.855). Overall, these results suggest NPs that are spherical in shape and having a rough surface. The roughness can be attributed to the natura of the used Ct polymer that was less prone to collapsing upon tapping by the AFM cantilever.

TEM results hence provides more detailed insights into the surface morphology and size of the NPs. From figure 3.15, the TEM showed perfectly round NPs with well identified edges and narrow size distribution in case of both control Ct and control CCC NPs. However, with regards to the 300W treated NPs, although the NPs were round in shape, they were not as smooth as the ones seen with the control group suggesting that potentially the treatment with microwave irradiation had some impact on the texture and appearance of Ct polymer.

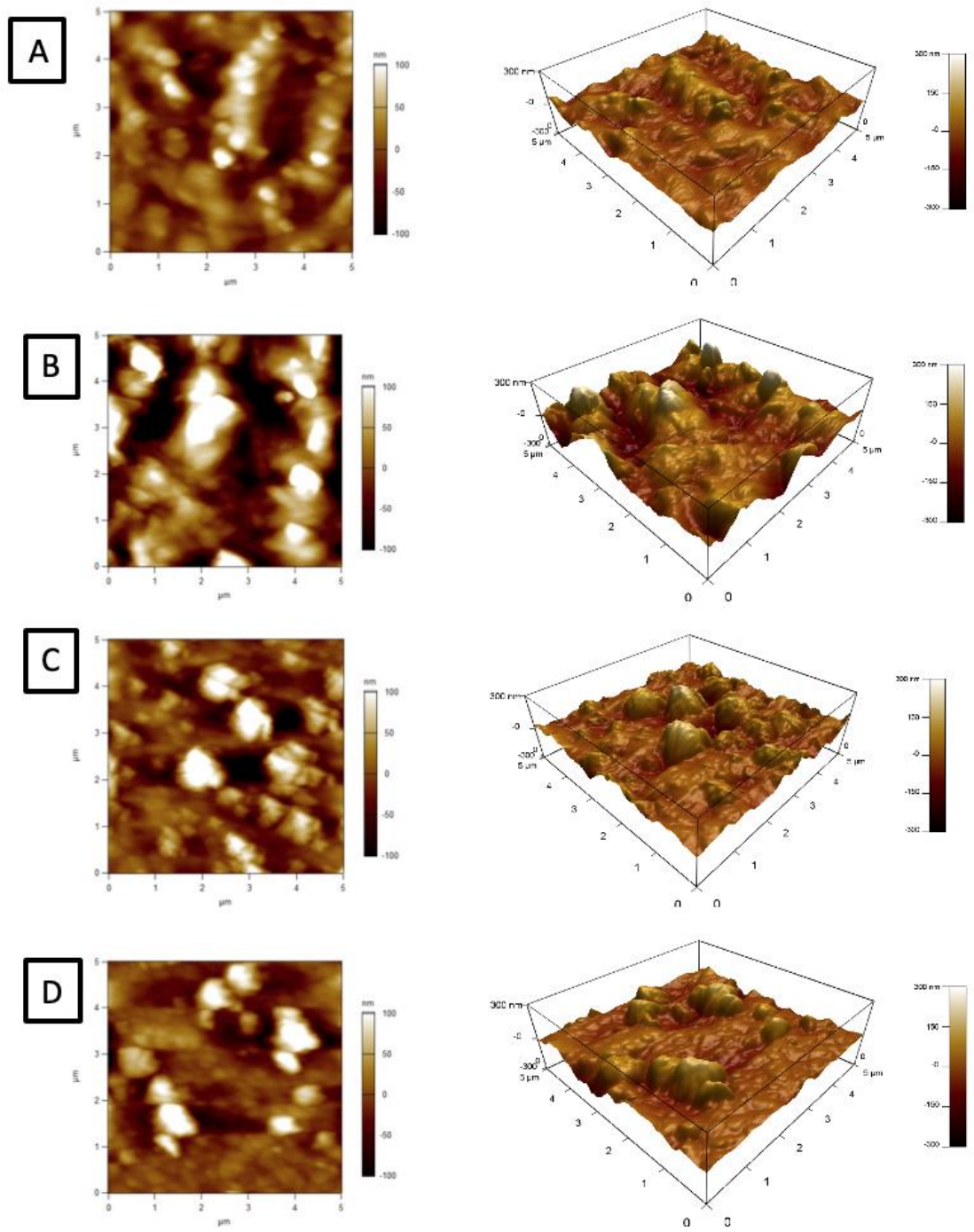

Figure 3.32: AFM analysis of the nanoparticles of A) Control Ct, B) 300W Ct, C) Control CCC, D) 300W CCC

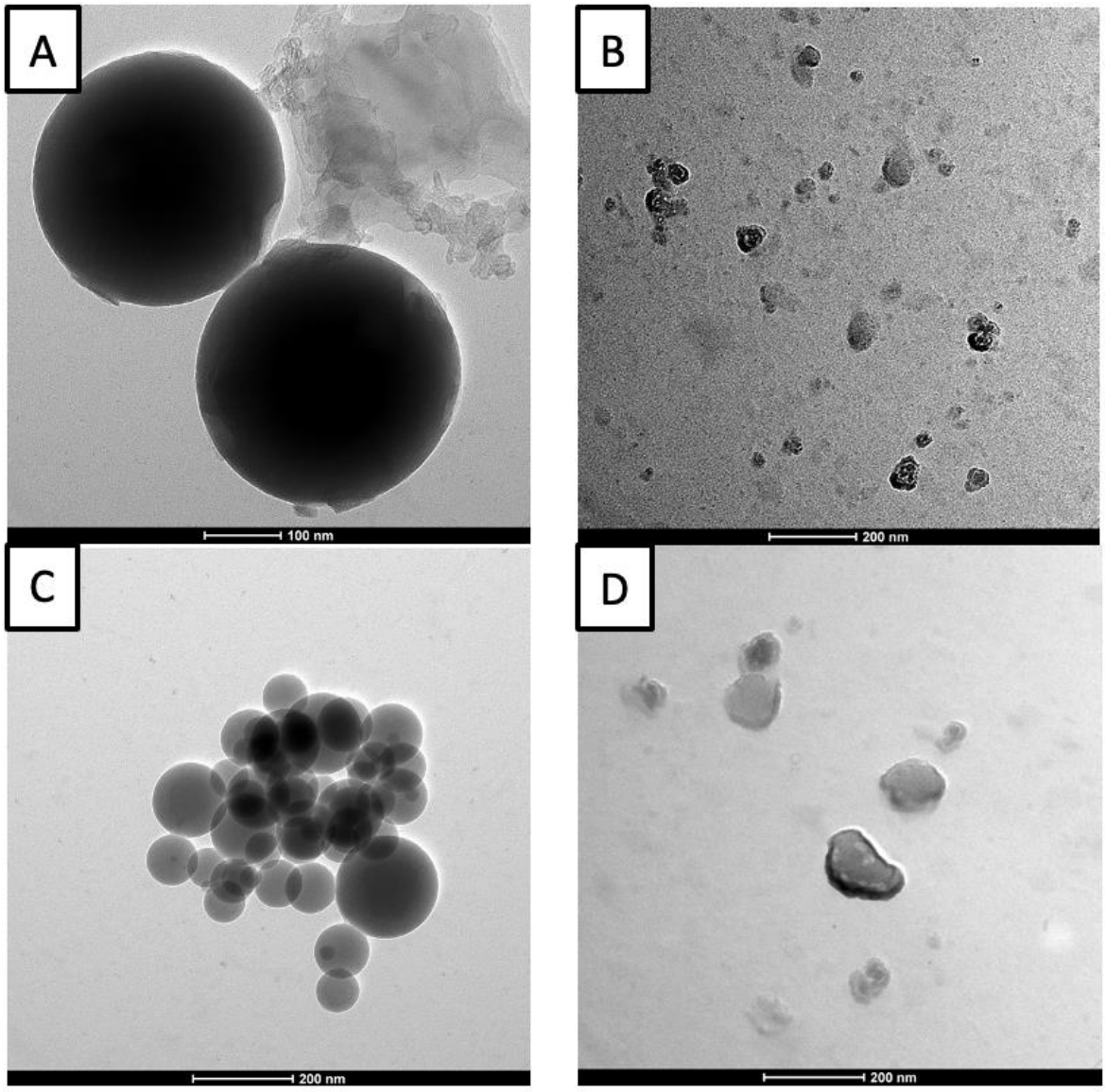

Figure 3.33: TEM Images of A) Control Ct, B) 300W Ct, C) Control CCC, D) 300W CCC

3.3.3 Stability studies on Ct and CCC NPs

The stability of Ct and CCC NPs at two different temperatures (RT and 4°C) was assessed to determine the appropriate storage temperature. The stability was additionally assessed every 7 days over a period of 28 days to study the changes in size, PDI and ZP of NPs with time. From figure 3.16 and by day 7, it can be noted that each of control Ct, 300W Ct, and 300W CCC are maintaining good stability (no significant changes in size, PDI and ZP with time in both temperatures). However, a significant increase in size of control CCC

by almost 4-folds at RT and around 2-fold at 4°C occurred. This can suggest that either transient agglomeration might have taken place because the size started decreasing after day 7, or that temperature had an influence on the size of the NPs, as this jump in size was not as evident in the control CCC NPs at 4°C. On the other hand, 300W CCC showed excellent stability profile at both storage conditions and in terms of size and PDI during the 28 days period. As expected, the empty Ct formulations in general maintained a nearly constant size throughout the 28-day period. A PDI around 0.5 was maintained. From table 3.5, it can be seen that and a positive and high ZP was also maintained in all samples (above +30 and +20 mV for Ct and CCC, respectively).

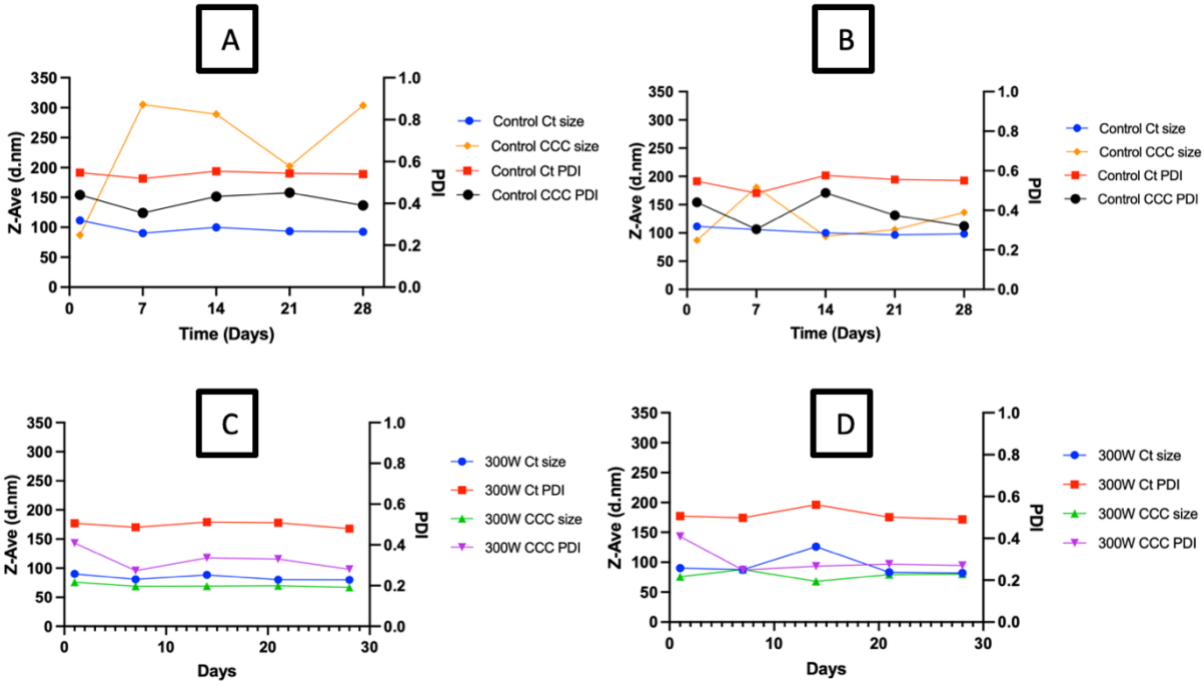

Figure 3.34: Changes in size and PDI of Control Ct & CCC at RT (A) and 4°C (B), and 300W Ct & CCC at RT (C) and 4°C (D) for days to 28.

Table 3.9: Zeta potential of of Control Ct & CCC at RT (A) and 4°C (B), and 300W Ct & CCC at RT (C) and 4°C (D).

	Day 1 ZP, RT	Day 7 ZP, RT	Day 14 ZP, RT	Day 21 ZP, RT	Day 28 ZP, RT
Control Ct	36 ± 2.36	34.3 ± 2.78	34.8 ± 1.23	35.1 ± 1.21	33.2±1.1
300W Ct	34.7 ± 2.68	35.1 ± 0.95	33.8 ± 1.55	34.2 ± 4.03	36.6±1.43
Control CCC	30 ± 1	24.2 ± 0.8	23.6 ± 1.15	32.6 ± 1.01	30.8±0.44
300W CCC	23.9 ± 1.5	27.1 ± 1.82	31.8 ± 0.85	26 ± 1.5	25.2±0.31
	Day 1 ZP, 4°C	Day 7 ZP, 4°C	Day 14 ZP, 4°C	Day 21 ZP, 4°C	Day 28 ZP, 4°C
Control Ct	36.0 ± 2.36	38.1 ± 0.47	37.4 ± 0.721	36.2 ± 1.25	35.7±1.04
300W Ct	34.7 ± 2.68	35.7 ± 0.92	34.9 ± 0.115	34.5 ± 0.52	35.47±2.4
Control CCC	30.0 ± 1.0	32.8 ± 0.59	31.6 ± 0.737	30.9 ± 1.19	31.8±0.72
300W CCC	23.9 ± 1.5	24.1 ± 0.50	23.8 ± 0.802	23.6 ± 0.7	24.73±0.74

3.4 In vitro Studies

3.4.1 In vitro drug release studies:

The in vitro drug release profiles of both control and 300W CCC NPs was tested to study the hypothesis whether the conjugation of CURC to Ct will result in a controlled release and will avoid the initial burst release seen with encapsulated drugs (149). The pH of PBS (release medium) was adjusted to 6.7 to simulate the colonic medium (as explained in section 1.1.1) and HCl was used to emulate the gastric acid in humans (12). After each time point, an Eppendorf® tube was sacrificed and its CURC content was calculated and represented in figure 3.17. The amount in each independent tube after each time point was calculated and presented in the figure without subtraction from the previous time point based on the followed procedure. From the figure, it can be noted that both Control and 300W CCC showed a slight burst release at first, followed by controlled release kinetics by maintaining

similar release over the tested period. However, with the 300W CCC NPs can be seen a slight initial increase in release in the first hour by around 5% (4.95%) compared with the following intervals, whereas it is not showing with control CCC NPs. This can be due to more curcumin being released with the dissolution of the outer layer of the 300W CCC NPs, because microwave irradiation resulted in smaller Ct molecules, which resulted in smaller NPs having higher surface area to interact with the solvent, and are hence more readily available for dissolution and releasing curcumin faster and more than control CCC NPs, as can be seen from figure 3.17. It is also noteworthy that the 300W CCC NPs outperformed the control CCC NPs and produced higher release of CURC after 96h (24.59% vs 16.90%, for 300W vs Control CCC NPs, respectively, p -value <0.0001).

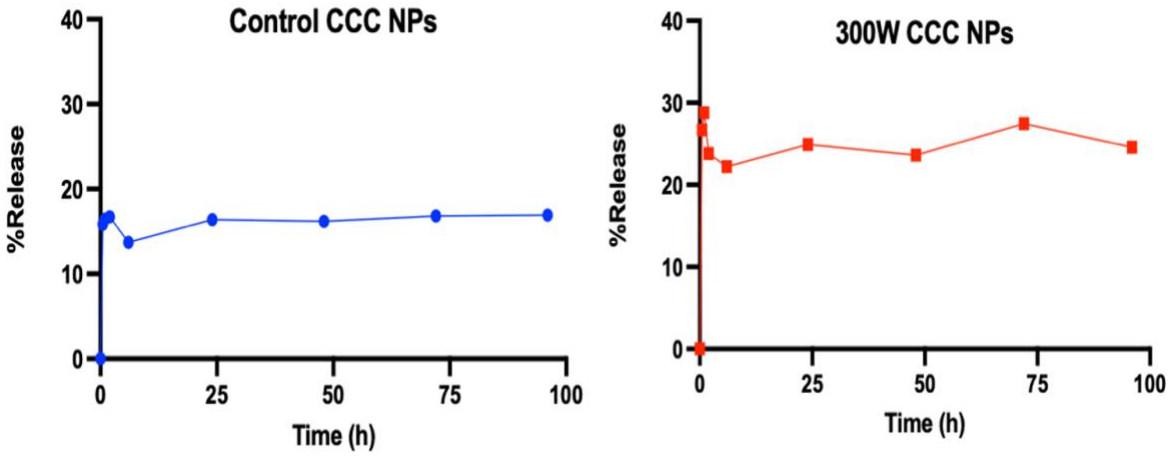

Figure 3.35: In vitro profiles of CURC release from A) control CCC and B) 300W CCC over 96 hours at pH 6.7.

3.4.2 In vitro cytotoxicity assay:

The cytotoxic effect of both control and 300W CCC, free curcumin, 5-FU as a positive control was assessed in the two colon cancer cell lines, HCT-116 and LoVo, using CCK8 assay. Untreated cells were considered as negative control. CCk8 is an activity and cell proliferations assay used for the purpose of determining cell viability. It contains 2-(2-

Methoxy-4-nitrophenyl)-3-(4-nitrophenyl)-5-(2,4-disulfophenyl)-2H-tetrazolium monosodium (WST-8) salt, which can be, in the presence of dehydrogenase in viable cells, reduced into the orange-colored, water soluble formazan. The optical density of this formazan can then be detected and used to estimate cell viability. Higher OD correlates to higher cell viability and lower cytotoxic effect and vice versa. CCK-8 has the advantage of exhibiting higher detecting sensitivity compared with other assays containing tetrazolium salt such as MTT (150). From figure 3.18 A, in general, a dose dependent cytotoxic effect is seen in HCT-116. A decrease in cell viability is seen with the increase in drug concentration for both control and 300W CCC. Furthermore, at the lowest dose, both formulations were able to significantly reduce cell viability compared to the negative control ($p \leq 0.001$ and for both), yet free CURC was still showing a superior effect to both at the lowest dose. However, with the increase in dose, the differences in performance between control CCC and 300W CCC started emerging. The 300W outperformed the control CCC as it showed no difference to CURC's cytotoxic effect at a concentration of 25 μM, and at the highest concentration (50 μM) the effect was superior free CURC ($p \leq 0.0001$) and comparable to the positive control 5-FU ($P > 0.5$). In the other hand, control CCC did not show any superiority over free CURC or 5-FU at any dose, however it showed a comparable effect to CURC at 50 μM.

For LoVo cell line, and from figure 3.18 B, a similar clear trend of a dose dependent response with regards to 300W CCC was seen. Nevertheless, this was not the case with the control CCC, which showed non-statistically significant decrease in cell viability with the increase in concentration from 12.5 to 25 μM (66.0% VS 61.1%, $P = 0.99$) and from 25 to 50 μM (61.1% vs 45.5%, $P = 0.157$). Both formulations showed comparable effect to free CURC at the lowest dose and up to the highest dose. It is also noteworthy that the two formulations also provided comparable effect to the positive control 5-FU, and the 300W CCC was even superior to 5-FU at a concentration of 50 μM ($P < 0.05$). By this, 300W CCC exhibits a

superior effect to control CCC in both HCT-116 and LoVo cell lines, and both formulations provide an effect that is at least comparable to free CURC.

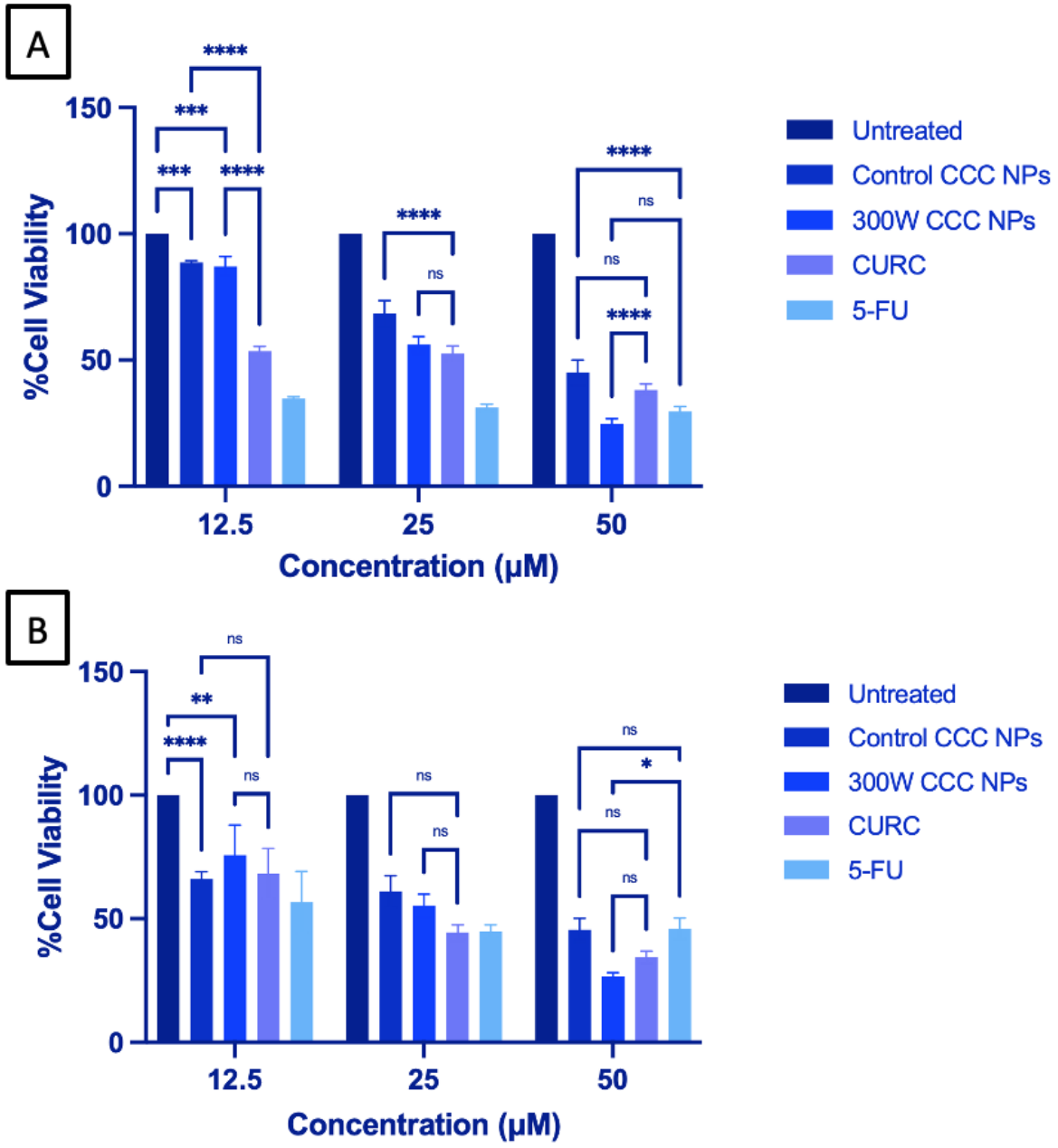

Figure 3.36: Cell viability of A) HCT-116 and B) LoVo cell lines treated after 48h. Statistical significance was determined using Two-way Anova test and Tukey multiple comparisons tests. P-value of ≤ 0.05 was considered statistically significant (**** P-value ≤ 0.0001; *** P-value ≤ 0.001; ** P-value ≤ 0.01; * P-value ≤ 0.05; ns P > 0.05).

CHAPTER IV: DISCUSSION

In this project I aimed to develop a novel approach for the conjugation of CURC in Ct nanoparticles. A detailed review of the etiology and incidence of colon and colorectal cancer has been presented in Chapter 1. One of the key constraints to realizing efficient therapeutics in cancer management is the indiscriminate effect of the anticancer agent on body, thus healthy cells get exposed to unwanted treatment. This is the main cause of side effects in anticancer therapy. Thus a paradigm in anticancer treatment is evolving, based on the use of targeted delivery of the therapeutic, thereby sparing the healthy cells from unwanted effect (151). Whilst this approach is rational and the source of intense research in the medical and pharmaceutical fields, the practicality in clinical practice of polymeric nano-formulations is deemed promising in providing solutions for problems seen in nanomedicine (152, 153). Another approach to managing cancer is by the use of anticancer agents of plant origin, and especially those that manifest equipotent anticancer effects and milder on normal tissue (154). Some of such anticancer agents may have specific affinity to cancer cells and able to arrest the growth of the cancer with no measurable effects on normal tissue. One such anticancer agent is CURC, a well-studied anticancer agent that is also widely used as a condiment (55). The fact that it is used as a condiment adds to the assurance of its safety for use as an anticancer agent. However, CURC is poorly soluble and its anticancer effects are not fully realized unless some form of modification to its chemical structure or formulation is done. In this project, I aimed to focus on formulation approach to improve the anticancer (colon cancer) efficacy of CURC. Nanoparticles have become an indispensable tool for the deployment of CURC into cancer tissue. This is because of their low particle size to volume ratio. Traditional nano-encapsulation methods of CURC involves the physical presence of CURC in the particle, with the possibility of leaching out freely. This will compromise any potential anticancer effects. Furthermore, for effect deployment of the nanoparticles into

tumors, it is desirable for the size of the nanoparticle to be as small as possible with the high payload, as described earlier. Putting all together, I developed a novel way of producing small sized nanoparticles. This entailed the application of microwave energy on Ct to depolymerize it and then conjugate the depolymerized Ct with CURC (CCC). This was then studied on colon cancer cell line to establish the degree of cytotoxicity. Extensive characterization was conducted at the various stages in order to understand the observed phenomena. The detailed results are presented in the results section and this section is dedicated to expounding on the key observations made.

The use of microwave energy was the rational choice as it provided environmentally friendly Ct defragmentation, with no significant impact on the main Ct chain or formation of other unwanted functional side products. NaCl was employed in the optimization trials to increase the transfer of the microwave energy in the media and accelerate Ct degradation as suggested by previous studies (127, 155). The microwave treated Ct exhibited a higher degree of absorption compared to the untreated, since depolymerization leads to the generation of polymer fragments with a higher degree of freedom and hence able to absorb the transmitted energy (156). The transmitted energy in the case of Ct yielded two notable peaks at 230 and 290nm. The peak at 230 is ascribable to n-σ* transition due to the NH_2 groups within Ct, whilst the 290nm peak is due to carbonyl and or carboxyl n-σ*transitions. NaCl added the ability to aid in the transmittance of the microwave energy.

The FTIR profiles of the microwave irradiated and control displayed identical peaks in all samples, which is indicative of the retention of the Ct backbone. This is true especially bonds ascribable to amide stretching (1650 cm^{-1}) and bending (1599 cm^{-1}) (125). Indeed, these moieties are relevant during the formulation Ct into nanoparticles. The intensities of these peaks appear to be less within the control Ct, which can be related to stearic hinderance of the indigenous groups prior irradiation. There is shortening of the amide III band at around

1310 cm^{-1}, which can be attributed to the removal acetyl groups. This in turn increases the degree of acetylation. We noticed that this phenomenon was more pronounced in the presence of NaCl. Also, the stretching due to amino groups between the region of 3200 cm^{-1} and 3500 cm^{-1}, is intense in the Ct irradiated without NaCl, which suggests that these groups remain unperturbed without NaCl. Crucially, there appears to be reduction in the degree of deacetylation in Ct treated with NaCl, which as stated earlier is contingent on the ability of NaCl to transfer the microwave energy more efficiently (157).

Ct is semi-crystalline and thus displays both crystalline and amorphous behavior. The peaks obtained from unmodified Ct are consistent with those observed in the literature (144, 158). The 300W treated Ct with NaCl displayed the lowest intensity of peaks, which is indicative of lowest crystallinity. These peaks were observed with an intensity of about 1443 at 2-θ angle of 8.86°, followed by 300W without NaCl (8.9°, 2210), 800W with NaCl (8.95°, 2511), and the highest in the untreated control Ct (8.85°, 2673). A possible explanation of the unexpectedly higher crystallinity with the higher power (800W) is attributable to the microwaves, whereby treatment was reported to preferentially degrade the amorphous regions of Ct initially, followed by the crystalline regions. This preferential degradation consequently leads to an initial increase in the crystallinity of the Ct. The main chains of Ct are constrained during the initiation of depolymerization by the hydrogen bonds and the disordered side chains that have more rotational freedom than the Ct main chai (118). However, as degradation progresses, (recall that the exposure intervals in the 300W Ct were double the exposure time in the 800W Ct), microwave overwhelms and destructs the remaining semi-crystalline structure, which subsequently leads to decreasing its crystallinity (118). The more amorphous the Ct is the more soluble it becomes, as further surface area will be exposed to interactions with the solvent.

The CN elemental analysis indicated that Ct exposed to 300W microwave energy with no NaCl presented the highest N percentage. This high level of N is consequential to the solubility of the degraded Ct since the lone pair of electrons are capable of attracting protons from water and hence going into solution. Thus, whilst it is true that NaCl promotes the transfer of microwave and thus its presence leads to a better degree of fragmentation, microwave irradiation without NaCl as shown here is crucial due to the likely increase in solubility.

The viscosity by flow time of the microwave irradiated Ct were all lowered and statistically significantly different from the untreated Ct. This is expected since there is an indirect correlation between polymer molecular weight and viscosity. The fragmentation causes a reduction in molecular weights. The flow time for 800W treated Ct was shorter than the 300W treated either with NaCl or without, which is attributable to the high-power fragmentation imposed by 800W microwave energy. Furthermore, 300W irradiation with NaCl significantly reduced the flow time, reaffirming the role of NaCl in augmenting the microwave fragmentation effects on Ct.

Thermal analysis provides a means of assessing transformations within chemicals subjected to some form of treatment. As stated earlier in the discussion, Ct displays semi-crystallinity. There is an exothermic peak that occurs at about 308°C, which has been attributed to degradation and glycosidic bond cleavage. It can also be ascribed to the melting of the semi-crystalline domains within Ct. The microwave Ct with NaCl produced eutectic impurities, which can be seen in their DSC thermogram at around 60^{o}C, which can be attributed to the use of NaCl. The absence of the peak at 308^{o}C can be explained whereby microwave treated Ct decomposes beyond 300^{o}C. This is expected because of the reduced molecular weight and hence prone to decomposition at a lower temperature compared to the parent Ct.

Solubility assessment indicated a significant increase in solubility with increase in microwave power. This is in line with the fragmentation process to low molecular weight entities which favor dissolution in aqueous media. The results agree with the data obtained from the XRD studies, where we observed a lower crystallinity in the 300W treated Ct compared to the 800W.

Following extensive characterization of the microwave treated Ct, it was time to conjugate CCC to CURC and then characterize the same. It is important to note that the microwave the microwave treated Ct chosen for conjugation along with the untreated Ct was thee 300W chitosan with no NaCl. This is for the following reasons:

1. The 800W power was hard to control with the use of normal domestic microwave oven such as in my case, hence, the maximum exposure interval that do. In addition, 800W power results showed higher crystallinity and lower solubility in comparison to 300W.
2. NaCl resulted in incomplete conjugation: CURC precipitated once the conjugates were dissolved indicating incomplete/unstable conjugation, unlike the 300W Ct not treated with NaCl and the normal untreated Ct.
3. Treatment with NaCl resulted in irregular shapes of Ct NPs when seen under SEM. Plus, the NPs' size after 21 days significantly increased and black precipitates were noticed with the Ct treated with NaCl, indicating poor stability.

The FTIR spectra obtained from the conjugate was distinctively different from either pure CURC or control Ct. Crucially, peaks akin to either Ct or CURC were also present in CCC. For example, the fingerprint stretching due to CURC is also present in the CCC between 400-700cm^{-1}. Also, the N-H bending in the amide I and II peaks has become shortened in the CCC spectrum compared with Ct alone. This suggests that the amine groups

in CCC has been consumed by carbonyl groups of CURC and subsequently converted to an imine (N=H). The analysis is a clear indication of the formation of the CCC conjugate.

Further analysis was conducted to assess the degree of crystalline transformation of the conjugate, whereby the strong crystalline patterns displayed by pure CURC is non-existent in the CCC. The CCC displays a smoothened intensity but retains some of the peak appearing at 2θ of 10^{o} and a tiny speck at 12^{o}. Herein, the conjugation process is suggested to disrupt the orderly crystal lattice of CURC by introducing more amorphous characteristics from Ct, resulting spectrum exhibit broader peaks or less defined crystalline patterns. The differences in crystallinity and the presence of new diffraction patterns in the CCC sample are indicative of structural changes at the molecular level, likely due to the formation of new covalent bonds between curcumin and chitosan. This aligns with the expectation of a Schiff base reaction altering the material's physical properties, including its crystalline structure.

Thermal profiles of CURC, CCC and unmodified Ct were compared and as expected melting point episode for CURC was exhibited at about 176^{o}C. This peak is manifestly absent in the CCC. This means that conjugation of CURC to Ct transforms the CURC to more amorphous configuration. An exothermic for the evaporation of water occurs at about 100oC and present in both Ct and CCC. This is an indication that the CCC retains some properties of the Ct. We may conclude that the DSC analysis indicates distinct thermal transitions that do not align with the known properties of either CURC or Ct alone, in support of the formation of a new substance.

CN analysis of the same three entities above yielded no peak concentration of N in CURC but about 6% for the CCC. Ct as expected with the amine moieties has 4% concentration for N. This is yet a strong indication of the of a successful conjugation between Ct and CURC with the N contributed by Ct. In the same vein, the percentage of C in CCC is about 40%, which must be a contribution of carbonyl moieties from Ct, whereby the carbonyl groups in

CURC reacts with the amine groups of Ct through a possible Schiff base formation. The results from the thermal analysis and the CN analysis provides strong evidence for the successful formation of a CCC conjugate.

Following the successful formation of the CCC conjugate, it was necessary to ascertain the yield. The yield obtained after conjugation of non-depolymerized Ct with CURC was 81.06% and matched at 81.15% in the 300W depolymerized Ct. This yield is considered high in comparison to other CURC formulations reported in the literature, such as This very high yield is a useful feature that is likely to be in concert with a high CURC loading in the eventual formulation of NP. The yield obtained from this study was high in comparison to other CURC containing formulations in the literature. For instance, Asif et al. produced CURC loaded Ct nanoparticles with a maximum 60% yield (54). Similarly, Nguyen, et al. fabricated amorphous CURC–Ct nanoparticle complex with a production yield of 40 ± 3% (159).

Prior to formulation of the NPs, I sought to ascertain the solubility of the CCC in various solvents. 1% Acetic acid, ethanol and water were used as the test solvents. The CCC was not soluble in either ethanol or water but dissolved completely in acetic acid at 1mg/ml. This solubility feature of CCC in acetic acid is a useful feature as regards to the formulation of NPs, since the ionic gelation proceeds in aqueous media when species are completely dissolved and chitosan obtains its cation (50). Thus, acetic acid was used for the formulation of the NP. Furthermore, the solubility of CURC in acidic media has another advantage because the tumor microenvironment is more acidic than the media surrounding normal tissues (132). Hence this can provide better solubility in the cancer media, and more CURC delivery to cancer cells. It is important to note that I followed another procedure for determining the solubility of CURC other than the conventional methods of reaching saturated equilibrium and then performing quantification using HPLC or spectroscopic

techniques (160). It was based on observation and on the success of nano-formulation. I relied on the fact that the success of ionic gelation requires solute to completely dissolve in the aqueous media (161), and the nanoparticles were successfully formed.

Equally important as the evaluation of the solubility profiles is the assessment of the stability of the CCC. Because Schiff bases are pH and acid-sensitive (162), the stability was assessed as a function of pH. By superimposing the spectra of the CCC with those obtained after exposure to the various pH media (2.15, 6.5 and 12) and then drying. It appears that exposure to pH 2.5 yielded the least distortions in the spectral profile. In the case of the pH 6.5 and pH 12, significant variations in the spectra of CCC and those obtained after exposure to the media was observed. Furthermore, the solution obtained in pH 2.15 was clear as opposed to the other two pH media. This is relevant given that the CCC, as stated earlier, must be in solution prior to the formulation into NP. We have earlier shown that the CCC dissolves well in acetic acid. The spectra obtained in the pH 2.15 medium is also indicative that the relevant moieties are intact, which is crucial during the ionic gelation into NPs. Zeta. Potential in all cases was maintained positive and above 20 mV, indicating good stability and lower risk of agglomeration between nanoparticles.

Following the thorough characterization and evaluation of the CCC, I was now poised to commence the formulation and characterization of CCC in NPs. The NPs were formulated by ionic gelation using sodium tripolyphosphate as the crosslinker. The NPs were characterized as regards to size, PDI and ZP. All the NP formulated displayed a ZP of positivity, which is attributed to the amine groups of Ct, albeit a slide decrease in the positive charge was seen after conjugation to CURC. The non-depolymerized Ct when transformed to NPs had a size of about 130 nm but CCC was crucially 95 nm. This addresses one of the aims of the research, whereby depolymerization, conjugation followed by nano-formulation yielded a smaller size compared to the non-depolymerized Ct. The retention of positive charge is a

relevant feature due to the possibility to interact with the negative moieties of sialic acid within the plasma membrane prior to traversing (111, 112). Furthermore, a high ZP reflects good repulsion forces between the particles, which intimates preferable stability profile and low risk of aggregation (148).

The morphology and topography of the NP was studied using TEM and AFM. Both techniques revealed that the particles are spherical. The results also indicate that the surface of the particles is smooth. The TEM revealed a perfectly spherical NPs with well identified edges and narrow size distribution in case of both control Ct and 300W CCC NPs. However, with regards to the 300W treated NPs, although the NPs were round in shape, it was not as smooth as the ones seen with the control group suggesting that potentially the treatment with microwave irradiation had some impact on the texture and appearance of Ct polymer.

Finally, the stability of the NP as a function of temperature over a 28-day period was assessed. The parameters assessed were the ZP, size and PDI. No significant changes in parameters were observed between the control Ct, 300W Ct and 300W CCC when stored at 4^{o}C. On the other hand, agglomeration and dramatic increase in size was observed in the control CCC NPs when stored at room temperature, pointing to the preference of storage below room temperature.

The in vitro release studies were chosen to be done at 37°C at a pH of 6.7 because, as described in section 1.1.2.1 and 1.1.1.1, the most common site in the colon affected by cancer with a percentage of 55% is the sigmoid colon, and this region has a slightly acidic pH of 6.7. this approach was followed by other studies investigating the effect of CURC-Ct nanoparticles in colorectal cancer (135, 163). The release kinetics of my formulation were found to be controlled prolonged release over a period of 96 h (4 days), which is comparable to other studies in the literature. Jacobson et al., and Idoudi et al., also succeeded to develop polymeric nanocarriers with sustained release kinetics (135, 164) The burst release seen in the first 1 hour was suggested to be either due to the diffusion of the drug from the polymer surface, or the swelling of the polymer (149).

Finally, in vitro cytotoxic assays of control and 300W showed a promising dose dependent cytotoxic effect of both control and 300W CCC NPs. However, the microwave -treated CCC NPs were more effective in both cell lines compared with the control CCC NPs. In HCT-116 cell lines and at a concentration of 50 uM, the 300W CCC NPs showed statistically significant reduction in the cell viability compared with free CURC and comparable cytotoxic effect to the positive control 5-FU. In addition, in LoVo cell line and at the highest concentration, 300W even outperformed 5-FU, the conventional chemotherapy known for the treatment of colon cancer. The reason might be because of the fact that LoVo cells possess APC mutation, which makes them resistant to 5-FU therapy (165). This can lead to interesting findings suggesting that the new formulation has a mechanism capable of evading the resistance, albeit it still needs confirmation by other investigational techniques. Whereas the effect of control CCC NPs was inferior to 300W CCC NPs in both cell lines, although it showed a comparable cytotoxic effect to both CURC and 5-FU at high doses.

CHAPTER IV: CONCLUSION AND FUTURE WORK

Ct is a multifunctional natural polymer that has versatile and unique biomedical features rendering it a useful in pharmaceutical and medical applications. The Mw of Ct is an important parameter to consider, to ensure efficient use of Ct. microwave irradiation seems an effective mean of depolymerizing Ct to produce lower molecular weight, which is needed for its role as a drug delivery system. CURC on the other hand was shown effective against colon cancer, yet limited with major restrictions including its low solubility in aqueous media, low bioavailability and absorption and rapid metabolism. The complexation of CURC with the water soluble Ct added the advantage of improving its water solubility. The conjugation instead of encapsulation increased CURC yield and loading capacity and produced smaller needed for efficient and targeted drug delivery. The NPs had a smaller size than the unmodified Ct but retained the positive charge and exhibited controlled release kinetics. The polydispersity was considered good as well. When assessed against human colon cancer lines, the elementary results of the new formulations showed a promising cytotoxic effect that is dose dependent and induced morphological changes in cancer cells. Future work will involve further in vitro studies including flow cytometry, cell cycle, cell apoptosis analysis, and western blotting. Besides, the assessment of the new formulation on other cell lines with distinct mutations and gene expressions will add more validity to the results obtained. In addition, in vivo assessment will be targeted to better understand the pharmacokinetic and effectiveness of the formulation in vivo.

Future studies will be aimed at ascertaining the following:

- Performing long term stability studies on the formulation.
- Performing an investigation on the cellular pathways involved in cell death.
- Western blotting assays.
- Performing in vitro studies comparing intravenous and oral administration routes.

- Performing an in vivo pharmacokinetic studies investigation on colon cancer infested animal models.

REFERENCES:

1. AmericanCancerSociety. What Is Colorectal Cancer? 2020 [updated June 29, 2020. Available from: https://www.cancer.org/cancer/types/colon-rectal-cancer/about/what-is-colorectal-cancer.html#:~:text=Colorectal%20cancer%20starts%20in%20the,to%20grow%20out%20of%20control.

2. (WHO) WHO. Colorectal cancer 2023 [updated July 11, 2023. Available from: https://www.who.int/news-room/fact-sheets/detail/colorectal-cancer#:~:text=Colon%20cancer%20is%20the%20second,and%20mortality%20rates%20were%20observed.

3. Lotfollahzadeh S, Recio-Boiles A, Cagir B. Colon cancer. 2023.

4. QNA. Qatar Cancer Society Organizes International Conference on Gastrointestinal Cancers in December 2023 [Available from: https://www.qna.org.qa/en/News%20Area/News/2023-11/14/0066-qatar-cancer-society-organizes-international-conference-on-gastrointestinal-cancers-in-december.

5. Valle L. Genetic predisposition to colorectal cancer: where we stand and future perspectives. World journal of gastroenterology: WJG. 2014;20(29):9828.

6. Hossain MS, Karuniawati H, Jairoun AA, Urbi Z, Ooi DJ, John A, et al. Colorectal cancer: a review of carcinogenesis, global epidemiology, current challenges, risk factors, preventive and treatment strategies. Cancers. 2022;14(7):1732.

7. Johnson CM, Wei C, Ensor JE, Smolenski DJ, Amos CI, Levin B, et al. Meta-analyses of colorectal cancer risk factors. Cancer causes & control. 2013;24:1207-22.

8. Wald A. The large bowel. Brocklehurst's Textbook of Geriatric Medicine and Gerontology: Elsevier; 2010. p. 661-77.

9. Amieva-Balmori M, Remes-Troche JM. Embryology of the anorectum. Anorectal Disorders: Elsevier; 2019. p. 1-7.

10. Morton DA, Foreman KB, Albertine KH. Chapter 10. Midgut and Hindgut. The Big Picture: Gross Anatomy. New York, NY: The McGraw-Hill Companies; 2011.

11. Maqbool A. Colon: structure, function, and disorders. 2023.

12. Fallingborg J. Intraluminal pH of the human gastrointestinal tract. Dan Med Bull. 1999;46(3):183-96.

13. Pimentel-Muiños FX. Autophagy in the gastrointestinal system and cross talk with microbiota. Autophagy in Health and Disease: Elsevier; 2022. p. 321-33.

14. Duan B, Zhao Y, Bai J, Wang J, Duan X, Luo X, et al. Colorectal cancer: an overview. Exon Publications. 2022:1-12.

15. Shussman N, Wexner SD. Colorectal polyps and polyposis syndromes. Gastroenterology report. 2014;2(1):1-15.

16. Bien SA, Su Y-R, Conti DV, Harrison TA, Qu C, Guo X, et al. Genetic variant predictors of gene expression provide new insight into risk of colorectal cancer. Human genetics. 2019;138:307-26.

17. Xiao J-b, Leng A-m, Zhang Y-q, Wen Z, He J, Ye G-n. CUEDC2: multifunctional roles in carcinogenesis. Frontiers in Bioscience-Landmark. 2019;24(5):935-46.

18. Cancer.Net. Lynch Syndrome 2023 [updated July, 2023. Available from: https://www.cancer.net/cancer-types/lynch-syndrome#:~:text=What%20is%20Lynch%20Syndrome%3F,polyposis%20colorectal%20cancer%20(HNPCC).

19. Wang Y, Zhou X, Song Y, Ji X, Zhang A, Zhang G, et al. The mismatch repair gene hPMS1 (human postmeiotic segregation1) is down regulated in oral squamous cell carcinoma. Gene. 2013;524(1):28-34.

20. Ditonno I, Novielli D, Celiberto F, Rizzi S, Rendina M, Ierardi E, et al. Molecular Pathways of Carcinogenesis in Familial Adenomatous Polyposis. International Journal of Molecular Sciences. 2023;24(6):5687.

21. Institute NC. Colon Cancer Treatment (PDQ®)–Patient Version 2022 [Available from: https://www.cancer.gov/types/colorectal/patient/colon-treatment-pdq#_93.

22. Testa U, Pelosi E, Castelli G. Colorectal cancer: genetic abnormalities, tumor progression, tumor heterogeneity, clonal evolution and tumor-initiating cells. Medical Sciences. 2018;6(2):31.

23. ElRuz R, Gupta I, Allouch A. Molecular Mechanisms of Colon Cancer Progression and Metastasis: Recent Insights and Advancements. 2020.

24. Keum N, Giovannucci E. Global burden of colorectal cancer: emerging trends, risk factors and prevention strategies. Nature reviews Gastroenterology & hepatology. 2019;16(12):713-32.

25. Ojo OA, Adeyemo TR, Rotimi D, Batiha GE-S, Mostafa-Hedeab G, Iyobhebhe ME, et al. Anticancer properties of curcumin against colorectal cancer: a review. Frontiers in Oncology. 2022;12:881641.

26. Rawla P, Sunkara T, Barsouk A. Epidemiology of colorectal cancer: incidence, mortality, survival, and risk factors. Gastroenterology Review/Przegląd Gastroenterologiczny. 2019;14(2):89-103.

27. Wong MC, Ding H, Wang J, Chan PS, Huang J. Prevalence and risk factors of colorectal cancer in Asia. Intestinal research. 2019;17(3):317-29.

28. Ribeiro MS, Wallace MB. Endoscopic Treatment of Early Cancer of the Colon. Gastroenterol Hepatol (N Y). 2015;11(7):445-52.

29. Vogel JD, Felder SI, Bhama AR, Hawkins AT, Langenfeld SJ, Shaffer VO, et al. The American Society of Colon and Rectal Surgeons clinical practice guidelines for the management of colon cancer. Diseases of the Colon & Rectum. 2022;65(2):148-77.

30. Kahnamoui K, Cadeddu M, Farrokhyar F, Anvari M. Laparoscopic surgery for colon cancer: a systematic review. Can J Surg. 2007;50(1):48-57.

31. Vitale I, Galluzzi L, Castedo M, Kroemer G. Mitotic catastrophe: a mechanism for avoiding genomic instability. Nature Reviews Molecular Cell Biology. 2011;12(6):385-92.

32. Vogel JD, Felder SI, Bhama AR, Hawkins AT, Langenfeld SJ, Shaffer VO, et al. The American Society of Colon and Rectal Surgeons Clinical Practice Guidelines for the Management of Colon Cancer. Dis Colon Rectum. 2022;65(2):148-77.

33. Wegner RE, Abel S, Monga D, Raj M, Finley G, Nosik S, et al. Utilization of Adjuvant Radiotherapy for Resected Colon Cancer and Its Effect on Outcome. Annals of Surgical Oncology. 2020;27(3):825-32.

34. Taieb J, Gallois C. Adjuvant Chemotherapy for Stage III Colon Cancer. Cancers (Basel). 2020;12(9).

35. Degirmencioglu S, Tanrıverdi O, Demiray AG, Senol H, Dogu GG, Yaren A. Retrospective comparison of efficacy and safety of CAPOX and FOLFOX regimens as adjuvant treatment in patients with stage III colon cancer. Journal of International Medical Research. 2019;47(6):2507-15.

36. Fang SH, Efron JE, Berho ME, Wexner SD. Dilemma of stage II colon cancer and decision making for adjuvant chemotherapy. Journal of the American College of Surgeons. 2014;219(5):1056-69.

37. Veronese ML, O'Dwyer PJ. Monoclonal antibodies in the treatment of colorectal cancer. European Journal of Cancer. 2004;40(9):1292-301.

38. Wu C. Systemic therapy for colon cancer. Surgical Oncology Clinics. 2018;27(2):235-42.

39. Abruzzo A, Zuccheri G, Belluti F, Provenzano S, Verardi L, Bigucci F, et al. Chitosan nanoparticles for lipophilic anticancer drug delivery: Development, characterization and in vitro studies on HT29 cancer cells. Colloids Surf B Biointerfaces. 2016;145:362-72.

40. Górnicka J, Mika M, Wróblewska O, Siudem P, Paradowska K. Methods to improve the solubility of curcumin from turmeric. Life. 2023;13(1):207.

41. Siemann DW. The unique characteristics of tumor vasculature and preclinical evidence for its selective disruption by Tumor-Vascular Disrupting Agents. Cancer Treat Rev. 2011;37(1):63-74.

42. Kang H, Rho S, Stiles WR, Hu S, Baek Y, Hwang DW, et al. Size-dependent EPR effect of polymeric nanoparticles on tumor targeting. Advanced healthcare materials. 2020;9(1):1901223.

43. Anitha A, Maya S, Deepa N, Chennazhi KP, Nair SV, Jayakumar R. Curcumin-Loaded N,O-Carboxymethyl Chitosan Nanoparticles for Cancer Drug Delivery. Journal of Biomaterials Science, Polymer Edition. 2012;23(11):1381-400.

44. Bae YH, Park K. Targeted drug delivery to tumors: myths, reality and possibility. J Control Release. 2011;153(3):198-205.

45. Cho K, Wang X, Nie S, Chen ZG, Shin DM. Therapeutic nanoparticles for drug delivery in cancer. Clin Cancer Res. 2008;14(5):1310-6.

46. Krishnamoorthy K, Mahalingam M. Selection of a suitable method for the preparation of polymeric nanoparticles: multi-criteria decision making approach. Adv Pharm Bull. 2015;5(1):57-67.

47. Calvo P, Remuñan-López C, Vila-Jato JL, Alonso MJ. Chitosan and Chitosan/Ethylene Oxide-Propylene Oxide Block Copolymer Nanoparticles as Novel Carriers for Proteins and Vaccines. Pharmaceutical Research. 1997;14(10):1431-6.

48. Hoang NH, Le Thanh T, Sangpueak R, Treekoon J, Saengchan C, Thepbandit W, et al. Chitosan nanoparticles-based ionic gelation method: a promising candidate for plant disease management. Polymers. 2022;14(4):662.

49. Fàbregas A, Miñarro M, García-Montoya E, Pérez-Lozano P, Carrillo C, Sarrate R, et al. Impact of physical parameters on particle size and reaction yield when using the ionic gelation method to obtain cationic polymeric chitosan–tripolyphosphate nanoparticles. International journal of pharmaceutics. 2013;446(1-2):199-204.

50. Pedroso-Santana S, Fleitas-Salazar N. Ionotropic gelation method in the synthesis of nanoparticles/microparticles for biomedical purposes. Polymer International. 2020;69(5):443-7.

51. Szymańska E, Winnicka K. Stability of chitosan-a challenge for pharmaceutical and biomedical applications. Mar Drugs. 2015;13(4):1819-46.

52. Hewlings SJ, Kalman DS. Curcumin: A Review of Its Effects on Human Health. Foods. 2017;6(10).

53. Gupta SC, Patchva S, Koh W, Aggarwal BB. Discovery of curcumin, a component of golden spice, and its miraculous biological activities. Clinical and experimental pharmacology and physiology. 2012;39(3):283-99.

54. Asif HM, Zafar F, Ahmad K, Iqbal A, Shaheen G, Ansari KA, et al. Synthesis, characterization and evaluation of anti-arthritic and anti-inflammatory potential of curcumin loaded chitosan nanoparticles. Scientific Reports. 2023;13(1):10274.

55. del Castillo MLR, López-Tobar E, Sanchez-Cortes S, Flores G, Blanch GP. Stabilization of curcumin against photodegradation by encapsulation in gamma-cyclodextrin:

A study based on chromatographic and spectroscopic (Raman and UV–visible) data. Vibrational Spectroscopy. 2015;81:106-11.

56. Vera-Ramirez L, Pérez-Lopez P, Varela-Lopez A, Ramirez-Tortosa M, Battino M, Quiles JL. Curcumin and liver disease. Biofactors. 2013;39(1):88-100.

57. Mahady GB, Pendland SL, Yun G, Lu ZZ. Turmeric (Curcuma longa) and curcumin inhibit the growth of Helicobacter pylori, a group 1 carcinogen. Anticancer Res. 2002;22(6c):4179-81.

58. Lestari ML, Indrayanto G. Curcumin. Profiles Drug Subst Excip Relat Methodol. 2014;39:113-204.

59. Zoi V, Galani V, Lianos GD, Voulgaris S, Kyritsis AP, Alexiou GA. The Role of Curcumin in Cancer Treatment. Biomedicines. 2021;9(9).

60. Anand P, Sundaram C, Jhurani S, Kunnumakkara AB, Aggarwal BB. Curcumin and cancer: an "old-age" disease with an "age-old" solution. Cancer letters. 2008;267(1):133-64.

61. Hu Q, Luo Y. Chitosan-based nanocarriers for encapsulation and delivery of curcumin: A review. International Journal of Biological Macromolecules. 2021;179:125-35.

62. PubChem. Compound Summary: Curcumin 2024 [updated 2024. Available from: https://pubchem.ncbi.nlm.nih.gov/compound/Curcumin.

63. DrugBank. Curcumin 2023 [Available from: https://go.drugbank.com/drugs/DB11672.

64. Mbese Z, Khwaza V, Aderibigbe BA. Curcumin and its derivatives as potential therapeutic agents in prostate, colon and breast cancers. Molecules. 2019;24(23):4386.

65. Rege SA, Arya M, Momin SA. Structure activity relationship of tautomers of curcumin: A review. Ukrainian food journal. 2019(8, Issue 1):45-60.

66. Jankun J, Wyganowska-Świątkowska M, Dettlaff K, Jelińska A, Surdacka A, Wątróbska-Świetlikowska D, et al. Determining whether curcumin degradation/condensation is actually bioactivation. International journal of molecular medicine. 2016;37(5):1151-8.

67. Zheng D, Huang C, Huang H, Zhao Y, Khan MRU, Zhao H, et al. Antibacterial mechanism of curcumin: A review. Chemistry & Biodiversity. 2020;17(8):e2000171.

68. Anand P, Thomas SG, Kunnumakkara AB, Sundaram C, Harikumar KB, Sung B, et al. Biological activities of curcumin and its analogues (Congeners) made by man and Mother Nature. Biochemical pharmacology. 2008;76(11):1590-611.

69. Peram MR, Jalalpure SS, Palkar MB, Diwan PV. Stability studies of pure and mixture form of curcuminoids by reverse phase-HPLC method under various experimental stress conditions. Food science and biotechnology. 2017;26(3):591-602.

70. Ahmed T, Gilani AH. Therapeutic potential of turmeric in Alzheimer's disease: curcumin or curcuminoids? Phytotherapy Research. 2014;28(4):517-25.

71. Gugulothu D, Fernandes C, Patravale V. A versatile high performance liquid chromatography method for simultaneous determination of three curcuminoids in pharmaceutical dosage forms. Pharm Anal Acta. 2012;3(04).

72. Kharat M, Du Z, Zhang G, McClements DJ. Physical and chemical stability of curcumin in aqueous solutions and emulsions: Impact of pH, temperature, and molecular environment. Journal of agricultural and food chemistry. 2017;65(8):1525-32.

73. Tønnesen HH, Másson M, Loftsson T. Studies of curcumin and curcuminoids. XXVII. Cyclodextrin complexation: solubility, chemical and photochemical stability. International journal of pharmaceutics. 2002;244(1-2):127-35.

74. Suresh D, Gurudutt K, Srinivasan K. Degradation of bioactive spice compound: curcumin during domestic cooking. European Food Research and Technology. 2009;228:807-12.

75. Giordano A, Tommonaro G. Curcumin and Cancer. Nutrients. 2019;11(10).

76. Johnson JJ, Mukhtar H. Curcumin for chemoprevention of colon cancer. Cancer letters. 2007;255(2):170-81.

77. Collett GP, Campbell FC. Curcumin induces c-jun N-terminal kinase-dependent apoptosis in HCT116 human colon cancer cells. Carcinogenesis. 2004;25(11):2183-9.

78. Haimovitz-Friedman A, Kolesnick RN, Fuks Z. Ceramide signaling in apoptosis. Br Med Bull. 1997;53(3):539-53.

79. Pricci M, Girardi B, Giorgio F, Losurdo G, Ierardi E, Di Leo A. Curcumin and colorectal cancer: from basic to clinical evidences. International journal of molecular sciences. 2020;21(7):2364.

80. Scott DW, Loo G. Curcumin-induced GADD153 gene up-regulation in human colon cancer cells. Carcinogenesis. 2004;25(11):2155-64.

81. Rashmi R, Kumar TS, Karunagaran D. Human colon cancer cells differ in their sensitivity to curcumin-induced apoptosis and heat shock protects them by inhibiting the release of apoptosis-inducing factor and caspases. FEBS letters. 2003;538(1-3):19-24.

82. Zhao L, Ding X, Khan IM, Yue L, Zhang Y, Wang Z. Preparation and characterization of curcumin/chitosan conjugate as an efficient photodynamic antibacterial agent. Carbohydrate Polymers. 2023;313:120852.

83. Idoudi S, Bedhiafi T, Hijji YM, Billa N. Curcumin and derivatives in nanoformulations with therapeutic potential on colorectal cancer. AAPS PharmSciTech. 2022;23(5):115.

84. Min Z, Zhu Y, Hong X, Yu Z, Ye M, Yuan Q, et al. Synthesis and biological evaluations of monocarbonyl curcumin inspired pyrazole analogues as potential anti-colon cancer agent. Drug Design, Development and Therapy. 2020:2517-34.

85. Dal Magro C, dos Santos AE, Ribas MM, Aguiar GP, Volfe CR, Lopes ML, et al. Production of curcumin-resveratrol cocrystal using cocrystallization with supercritical solvent. The Journal of Supercritical Fluids. 2021;171:105190.

86. Lu J, Rohani S. Polymorphism and crystallization of active pharmaceutical ingredients (APIs). Current Medicinal Chemistry. 2009;16(7):884-905.

87. Kumar S, Kesharwani SS, Mathur H, Tyagi M, Bhat GJ, Tummala H. Molecular complexation of curcumin with pH sensitive cationic copolymer enhances the aqueous solubility, stability and bioavailability of curcumin. European Journal of Pharmaceutical Sciences. 2016;82:86-96.

88. Schiff H. Mittheilungen aus dem Universitätslaboratorium in Pisa: eine neue Reihe organischer Basen. Justus Liebigs Annalen der Chemie. 1864;131(1):118-9.

89. Hussain Z, Yousif E, Ahmed A, Altaie A. Synthesis and characterization of Schiff's bases of sulfamethoxazole. Organic and medicinal chemistry letters. 2014;4(1):1-4.

90. Di Bernardo P, Zanonato P, Tamburini S, Tomasin P, Vigato P. Complexation behaviour and stability of Schiff bases in aqueous solution. The case of an acyclic diimino (amino) diphenol and its reduced triamine derivative. Dalton Transactions. 2006(39):4711-21.

91. Dhar DN, Taploo C. Schiff bases and their applications. J Sci Ind Res. 1982;41(8):501-6.

92. Przybylski P, Huczyński AW, Pyta KK, Brzezinski B, Bartl F. Biological properties of Schiff bases and azo derivatives of phenols. Current Organic Chemistry. 2009;13.

93. Tong R, Tang L, Ma L, Tu C, Baumgartner R, Cheng J. Smart chemistry in polymeric nanomedicine. Chemical Society Reviews. 2014;43(20):6982-7012.

94. Guzman-Villanueva D, El-Sherbiny IM, Herrera-Ruiz D, Smyth HD. Design and in vitro evaluation of a new nano-microparticulate system for enhanced aqueous-phase solubility of curcumin. BioMed research international. 2013;2013.

95. Seljak KB, Kocbek P, Gašperlin M. Mesoporous silica nanoparticles as delivery carriers: An overview of drug loading techniques. Journal of Drug Delivery Science and Technology. 2020;59:101906.

96. Nair KL, Thulasidasan AKT, Deepa G, Anto RJ, Kumar GV. Purely aqueous PLGA nanoparticulate formulations of curcumin exhibit enhanced anticancer activity with dependence on the combination of the carrier. International journal of pharmaceutics. 2012;425(1-2):44-52.

97. Gao Y, Li Z, Sun M, Guo C, Yu A, Xi Y, et al. Preparation and characterization of intravenously injectable curcumin nanosuspension. Drug delivery. 2011;18(2):131-42.

98. Li H, Zhang N, Hao Y, Wang Y, Jia S, Zhang H, et al. Formulation of curcumin delivery with functionalized single-walled carbon nanotubes: characteristics and anticancer effects in vitro. Drug delivery. 2014;21(5):379-87.

99. Gaspar VM, Moreira AF, de Melo-Diogo D, Costa EC, Queiroz JA, Sousa F, et al. Multifunctional nanocarriers for codelivery of nucleic acids and chemotherapeutics to cancer cells. Nanobiomaterials in Medical Imaging: Elsevier; 2016. p. 163-207.

100. Elieh Ali Komi D, Sharma L, Dela Cruz CS. Chitin and its effects on inflammatory and immune responses. Clinical reviews in allergy & immunology. 2018;54:213-23.

101. Jiang T, James R, Kumbar SG, Laurencin CT. Chitosan as a biomaterial: structure, properties, and applications in tissue engineering and drug delivery. Natural and synthetic biomedical polymers: Elsevier; 2014. p. 91-113.

102. Samar MM, El-Kalyoubi M, Khalaf M, Abd El-Razik M. Physicochemical, functional, antioxidant and antibacterial properties of chitosan extracted from shrimp wastes by microwave technique. Annals of Agricultural Sciences. 2013;58(1):33-41.

103. Hwang J-K, Shin H-H. Rheological properties of chitosan solutions. Korea-Australia Rheology Journal. 2000;12(3_4):175-9.

104. Aranaz I, Alcántara AR, Civera MC, Arias C, Elorza B, Heras Caballero A, et al. Chitosan: An overview of its properties and applications. Polymers. 2021;13(19):3256.

105. ChemicalBook. Chitosan 2023 [Available from: https://www.chemicalbook.com/ChemicalProductProperty_EN_CB1479274.htm.

106. Romanazzi G, Gabler FM, Margosan D, Mackey BE, Smilanick JL. Effect of chitosan dissolved in different acids on its ability to control postharvest gray mold of table grape. Phytopathology. 2009;99(9):1028-36.

107. Lizardi-Mendoza J, Monal WMA, Valencia FMG. Chemical characteristics and functional properties of chitosan. Chitosan in the preservation of agricultural commodities: Elsevier; 2016. p. 3-31.

108. Jiang Y, Fu C, Wu S, Liu G, Guo J, Su Z. Determination of the deacetylation degree of chitooligosaccharides. Marine drugs. 2017;15(11):332.

109. Wenling C, Duohui J, Jiamou L, Yandao G, Nanming Z, Xiufang Z. Effects of the degree of deacetylation on the physicochemical properties and Schwann cell affinity of chitosan films. Journal of biomaterials applications. 2005;20(2):157-77.

110. Lv S. High-performance superplasticizer based on chitosan. Biopolymers and biotech admixtures for eco-efficient construction materials: Elsevier; 2016. p. 131-50.

111. Nishino M, Matsuzaki I, Musangile FY, Takahashi Y, Iwahashi Y, Warigaya K, et al. Measurement and visualization of cell membrane surface charge in fixed cultured cells related with cell morphology. PLoS One. 2020;15(7):e0236373.

112. Aibani N, Rai R, Patel P, Cuddihy G, Wasan EK. Chitosan nanoparticles at the biological interface: Implications for drug delivery. Pharmaceutics. 2021;13(10):1686.

113. Matica MA, Aachmann FL, Tøndervik A, Sletta H, Ostafe V. Chitosan as a wound dressing starting material: Antimicrobial properties and mode of action. International journal of molecular sciences. 2019;20(23):5889.

114. Chokradjaroen C, Rujiravanit R, Watthanaphanit A, Theeramunkong S, Saito N, Yamashita K, et al. Enhanced degradation of chitosan by applying plasma treatment in combination with oxidizing agents for potential use as an anticancer agent. Carbohydrate Polymers. 2017;167:1-11.

115. Shao J, Yang Y, Zhong Q. Studies on preparation of oligoglucosamine by oxidative degradation under microwave irradiation. Polymer Degradation and Stability. 2003;82(3):395-8.

116. Pandit A, Indurkar A, Deshpande C, Jain R, Dandekar P. A systematic review of physical techniques for chitosan degradation. Carbohydrate Polymer Technologies and Applications. 2021;2:100033.

117. El Knidri H, Belaabed R, Addaou A, Laajeb A, Lahsini A. Extraction, chemical modification and characterization of chitin and chitosan. International journal of biological macromolecules. 2018;120:1181-9.

118. Li K, Xing R, Liu S, Qin Y, Meng X, Li P. Microwave-assisted degradation of chitosan for a possible use in inhibiting crop pathogenic fungi. International Journal of Biological Macromolecules. 2012;51(5):767-73.

119. Wasikiewicz JM, Yeates SG. “Green” molecular weight degradation of chitosan using microwave irradiation. Polymer Degradation and Stability. 2013;98(4):863-7.

120. Jafari H, Delporte C, Bernaerts KV, De Leener G, Luhmer M, Nie L, et al. Development of marine oligosaccharides for potential wound healing biomaterials engineering. Chemical Engineering Journal Advances. 2021;7:100113.

121. Li Y, Yang Y, Huang Z, Luo Z, Qian C, Li Y, et al. Preparation of low molecular chitosan by microwave-induced plasma desorption/ionization technology. International Journal of Biological Macromolecules. 2021;187:441-50.

122. Journot CM, Nicolle L, Lavanchy Y, Gerber-Lemaire S. Selection of water-soluble chitosan by microwave-assisted degradation and pH-controlled precipitation. Polymers. 2020;12(6):1274.

123. Sun T, Zhou D, Xie J, Mao F. Preparation of chitosan oligomers and their antioxidant activity. European Food Research and Technology. 2007;225:451-6.

124. Sun T, Zhou D, Mao F, Zhu Y. Preparation of low-molecular-weight carboxymethyl chitosan and their superoxide anion scavenging activity. European polymer journal. 2007;43(2):652-6.

125. Cheng J, Zhu H, Huang J, Zhao J, Yan B, Ma S, et al. The physicochemical properties of chitosan prepared by microwave heating. Food Science & Nutrition. 2020;8(4):1987-94.

126. Zhang Y, Zhang H, Chen S, Fu H, Zhao Y. Microwave-assisted degradation of chitosan with hydrogen peroxide treatment using Box-Behnken design for enhanced antibacterial activity. International Journal of Food Science & Technology. 2018;53(1):156-65.

127. Basit HM, Mohd Amin MCI, Ng S-F, Katas H, Shah SU, Khan NR. Formulation and evaluation of microwave-modified chitosan-curcumin nanoparticles—A promising nanomaterials platform for skin tissue regeneration applications following burn wounds. Polymers. 2020;12(11):2608.

128. Kocak N, Sahin M, Akin I, Kus M, Yilmaz M. Microwave assisted synthesis of chitosan nanoparticles. Journal of Macromolecular Science, Part A. 2011;48(10):776-9.

129. Hiep NT, Khon HC, Niem VVT, Toi VV, Ngoc Quyen T, Hai ND, et al. Microwave-assisted synthesis of chitosan/polyvinyl alcohol silver nanoparticles gel for wound dressing applications. International Journal of Polymer Science. 2016;2016.

130. Elsayed Mahmoud D, Billa N. Physicochemical modifications in microwave-irradiated chitosan: biopharmaceutical and medical applications. Journal of Biomaterials Science, Polymer Edition. 2024:1-18.

131. Galema SA. Microwave chemistry. Chemical Society Reviews. 1997;26(3):233-8.

132. Lee S-H, Griffiths JR. How and why are cancers acidic? Carbonic anhydrase IX and the homeostatic control of tumour extracellular pH. Cancers. 2020;12(6):1616.

133. Bogdanov A, Bogdanov A, Chubenko V, Volkov N, Moiseenko F, Moiseyenko V. Tumor acidity: From hallmark of cancer to target of treatment. Frontiers in Oncology. 2022;12:979154.

134. Saranya TS, Rajan VK, Biswas R, Jayakumar R, Sathianarayanan S. Synthesis, characterisation and biomedical applications of curcumin conjugated chitosan microspheres. Int J Biol Macromol. 2018;110:227-33.

135. Idoudi S, Hijji Y, Bedhiafi T, Korashy HM, Uddin S, Merhi M, et al. A novel approach of encapsulating curcumin and succinylated derivative in mannosylated-chitosan nanoparticles. Carbohydrate Polymers. 2022;297:120034.

136. Gupta KC, Jabrail FH. Effects of degree of deacetylation and cross-linking on physical characteristics, swelling and release behavior of chitosan microspheres. Carbohydrate polymers. 2006;66(1):43-54.

137. Sheng JJ. Chapter 5 - Polymer Flooding. In: Sheng JJ, editor. Modern Chemical Enhanced Oil Recovery. Boston: Gulf Professional Publishing; 2011. p. 101-206.

138. Esfandiarpour-Boroujeni S, Bagheri-Khoulenjani S, Mirzadeh H, Amanpour S. Fabrication and study of curcumin loaded nanoparticles based on folate-chitosan for breast cancer therapy application. Carbohydrate polymers. 2017;168:14-21.

139. Hassan AF, Hussein O, Al-Barazenji T, Allouch A, Kamareddine L, Malki A, et al. The effect of novel nitrogen-based chalcone analogs on colorectal cancer cells: Insight into the molecular pathways. Heliyon. 2024.

140. Clarke CN, Kopetz ES. BRAF mutant colorectal cancer as a distinct subset of colorectal cancer: clinical characteristics, clinical behavior, and response to targeted therapies. Journal of Gastrointestinal Oncology. 2015;6(6):660.

141. El-Sawy NM, Abd El-Rehim HA, Elbarbary AM, Hegazy E-SA. Radiation-induced degradation of chitosan for possible use as a growth promoter in agricultural purposes. Carbohydrate Polymers. 2010;79(3):555-62.

142. Yen M-T, Yang J-H, Mau J-L. Physicochemical characterization of chitin and chitosan from crab shells. Carbohydrate polymers. 2009;75(1):15-21.

143. Zhang D, Jiang L, Zong J, Chen S, Ma C, Li H. Incorporated α-amylase and starch in an edible chitosan–procyanidin complex film increased the release amount of procyanidins. RSC advances. 2017;7(89):56771-8.

144. Dey SC, Al-Amin M, Rashid TU, Sultan MZ, Ashaduzzaman M, Sarker M, et al. Preparation, characterization and performance evaluation of chitosan as an adsorbent for remazol red. Int J Latest Res Eng Technol. 2016;2(2):52-62.

145. Ferrero F, Periolatto M. Antimicrobial finish of textiles by chitosan UV-curing. Journal of nanoscience and nanotechnology. 2012;12(6):4803-10.

146. Sayyar Z, Jafarizadeh-Malmiri H. Temperature effects on thermodynamic parameters and solubility of curcumin O/W nanodispersions using different thermodynamic models. International journal of food engineering. 2019;15(1-2):20180311.

147. Danaei M, Dehghankhold M, Ataei S, Hasanzadeh Davarani F, Javanmard R, Dokhani A, et al. Impact of particle size and polydispersity index on the clinical applications of lipidic nanocarrier systems. Pharmaceutics. 2018;10(2):57.

148. Arozal W, Louisa M, Rahmat D, Chendrana P, Sandhiutami NMD. Development, characterization and pharmacokinetic profile of chitosan-sodium tripolyphosphate nanoparticles based drug delivery systems for curcumin. Advanced Pharmaceutical Bulletin. 2021;11(1):77.

149. Mohammed MA, Syeda JT, Wasan KM, Wasan EK. An overview of chitosan nanoparticles and its application in non-parenteral drug delivery. Pharmaceutics. 2017;9(4):53.

150. Cai L, Qin X, Xu Z, Song Y, Jiang H, Wu Y, et al. Comparison of cytotoxicity evaluation of anticancer drugs between real-time cell analysis and CCK-8 method. ACS omega. 2019;4(7):12036-42.

151. Estanqueiro M, Amaral MH, Conceição J, Lobo JMS. Nanotechnological carriers for cancer chemotherapy: the state of the art. Colloids and surfaces B: Biointerfaces. 2015;126:631-48.

152. Shi J, Xiao Z, Kamaly N, Farokhzad OC. Self-assembled targeted nanoparticles: evolution of technologies and bench to bedside translation. Accounts of chemical research. 2011;44(10):1123-34.

153. Makadia HK, Siegel SJ. Poly lactic-co-glycolic acid (PLGA) as biodegradable controlled drug delivery carrier. Polymers. 2011;3(3):1377-97.

154. Prakash O, Kumar A, Kumar P. Anticancer potential of plants and natural products. Am J Pharmacol Sci. 2013;1(6):104-15.

155. Xing R, Liu S, Yu H, Guo Z, Wang P, Li C, et al. Salt-assisted acid hydrolysis of chitosan to oligomers under microwave irradiation. Carbohydrate Research. 2005;340(13):2150-3.

156. Wang C, Xu W, Zhang C, Wang M, Wang X. Microwave wireless power transmission technology index system and test evaluation methods. EURASIP Journal on Advances in Signal Processing. 2022;2022(1):16.

157. Mathaba M, Daramola MO. Effect of chitosan's degree of deacetylation on the performance of pes membrane infused with chitosan during amd treatment. Membranes. 2020;10(3):52.

158. Morsy M, Mostafa K, Amyn H, El-Ebissy AA-h, Salah AM, Youssef MA. Synthesis and characterization of freeze dryer chitosan nano particles as multi functional eco-friendly finish for fabricating easy care and antibacterial cotton textiles. Egyptian Journal of Chemistry. 2019;62(7):1277-93.

159. Nguyen MH, Yu H, Kiew TY, Hadinoto K. Cost-effective alternative to nano-encapsulation: amorphous curcumin–chitosan nanoparticle complex exhibiting high payload and supersaturation generation. European journal of pharmaceutics and biopharmaceutics. 2015;96:1-10.

160. Larsson J. Methods for measurement of solubility and dissolution rate of sparingly soluble drugs. 2009.

161. Giri TK. 5 - Nanoarchitectured Polysaccharide-Based Drug Carrier for Ocular Therapeutics. In: Holban AM, Grumezescu AM, editors. Nanoarchitectonics for Smart Delivery and Drug Targeting: William Andrew Publishing; 2016. p. 119-41.

162. Su H, Zhang W, Wu Y, Han X, Liu G, Jia Q, et al. Schiff base-containing dextran nanogel as pH-sensitive drug delivery system of doxorubicin: Synthesis and characterization. Journal of Biomaterials Applications. 2018;33(2):170-81.

163. Idoudi S, Bedhiafi T, Sahir F, Hijji Y, Uddin S, Merhi M, et al. Studies on anti-colon cancer potential of nanoformulations of curcumin and succinylated curcumin in mannosylated chitosan. International Journal of Biological Macromolecules. 2023;235:123827.

164. Jacobson GB, Shinde R, Contag CH, Zare RN. Sustained release of drugs dispersed in polymer nanoparticles. Angewandte Chemie (International ed in English). 2008;47(41):7880.

165. Das D, Preet R, Mohapatra P, Satapathy SR, Siddharth S, Tamir T, et al. 5-Fluorouracil mediated anti-cancer activity in colon cancer cells is through the induction of Adenomatous Polyposis Coli: Implication of the long-patch base excision repair pathway. DNA repair. 2014;24:15-25.